Comparison of Various Types of Modified Biochar for Optimal PFOS/PFOA Adsorption

by

Gabrielle Frances Gray

A thesis submitted in partial fulfillment of the requirements for the degree of

Master of Science

in

Environmental Engineering

Department of Civil and Environmental Engineering
University of Alberta

Abstract

The increasing abundance of per- and polyfluoroalkyl substances (PFAS) has attracted growing interest due to concern about the potential hazards to public health and ecosystems. Due to PFAS toxicity, mobility, environmental persistence, and strong bioaccumulation, they are being further investigated. Long-chain perfluorooctane sulfonic acid (PFOS) and perfluorooctanoic acid (PFOA) are most often detected in aquatic environments even though their use has been limited by recent regulations. However, most adsorption studies are focused on their removal using deionized water instead of wastewater. In this research, the removal of PFOS in wastewater was investigated using four different types of municipal sludge-produced biochars, where the metal-enhanced ferric chloride ($FeCl_3$)-modified biochar showed the most promising adsorption of PFOS and PFOA. $FeCl_3$-modified biochar was characterized via x-ray diffraction (XRD), x-ray photoelectron spectroscopy (XPS), Fourier transform infrared (FTIR), thermogravimetric analyzer (TGA), and Brunauer–Emmett–Teller (BET) method. The results indicated that physical adsorption might play a dominant role in the removal process. The $FeCl_3$-modified biochar exhibited a high removal efficiency of PFOS and PFOA, 99.89% and 94.34%, respectively, with an initial concentration of 25 mg L^{-1}, for PFOS and PFOA and an adsorbent dosage of 0.5 g L^{-1} and 0.75 g L^{-1}, respectively. The possible adsorption mechanism was proposed, and the enhanced removal ability was due to the improved specific surface area, and pore volume. Functional groups in the biochar, such as Fe, were also responsible for the enhanced removal ability, which also might be the reason for the better performance of the $FeCl_3$-modified biochar than other modified biochars. Moreover, the adsorption process was best described using the Langmuir and pseudo-second-order models. The desorption and regeneration of $FeCl_3$-modified biochar for the removal of PFOS and PFOA were also determined. No desorption of PFOS was observed at 24 hrs or 7

days and a 5.3% desorption of PFOA was seen after 7 days. The regeneration of $FeCl_3$-modified biochar for PFOS and PFOA adsorption was evaluated over five cycles. After the first regeneration cycle, the $FeCl_3$-modified biochar removed 84.68% of PFOS with the removal decreasing with each cycle to 33.47%. PFOA removal increased with the first regeneration cycle to 100% and was maintained for four cycles before reducing to 99.08% after the fifth regeneration cycle. Overall, the $FeCl_3$-modified biochar would be a promising and effective adsorbent for PFOS and PFOA removal, due to its removal efficiency and cost-effective and environmentally friendly advantages.

Preface

The research described in this thesis is an original work by Gabrielle Frances Gray. The thesis was written and performed under the supervision of Dr. Mohamed Gamal El-Din in the Department of Civil and Environmental Engineering at the University of Alberta. The thesis is designed as a paper format with Sections 3 and 4 representing stand-alone papers that have been or will be submitted for publication. I conducted the experimental work and prepared the manuscript with the help of research assistants, Ph.D. students, and post-doctoral fellows in our research group.

Dedication

This thesis is dedicated to my parents.

For their endless love, support, and encouragement.

Acknowledgements

Firstly, I would like to thank Dr. Mohamed Gamal El-Din for his constant guidance and supervision. I am inspired by his dedication to seeking knowledge and excellence in all his works. Furthermore, I am grateful for the wealth of knowledge he was always willing to share and for challenging me to excel. I am honored that he has given me the opportunity to work as a part of his team. I would also like to thank Dr. Pamela Chelme-Ayala who was always willing to give her time to discuss my findings and answer my questions. I am immensely grateful for her words of encouragement in times of doubt and for providing insight into my data, presentation, and thesis. I would like to sincerely thank Ph.D. student Deborah Crominski da Silva Medeiros for her help, guidance, and knowledge in the field of biochar production and adsorption. I would also like to acknowledge the financial support received from the Natural Sciences and Engineering Research Council of Canada (NSERC) Collaborative Research and Discovery Grant Program and EPCOR Water Services.

I would also like to thank my friends and family for encouraging and reassuring me throughout the duration of my master's degree. For providing me safe space where I could voice both my worries and triumphs. I sincerely thank and acknowledge that I would not be where I am today without their love and support.

Table of Contents

List of Tables

List of Figures

Abbreviations

AC
: Activated Carbon

AOPs
: Advanced Oxidation Processes

BdAC
: Bamboo-derived Activated carbon

BET
: Brunauer, Emmett, and Teller

CdB
: Corn-derived biochar

COD
: Chemical Oxygen Demand

DI
: Deionized water

DTG
: Derivative of thermogravimetric

DWTP
: Drinking Water Treatment Plant

EDX
: Energy dispersive X-ray spectrometer

EfOM
: Effluent Organic Matter

FTIR
: Fourier transform infrared

GAC
: Granular activated carbon

HWC
: Hardwood biochar

MAC

Maximum acceptable concentration

MIP-CMS

Molecularly imprinted carbon microspheres

MS

Mass spectrometry

MSB

Maize Strat Biochar

MWNT

Multi-walled carbon nanotubes

NIP-CMS

Non-imprinted carbon microspheres

PAC

Powdered activated carbon

PFAS

Poly- and perfluoroalkyl substances

PFBS

Perfluorobutane sulfonic acid

PFCAs

Perfluorocarboxylic acids

PFOA

Perfluorooctanoic acid

PFOS

Perfluorooctane sulfonic acid

PFSAs

Perfluoroalkyl sulfonates

PPM

Parts Per Million

PWC

Pinewood biochar

QCB

Quaternized Cotton Biochar

RPM

Revolutions Per Minute

SE

Secondary Effluent

SWNT

Single-walled nanotubules

TGA

Thermogravimetric analyzer

TKN

Total Kjeldahl Nitrogen

TOC

Total Organic Carbon

TOF

Time of Flight

UPLC

Ultra-high performance liquid chromatography

UV

Ultraviolet

WSB

Willow Sawdust Biochar

WW

Wastewater

WWTP

Wastewater Treatment Plant

XPS

X-ray photoelectron spectroscopy

XRD

X-ray diffractometer

1. Introduction and Research Objectives

1.1. Background and Motivation

1.1.1. Per-and polyfluoroalkyl Substances

Per- and polyfluoroalkyl substances (PFAS) are a large, complex group of human-made compounds that do not occur naturally in the environment. Due to PFAS water resistance, acid-base resistance, surface activity, and chemical/thermal stability, they are used in numerous industries such as aerospace, automotive, construction, and electronics. They are widely used as coating materials, firefighting foams, metal plating solutions, clothing, plastic bottles, and polymers (Hassan et al., 2020). PFAS have been manufactured and used in a variety of industries worldwide since the 1940s. The use, sale, and import of perfluorooctanoic acid (PFOA)/ perfluorooctane sulfonate (PFOS) or PFOS/PFOA-containing products was prohibited in Canada in 2008, with the exception of firefighting and military products (Government of Canada, 2021). Perfluorooctanoic acid (PFOA) and perfluorooctane sulfonate (PFOS) are the most common PFAS found in the environment and are the most well-studied. PFOS and PFOA are further classified into PFAS subgroups as perfluoroalkyl sulfonates (PFSAs) and perfluorocarboxylic acid (PFCAs). PFOS and PFOA are persistent in the environment and resistant to typical environmental degradation processes, primarily due to the chemical bond between the carbon and fluorine atoms being extremely strong and stable. The strength of the C-F bond provides PFAS with both chemical and thermal stability (Hamid & Li, 2016). Due to the low polarizability of fluorine atoms, PFAS exhibit hydrophobic and lipophobic properties. PFAS have been classified as a persistent organic pollutant of significant concern (Government of Canada, 2021; EPA 2022). They are widely distributed across all trophic levels and are found in soil, air, and groundwater. Long-range

atmospheric transport provides a pathway for PFAS to be distributed even to remote areas including the Arctic and Antarctic. Bioaccumulation and biomagnification of PFAS increase as the length of the carbon chain does (Gagliano et al., 2020; Panieri et al., 2022). The toxicity, mobility, and bioaccumulation potential of PFOS and PFOA result in potential adverse effects on the environment and human health. They can bind to blood proteins and have long half-lives in humans (Pachkowski et al., 2019). Due to their widespread use, they can be found in the blood of humans and animals worldwide. They are also present at low levels in various food products. The half-life of PFOS and PFOA in humans ranges from 2.3 to 5.4 years (EPA, 2022). PFAS exposure in humans is linked to cancer, obesity, elevated cholesterol, immune suppression, ulcerative colitis, endocrine disruption, and renal dysfunction in children. (Gagliano et al., 2020; Pachkowski et al., 2018; Government of Canada, 2018; EPA, 2022). Chou & Lin (2020) research showed that PFOS interfere with mitochondrial beta-oxidation of fatty acids affecting the transcriptional activity in the liver of rodents and PFOS can alter lipid metabolism changing serum lipids. Zeng et al. (2019) discussed the bioaccumulation of PFOS is most prevalent in the liver causing hepatoxicity through interference with fat metabolism, disrupting cell cycle progression, and causing oxidative stress. Zeng et al. (2019) and Chou & Lin (2020) outline that the toxicity of PFOS mainly involve oxidative stress and competitive binding to protein receptors, causing physiological process disruption with fatty acids.

A PFOA oral non-cancer reference dose (RfD) of 0.2 ng/kg/day was derived by the EPA in 2016. The maximum acceptable concentration (MAC) of PFOA in drinking water was determined to be 0.2 $\mu g\ L^{-1}$. The EPA has determined that a PFOA concentration of 0.5 $\mu g\ L^{-1}$ in drinking water would correspond to a one-in-a-million increased risk of cancer, based on this slope factor

(EPA, 2022). PFOS has a MAC of 0.6 μg L^{-1} in drinking water. The effects of PFOS and PFOA are additive, and their corresponding MACs should not exceed 1 μg L^{-1} (EPA, 2022). The EPA established drinking water health advisories of 70 parts per trillion (0.07 μg L^{-1}) for the combined concentrations of PFOS and PFOA. The American Conference of Governmental Industrial Hygienists (ACGIH) has classified PFOA as a Group A3 carcinogen, a confirmed animal carcinogen with unknown relevance to humans (Zeng et al., 2019; Chou & Lin, 2020). The International Agency for Research on Cancer (IARC) has classified PFOS as Group 2B, a possible carcinogen to humans (Arrieta-Cortes et al., 2017; Chou & Lin, 2020; Son et al., 2020). Some cancer effects have been observed in humans after PFOS exposure; however, no clear links have been established. PFOA is third on the EPA's Contaminant Candidate List for consideration for regulation in drinking water. PFOS are fourth on the drinking water contaminant candidate list and are currently not subject to any proposed or promulgated national primary drinking water regulations but are known or anticipated to occur in public water systems. In the 1990s, PFOS was known to be widespread in the blood of the general population. Animal studies show that PFOS is well absorbed orally and distributed mainly in the serum and the liver. At the lowest level of exposure, non-cancer effects such as reproductive and developmental effects, liver effects, and changes in serum lipid levels occur in animals (EPA, 2022). Through the PFOA Stewardship Program, companies have committed to reducing PFOA product content and emissions by 95 percent in 2010 and eliminating its use by 2015. PFOS was added to the list of persistent organic pollutants (POPs) at the Stockholm Convention in 2009 (Chen et al., 2017).

The public can be exposed to PFAS through many different sources including, food, consumer products, dust, and drinking water (Vo et al., 2022; Hamid & Li, 2016). The main sources of exposure are food and consumer products, but concentrations in drinking water can increase in

areas where water is contaminated. In drinking water, PFAS concentrations are usually below 0.001 µg L^{-1}. PFOA and PFOS levels in the Vaal River in South Africa range from 0.4 – 96.4 ng L^{-1} and 0.4 – 13.23 ng L^{-1}, respectively, while lower concentrations were detected in lake waters, with values of 0.4 – 11.65 ng L^{-1} for PFOA and 0.4 – 2.53 ng L^{-1} for PFOS (Panieri et al., 2022). Based on a study by Yuen et al. (2022), the PFOA concentration in natural water range from 0.11 – 0.97 mg L^{-1} and 0.09 – 0.92 mg L^{-1} in municipal wastewater.

1.2. Research Scope and Objectives

This research focuses on using different engineered municipal sludge-produced biochars for the adsorption of various PFAS present in wastewater. Five engineered biochars were produced using municipal sludge and modified. The biochar was used to remove PFAS from wastewater through adsorption. The biochar evaluated includes non-modified sludge biochar, $FeCl_3$-modified sludge biochar, $ZnCl_2$-modified sludge biochar, KOH-modified sludge biochar, and $FeCl_3$/$ZnCl_2$-modified sludge biochar.

The main objective of this research is to determine the adsorption kinetics, adsorption isotherms, desorption, and regeneration of PFAS using different engineered municipal sludge-produced biochar. These different biochar types were compared to determine the most efficient treatment option to deal with PFAS in pre-UV secondary effluent. Most adsorption experiments reported previously in the literature were performed with deionized water (DI) spiked with PFAS, thus the effect on natural organic matter (NOM) and effluent organic matter (EfOM) were not considered. NOM and EfOM often play a competitive role in the adsorption process (Kothawala et al., 2017; Gagliano et al., 2020).

The objectives of the adsorption study are to:

(1) Evaluate different municipal sludge-engineered biochars (non-modified sludge biochar, $FeCl_3$-modified sludge biochar, $ZnCl_2$-modified sludge biochar, KOH-modified sludge biochar, and $FeCl_3$/$ZnCl_2$-modified sludge biochar).

(2) Determine the effect of adsorbent type, dosage, and the equilibrium time required for the adsorption of PFAS

(3) Understand the adsorption kinetics and adsorption mechanisms for the adsorption of PFAS compounds.

(4) Evaluate the adsorption performance of two PFAS compounds in terms of their distinct structures and characteristics.

(5) Understand the biochar desorption and regeneration for the adsorption of PFAS compounds.

(6) Determine the adsorption capacity of biochar to adsorb PFAS compounds in wastewater.

1.3. Hypotheses

It was hypothesized that a low concentration of modified biochar would be needed to effectively remove PFAS compounds from wastewater and equilibrium would be reached at moderate contact times (within 24 hours).

1.4. Thesis Outline

This thesis has been separated into six sections, which are organized by a logical succession of information required for the study to be completed.

Section 1 discusses the background of the environmental issues related to PFAS persistence in the ground, surface, and treatment waters. Environmental and public health concerns associated

with the presence of PFAS are described as well as regulatory standards for PFOS and PFOA compounds. The first section also documents the research objectives, hypothesis, and thesis organization.

Section 2 is an extensive literature review including adsorption fundamentals: physical and chemical adsorption, critical parameters of adsorption, adsorption kinetics, adsorption isotherms, desorption, and regeneration of adsorbents. PFAS classification and the effect of chain length are discussed. This section also focuses on the potential destruction and separation treatment methods for the removal of PFAS.

Section 3 describes the experimental method and materials used throughout the study including the chemicals, instrumentation, and adsorbent and solute characterization. The experimental setup for evaluation of adsorbent type, adsorbent dosage, adsorption kinetics, adsorption isotherms, desorption, and regeneration are described. It also outlines the linearized equations for kinetic and isotherm models and the significance of high correlation values.

Section 4 evaluates the adsorbent type, adsorbent dosage, adsorption kinetics, adsorption isotherms, desorption, and regeneration. It also entails the results of the adsorbent and solute characterization. The research provided insight into the feasibility of using engineered municipal sludge biochar as an efficient treatment method in wastewater.

Section 5 summarizes the major findings and conclusions drawn from the data presented in section four.

Section 6 highlights recommendations for future work to be completed in this research area and the current limitations.

2. Literature Review

2.1. Adsorption Fundamentals

2.1.1. Physical and Chemical Adsorption

Adsorption uses a suitable interface to accumulate substances from a solution. It is a mass transfer operation, where a constituent in the liquid phase is transferred to the solid phase through diffusion. The adsorbate is the substance being removed and the adsorbent is the material which the adsorbate accumulates onto. It is through chemical or physical adsorption that the adsorbate is bound to the adsorbent.

Physical adsorption is the weak intermolecular forces such as hydrogen bonding, van der Waals Forces, electrostatic forces, and hydrophobic interactions that occur between the adsorbate and the adsorbent. The adsorption sites are assumed to be non-specific, so the adsorbate is not attached to a singular site of the adsorbent, meaning either monolayer or multiplayer adsorption may occur (Tchobanoglous et al., 2014). Due to the low associated heat of physical adsorption, it is usually a reversible adsorption process.

Chemical adsorption or chemisorption occurs when a chemical bond such as a covalent bond or ionic bond forms between the adsorbate and adsorbent. The adsorption is assumed to occur in specific sites allowing for monolayer adsorption to occur. This process is not favorable as this process is considered irreversible adsorption (Tchobanoglous et al., 2014).

There is also the possibility of co-occurrence of physical and chemical adsorption as several different adsorption processes can occur during wastewater treatment. The dominant adsorption process will depend on the type of adsorbate and adsorbent, wastewater characteristics, and other factors (Vo et al., 2021).

Hydrophobic and electrostatic interactions are considered the dominant mechanisms that govern PFAS adsorption for many adsorbent materials (Gagliano et al., 2020; Inyang & Dickenson, 2017; Yu et al., 2009). Hydrogen bonding and covalent bonding also play an important role in the adsorption of PFAS. PFAS chemical and physical properties including surface functional groups, polarity, and porosity are considered the main factors affecting PFAS adsorption efficiency.

2.1.2. Parameters Affecting Adsorption of PFAS

The adsorption efficiency of PFAS onto the adsorbent depends on operational parameters such as initial PFAS concentration, adsorbent type, and adsorbent dosage. It is important to optimize the adsorbent dose, as an insignificant amount of adsorbent will not maximize PFAS removal. However, exceeding the optimal adsorbent dose can cause aggregation issues in the solution reducing the removal efficiency. Aggregation issues reduce the number of available sites for PFAS to attach while aiding in the promotion of desorption (Militoa et al., 2021; Gagliano et al., 2020; Momina et al., 2018). The PFAS initial concentration in an adsorption study is important to evaluate the potential removal in municipal and industrial applications.

The most important physical properties for biochar adsorption include surface area and porous properties. There are three pore size classifications, micropores (<2 nm), mesopores (2–50 nm), and macropores (>50 nm) based on the International Union of Pure and Applied Chemistry (IUPAC) (Zdravkov et al., 2007). Using the properties of the adsorbent (molecule size) and the adsorbate (pore size/volume, and surface area), the adsorption capacity can be predicted. An increase in adsorption capacity can be observed when the mesopore volume is increased, as the micropores can be reached and larger contaminant molecules can be adsorbed (Tchobanoglous et

al., 2014). The PFAS chain length is the dominant structural feature influencing adsorption (Higgins & Luthy, 2006).

Two equations are commonly used to evaluate adsorption data: the removal rate (Eq. 2.1) and the adsorption capacity (Eq. 2.2). Where q_t is the adsorption capacity at time *t* (mg g^{-1}), C_0 is the pollutant concentration at time 0 (mg L^{-1}), C_t is the pollutant concentration at time *t* (mg L^{-1}), *m* is the mass of adsorbent material (g), and *V* is the volume of the solution (L). The removal rate determines how much of the pollutant was removed from the initial solution. Showing the efficiency of adsorbate adsorbed onto the adsorbent. The adsorption capacity depicts the amount of pollutant removed by the adsorbent.

$$Removal\ (\%) = \frac{(C_0 - C_t)}{C_0} \times 100\% \qquad \text{(Eq. 2.1)}$$

$$q_t = \frac{(C_0 - C_t)}{m}\ V \qquad \text{(Eq. 2.2)}$$

2.1.3. Adsorption Kinetics

The kinetics of adsorption determines how quickly an adsorbate attaches to the adsorbent surface. The adsorption kinetics are evaluated by the concentration of adsorbate at increasing time intervals until equilibrium is reached, known as the equilibrium time. Based on Worch (2012), the adsorption process can be characterized by four consecutive steps: (1) The adsorbate is transferred from the liquid phase to the hydrodynamic boundary layer located around the adsorbent particle. (2) Film or external diffusion occurs when the adsorbate is transported through the boundary layer onto the surface of the absorbent. (3) Interparticle diffusion takes place as the adsorbent molecule is transferred into the interior of the adsorbent particle. (4) Equilibrium is the final step as energetic interaction occurs between the adsorbate molecule and the final adsorption sites. The first and fourth steps are thought to be very fast and steps two and three are the rate-limiting steps.

The adsorption kinetics for PFOS and PFOA compounds were analyzed using four common linear kinetic models including pseudo-first order (PFO), pseudo-second order (PSO), Elovich, and interparticle diffusion (IPD) (Weber and Morris). The pseudo-first order (PFO) was created by Lagergren in 1898 describing the rate of change of solute with time is directly proportional to the difference in the adsorption equilibrium capacity and the amount adsorbed. The PFO kinetic model has been widely used to describe adsorption kinetic for both liquid (DI and WW) and solid (soil) systems (Simonin, 2016). The PSO kinetic model suggests the adsorption capacity is proportional to the number of active sites on the adsorbent (Inyang & Dickenson, 2017; Jang et al., 2018). Based on the PFO and PSO kinetic parameters the adsorption rate of various PFAS compounds can be compared providing insight into the role different properties play on adsorption.

The Elovich model originally developed by Turner in 1975 describes the chemical adsorption of gases on solid but was further refined to suitably describe systems with heterogeneous adsorbent surfaces (Ho et al., 2017). It is now commonly used to describe the adsorption of pollutants from aqueous solutions (Inyang & Dickenson, 2017; Guo et al., 2017). The Elovich model assumes that the adsorbent surface is energetically heterogeneous and indicates important interactions between the pollutant and the adsorbent (Inyang & Dickenson, 2017; Guo et al., 2017; Ho et al., 2017; Jang et al., 2018).

The IPD model was used to evaluate the diffusion mechanism during the adsorption process. There are four steps of adsorption (bulk diffusion, film/external diffusion, pore diffusion, and equilibrium steps) are presented as four linear plots. IPD models with multiple mass transfer processes other than just intraparticle diffusion may be playing an important role in the adsorption process. If the IPD model does not pass through the origin when fitted to experimental data, the role of bulk, film, and pore diffusion must be taken into consideration as interparticle diffusion is

not the only rate-limiting mass transfer process (Song et al., 2021; Benally et al., 2019). Among all the diffusion regions, pore diffusion requires the longest time and has the lowest rate constant. As the adsorbate must diffuse through the bulk and film layers before pore diffusion occurs.

The suitability of a kinetic model for experimental data is evaluated based on the correlation coefficient (R^2) provided by the fitting of a linear plot to the data, in which the highest R^2 is favorable. Aiding in the determination of the most accurate kinetic parameters for comparing multiple PFAS compound adsorption behaviours.

Four equations are commonly used to evaluate adsorption data: PFO (Eq. 2.3), PSO (Eq. 2.4), Elovich (Eq. 2.5), and IPD (Eq. 2.6). Where q_e is the adsorption capacity at equilibrium (mg g^{-1}), q_t is the adsorption capacity at time t (mg g^{-1}), K_{PFO} is the pseudo-first order rate constant (h^{-1}), K_{PSO} is the pseudo-second order rate constant (h^{-1}), α is the initial adsorption rate (mg g^{-1} min^{-1}), β is the constant related to the extent of surface coverage and activation energy (g mg^{-1}), k_i is the intraparticle diffusion constant (mg g^{-1} $min^{-0.5}$), and c_i is the thickness of the boundary layer.

$$\ln(q_e - q_t) = \ln q_e - K_{PFO} t \quad \text{(Eq. 2.3)}$$

$$\frac{t}{q_t} = \frac{1}{K_{PSO} q_e^2} + \frac{t}{q_e} \quad \text{(Eq. 2.4)}$$

$$q_t = \frac{1}{\beta} \ln(\alpha\beta) + \frac{1}{\beta} \ln(t) \quad \text{(Eq. 2.5)}$$

$$q_t = k_i t^{0.5} + c_i \quad \text{(Eq. 2.6)}$$

2.1.4. Adsorption Isotherms

Adsorption isotherms depict the relationship between the adsorbate in the liquid phase and the amount of adsorbate adsorbed to the surface of the adsorbent at equilibrium. The adsorption equilibrium is a critical component in determining not only the adsorption isotherms but in understanding the adsorption mechanisms as well. The adsorption equilibrium is described as the

point when the adsorbate adsorbed by the adsorbent is at a maximum and no more adsorbates can be adsorbed. Adsorption isotherms are important for the evaluation of adsorbate-adsorbent interaction and adsorption capacity.

The Langmuir (1918) and Freundlich (1906) models are commonly used to describe adsorption isotherms. The Langmuir model (Eq. 2.7) states that adsorption occurs only on specific sites and assumes the following: (1) there are a fixed number of accessible sites available on the adsorbent surface with the same energy, (2) adsorption occurs in monolayer so, once an adsorbent site is occupied adsorption cannot overlap (Yu et al., 2009; Ochoa-Herrera & Sierra-Alvarez, 2008). So, there are a limited amount of adsorption sites, and they are homogeneous. Whereas it is assumed that the adsorbent surface is heterogeneous in the Freundlich model (Senevirathna et al., 2010; Umpleby et al., 2001). In the Freundlich model, it is also assumed that adsorption occurs in multilayers, meaning more than one adsorbate molecule can attach to a single site and they have different energies (Umpleby et al., 2001).

Two equations are commonly used to evaluate adsorption data: Langmuir (Eq. 2.7), and Freundlich (Eq. 2.8). Where q_{max} is the maximum adsorption capacity (mg g^{-1}), b_L is Langmuir affinity constant (L mg^{-1}), K_f is Freundlich adsorption coefficient, and n_f is Freundlich heterogeneity parameter.

$$\frac{C_e}{q_e} = \frac{1}{b_L\, q_{max}} + \frac{1}{q_{max}} C_e \qquad \text{(Eq. 2.7)}$$

$$\log q_e = \log K_f + \frac{1}{n_f} \log C_e \qquad \text{(Eq. 2.8)}$$

2.1.5. Potential of PFAS leaching from spent adsorbent

The purpose of the desorption experiments is to detect if the PFAS compound adsorbed is leaching from the biochar when in contact with wastewater for an extended period of time. The

occurrence of desorption increases as the PFAS compounds' chain length decreases, the shorter the chain length, the higher the rate of desorption (Yadav et al., 2022). Assessing the desorption provides insight into the partitioning of the PFAS compounds from the adsorbent. Based on the literature PFOA has a higher desorption rate than PFOS showing 41.6% desorption compared to 11.1% desorption (Askeland et al., 2020).

2.1.6. Regeneration of spent adsorbent

The economic feasibility often depends on the regeneration and reactivation of the biochar once the adsorption capacity is reached. The operating time of an adsorption unit is limited by the capacity of the adsorbent. Regeneration describes the process of recovering the adsorption capacity of the spent material. Through regeneration experiments, the adsorption efficiency of used/spent adsorbent can be determined (Gagliano et al., 2020). Several different methods can be used to regenerate the adsorbent although little research has been conducted in the regeneration of spent adsorbent for PFOS and PFOA adsorption. Chemical regeneration is achieved through the desorption of a compound using a solvent, whereas thermal regeneration employs high temperatures to break the bonds between the adsorbent and the adsorbate. Thermal regeneration is favorable as the chemical regeneration solvent must be further treated to dispose of the PFOS and PFOA compounds now present. As stated in section 2.3 PFAS potential treatment, the feedstock and preparation of the material will affect the regeneration characteristics (Guo et al, 2018; Elanchezhiyan et al., 2021). The thermal regeneration capacity depends on the temperature and time used to recover the adsorption capacity (Sörengård et al., 2020; Momina, 2018). Based on the current literature investigation of regeneration, between 1 and 5 cycles are used for a comprehensive evaluation (Gagliano et al., 2020; Chen et al., 2017). The adsorption capacity of the biochar is expected to decrease after each regeneration cycle as some PFAS fragments will

remain on the adsorbent surface. When full desorption of the PFAS compound is not achieved during regeneration, there are fewer active sites available for the PFAS compounds to attach.

2.2. Effect of Chain Length on Adsorption

Per-and polyfluoroalkyl substances (PFAS) refer to a large group of anthropogenic aliphatic compounds. PFAS can be distinguished based on their terminal functional groups such as perfluorocarboxylic acids (PFCAs) and perfluoroalkyl sulfonates (PFSAs). PFAS subgroups can be distinguished based on their carbon chain length. As described by the Organization for Economic Cooperation and Development (OECD), long-chain compounds refer to PFCAs with eight or more carbons and PFSAs with six or more carbons. Short-chain compounds refer to PFCAs with seven or fewer carbons and PFSAs with five or fewer carbons (Chen et al., 2017; Zhao et al., 2016). PFAS bioaccumulation and biomagnification increase as the chain length increases. PFSAs have a higher tendency to bioaccumulate than PFCAs with the same chain length due to their high solubility. With increasing carbon-chain length and replacement of hydrogen by fluorine, PFAS become more chemically inert. However, the water solubility decreases as the chain length increases (Murruy et al., 2021; Gagliano et al., 2020). Based on the octanol/water partition coefficients (K_{ow}), PFAS become more lipophilic as the chain-length increases.

PFOS and PFOA have the same perfluorocarbon chain length, containing eight carbon molecules. PFOS and PFBS are similar in structure as they have the same sulphonic group. They differ as PFBS have a shorter C-F chain length containing six carbon molecules. The hydrophobicity of a PFAS increases as the chain length of the compound increases.

2.3. Potential Treatment of PFAS

PFAS has been shown to be toxic, persistent, and bioaccumulative in the environment. The fluorine-carbon bond is one of the strongest known in nature. As a result, PFAS are very resistant to many different treatment options. Typically, long-chain PFAS such as PFOS and PFOA tend to accumulate in sludge while short-chain PFAS such as PFBS are detected in wastewater treatment plants (WWTPs) and drinking water treatment plants (DWTPs) effluent (Dalahmeh et al., 2019; Zhao et al., 2016).

Various treatment options have been applied to remove PFAS from these systems and the environment. These different technologies can be described by two categories, destruction, and separation. The destruction technologies being studied include photochemical, ultraviolet radiation, electrochemical oxidation, sono-chemical treatment, and plasma treatment (Dai et al., 2019; Kucharzyk et al., 2017). Destruction technologies are tasked with breaking down contaminants (PFAS) into less toxic products (fluoride).

Advanced oxidation processes (AOPs) have demonstrated effectiveness in degrading PFOS and PFOA, this includes photolysis, photochemical oxidation, photocatalysis, and electrochemical oxidation technology. Direct photolysis uses UV radiation to break apart C-F bonds in PFAS, however, only partial degradation has been achieved (Dalahmeh et al., 2019; Guo et al., 2018). Indirect photolysis, such as photochemical oxidation, uses a light source (UV, solar) and the generation of highly reactive radicals such as hydroxyl radical (•OH), superoxide radical ($O_2^{\bullet-}$), hydroperoxyl radical (HO_2^-), and sulfate radical ($SO_4^{\bullet-}$) to degrade PFAS (Yang et al., 2020; Trojanowicz et al., 2018; Schröder & Meesters, 2005). Hydrogen peroxide (H_2O_2), ozone (O_3), and peroxymonosulfate (HSO_5^-) are commonly used to produce these radicals. Photocatalytic oxidation involves a light source, an oxidant, and a catalyst. A variety of catalysts can be used such

as ferrous ion (Fe (II)), hydrogen peroxide (H_2O_2), titanium oxide (TiO_2), tin oxide (SnO_2), magnesium dioxide (MgO_2), indium (III) oxide (In_2O_3), and gallium (III) oxide (β-Ga_2O_3) (Yuan et al., 2022; Xu et al., 2017). The removal/degradation results for a combination of photocatalytic oxidation, catalyst, and peroxymonosulfate are displayed in Appendix: AOP Data.

Electrochemical oxidation processes (EOPs) utilize electricity instead of heat or chemicals to break C-F bonds. However, the use of electrochemical oxidation forms toxic by-products such as hydrogen, fluorine, and chlorine gas, which may require additional treatment (Liu et al., 2021).

Sono-chemical oxidation degrades PFAS by applying high temperatures and pressures through the acoustic cavitation process. The sound waves collapse the bubbles during the pyrolytic reaction of the PFAS compounds at the vapour/water interface (Yadav et al., 2021; Guo et al., 2018; Kucharzyk et al., 2017).

Plasma technology has grown more popular in recent decades as the process is not affected by other contaminants in the degradation of PFAS. Plasma is formed when heat or energy is added to ionize an electrically charged gas (most often argon) (Liu et al., 2021; Trojanowicz et al., 2018). Plasma is categorized into two types, thermal and non-thermal. Non-thermal plasma is preferable in water treatment applications as both highly reactive and reductive species are produced. This is achieved when an electrical discharge is generated between a high voltage and a grounded electrode (Liu et al., 2021; Yadav et al., 2021; Gagliano et al., 2020). Sequential defluorination has been observed with most degradation processes, breaking down long-chain PFAS into short-chain PFAS. Although, many of these destruction methods have been found to be insufficient as the high energy demands, associated capital, operation, and maintenance costs are determined to be uneconomical for scaling up. Further investigation is still ongoing for destructive technologies; however, adsorption processes still have higher performance efficiency for the removal of PFAS.

Separation technologies include adsorption, membrane filtration, and coagulation-flocculation. The physicochemical properties of PFOS and PFOA have rendered many conventional treatment technologies such as biological degradation, oxidation, reduction, and coagulation followed by sedimentation/filtration ineffective (Yadav et al., 2022; Gagliano et al., 2020). However, common treatment options such as powdered activated carbon (PAC), granular activated carbon (GAC), ion exchange resins, reverse osmosis (RO), and nanofiltration (NF), have been identified for removing PFAS (Banks et al., 2020). Membrane technologies have the capability to be the most effective and efficient at removing PFAS, long-chain, and short-chain. However, they are costly to operate, they produce residual PFAS concentrate, and are not a viable solution for developing countries (Yadav et al., 2022; Hang et al., 2015). Adsorption is an established technology for the removal of PFAS and provides a more economical performance compared to high-pressure membrane processes.

Adsorption onto activated carbon (AC) is the currently accepted remediation technology for groundwater impacted by PFOS and PFOA. AC has been investigated and implemented in full-scale treatment operations to remove organic pollutants from drinking water and wastewater. However, the use of AC is usually used as a polishing treatment after completing normal biological treatment. Where the AC is used to remove any remaining dissolved organic matter (Tchobanoglous et al., 2014). GAC consistently removes PFOS/PFOA with an efficiency of more than 90%, with PAC reported to have a higher removal efficiency than GAC with a shorter equilibrium time as seen in Tables 2.3 to 2.5. This is due to PAC increased surface area compared to GAC. It is also reported that high temperatures of 800 °C are necessary to destroy the PFOS and PFOA adsorbed to GAC/PAC (Gagliano et al., 2020; Tchobanoglous et al., 2014). There is concern for the potential for smaller chain PFAS (four or six carbons) like PFB to break through the

PAC/GAC media within shorter timeframes than their longer chain equivalents. A variety of materials has been tested in recent years to produce AC with enlarged pores and increased adsorption surface.

Biochar has been extensively researched for the removal of metals, organic pollutants, and nutrients from wastewater (WW) and has the potential to effectively remove PFAS. Adsorbents such as biochar have the potential to reduce toxicity during the WW treatment process. Biochar is a carbon-rich solid created through the pyrolysis of biomass such as crop and forest residues, bamboo, wood chips, algae, manure, and organic municipal solid wastes (sludge) (Militao et al., 2021; Xiang et al., 2020). The contaminants present in the sludge feedstock are removed during the biochar production process. The presence of gas and stream during the pyrolysis process develops the porous structure of the material, creating a large internal surface area (Tchobanoglous et al., 2014). The effectiveness of a biochar is dependent on the type of feedstock and thermochemical condition under which it is created. This also affects the pore-size distribution and regeneration characteristics. Hydrophobic interaction is the driving mechanism for biochar adsorption of PFAS. Engineered biochar modified with metal-containing functional group have shown increased performance, enhancing electrostatic interaction and ion exchange mechanisms (Vo et al., 2021; Militao et al., 2021; Hassan et al., 2020). Biochar is a less expensive alternative to AC as production is less energy intensive and biochar is often created from a waste product such as sludge, agricultural residue, and plant/animal biomass (Tchobanoglous et al., 2014).

Table 2.1: Summary of PFOS adsorption technologies.

Adsorbent Type	Adsorbent Dose (mg L^{-1})	Compound Dose (mg L^{-1})	Adsorption condition		Adsorption Capacity (mg g^{-1})	References
GAC Calgon	1000	15-150	Media	Di	236.4	
			pH	7.2		

			Temperature	30°C		Ochoa-Herrera and Sierra-Alvarez, 2008)
GAC	100	20-300	Media pH Temperature rpm Contact time	Di 5 25°C 140 48 hrs	390.1	Chen et al., 2011
PAC	100-130	20-300	Media pH Temperature rpm Contact time	DI 5 25°C 150 12 hrs	520.13	Yu et al., 2009; Chen et al., 2011
SWNT	200-1200	1-500	Media pH Temperature rmp Contact time	DI 7 25°C 150 2 hrs	712	Chen et al., 2011
CdB (T: 200-700C)	200	5-10	Media pH Temperature rpm Contact time	DI 7 25°C 150 48 hrs	135.53-169.90	Guo et al., 2017
MWNT	50	0.05 - 10	Media pH Temperature	DI 6.5 25°C	5.00	Li et al., 2017
Chitosan (MIP)	100	20-550	Media pH Temperature Contact time	DI 5 25°C 36 hrs	1455.52	Yu et al., 2009
Chitosan (NIP)	100	20-550	Media pH Temperature Contact time	DI 5 25°C 36 hrs	1203.51	Yu et al., 2009
MIP-CMS			Media pH Temperature rmp Contact time	DI 3 25°C 150 2 hrs	75.99	Guo et al., 2018
NIP-CMS			Media pH Temperature rmp Contact time	DI 3 25°C 150 2 hrs	43.94	Guo et al., 2018
13X zeolite	1000	15-150	Media pH Temperature	DI 7.2 30°C	12	Ochoa-Herrera and Sierra-Alvarez, 2008)

NaY80 zeolite	1000	15-150	Media pH Temperature	DI 7.2 30°C	114.7	Ochoa-Herrera and Sierra-Alvarez, 2008)
WSB	200-1200	1-500	Media pH Temperature Rpm Contact time	DI 7 25°C 150 384 hrs	91.6	Chen et al., 2011
MSB	200-1200	1-500	Media pH Temperature rpm Contact time	DI 7 25°C 150 384 hrs	164	Chen et al., 2011
QCB	100	95-460	Media pH Temperature rpm	DI 5 25°C 150	1650.43	Deng et al., 2012

Table 2.2: Summary of PFOA adsorption technologies.

Adsorbent Type	Adsorbent Dose (mg L^{-1})	Compound Dose (mg L^{-1})	Adsorption condition		Adsorption Capacity (mg g^{-1})	References
AC Calgon	1000	15-150	Media pH Temperature	Di 7.2 30°C	112	Ochoa-Herrera and Sierra-Alvarez, 2008)
AC Calgon	100	20-250	Media Temperature rpm Contact time	DI 25°C 150 168 hrs	194.6	Yu et al., 2009
GAC	100	20-250	Media Temperature rpm Contact time	DI 25°C 150 168 hrs	277.42	Yu et al., 2009
PAC	100	20-250	Media Temperature rpm Contact time	DI 25°C 150 12 hrs	161.48	Yu et al., 2009
SWNT	250	3.8-259	Media pH Temperature Contact time	DI 6 25°C 3 d	78.67	Wang et al., 2016
MWNT	100	0.5-10	Media	DI	2.69	Li et al., 2011

			pH	6.5		
			Temperature	25°C		
BdAC	120	200	Media	WW	372.6	Du et al., 2015
			pH	4		
			rpm	170		
			Temperature	25°C		
			Contact time	48 hrs		
HWC			Media	WW	31.7	Inyang & Dickenson, 2017
			pH	7.2		
			Temperature	22°C		
			Contact time	30 d		
PWC			Media	WW	27.7	Inyang & Dickenson, 2017
			pH	7.2		
			Temperature	22°C		
			Contact time	30 d		
QCB	100	78.67-381	Media	DI	1283.61	Deng et al., 2012
			pH	5		
			Temperature	25°C		
			rpm	150		

Table 2.3: Summary of PFB adsorption technologies.

Adsorbent Type	Adsorbent Dose (mg L^{-1})	Compound Dose (mg L^{-1})	Adsorption condition		Adsorption Capacity (mg g^{-1})	References
AC Calgon	250	6-247	Media	DI	51.01	Wang et al., 2016
			pH	6		
			Temperature	25°C		
			Contact time	3 d		
GAC Calgon	1000	15-150	Media	DI	98.7	Ochoa-Herrera and Sierra-Alvarez, 2008)
			pH	7.2°C		
			Temperature	25°C		

3. Experimental Method and Materials

3.1. Effluent, Sludge, and Chemicals

Pre-UV secondary effluent (SE) and the sludge were collected from a local wastewater treatment plant (Edmonton, Alberta, Canada) and stored at 4°C in a cold room. The sludge used

in this study was a mixture of primary and secondary sludge collected at the end of the anaerobic digester of biosolids (solids handing).

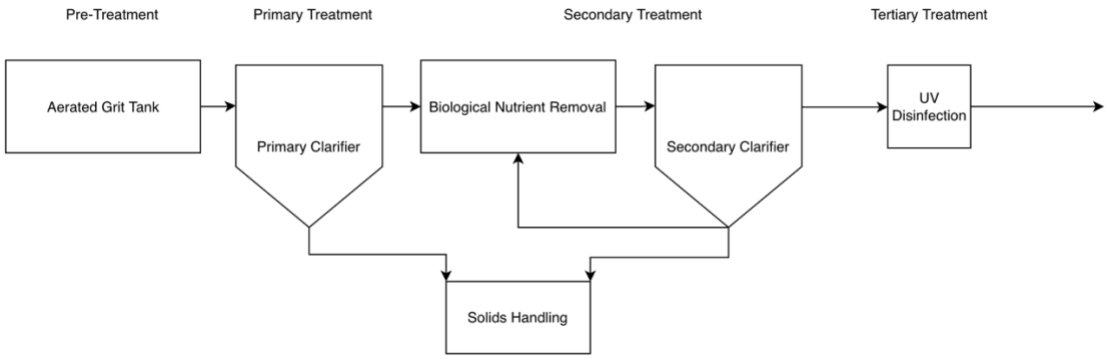

Figure 3.1: Wastewater treatment plant flowchart.

Model compounds PFOS (98%), PFOA (96%), and PFBS (97%) were purchased from Sigma Aldrich (Germany). Stock solutions for PFOS, PFOA, and PFBS were prepared at 25 mg L^{-1} using pre-UV secondary effluent wastewater, kept in a borosilicate dark glass bottle, and stored at 4°C in the dark. Other chemicals utilized were sodium chloride (NaCl), ferric chloride hexahydrate ($FeCl_3 \cdot 6H_2O$), zinc chloride anhydrous (98%) ($ZnCl_2$), potassium hydroxide (KOH), hydrochloric acid (37%) (HCl), sodium hydroxide (NaOH) (95%), and hydrochloric acid (HCl) 37% were purchased from Fisher Scientific (New Jersey, USA) and all analytical grade (ACS). Pure nitrogen gas (N_2) (99%) was used at various stages during this study, such as biochar production, regeneration, and point of zero charge determination. The characteristics of the PFAS model compounds used throughout this study are displayed in Table 3.1. Ultra-pure water (Synergy UV, MilliporeSigma, USA) was used in the dilution of NaCl, $FeCl_3 \cdot 6H_2O$, and HCl.

Table 3.1: PFAS characteristics.

Compound	Perfluorooctane sulfonic acid (PFOS)	Perfluorooctanoic acid (PFOA)	Perfluorobutane sulfonic acid (PFBS)	Reference

Acronym	PFOS	PFOA	PFBS	(U.S National Library of Medicine, 2022)
Formula	$C_8F_{17}SO_3H$	$C8HF_{15}O_2$	$C_4HF_9O_3S$	
Chain Length	C8	C8	C4	
MW (g mol^{-1})	500.13	414.07	300.10	
Log K_{ow}	4.49	4.81	1.82	
Solubility in water (mg L^{-1}) @ 25 °C	550	3300	344	
Vapour Pressure (mm Hg)	6×10^{-3}	3.16×10^{-2}	2.68×10^{-2}	
pKa	-3.27	0.50	-3.57	
Density (g/cm^3)	1.84	1.79	1.85	

3.2. Biochar Production

The municipal sludge was dried in an oven (Fisherbrand™ Isotemp™, Fisher Scientific, USA) at 105°C for 24 h, crushed using a ball milling process (MM400, Retsch, Germany) at 30 s^{-1} frequency for 50 sec operation time to obtain a homogeneous powder, and stored in air-tight glass containers.

The non-modified and modified biochars (Figure 3.2) were produced by pyrolysis at 600°C under oxygen-free conditions (supplying 99% pure N_2 at 2 L min^{-1}) in a muffle furnace (Lindberg Blue M, Thermo Scientific™, USA) at heating rate of 10°C min^{-1} and residence time at 600°C of 2 h. Oxygen-free conditions were maintained for cooling down time.

The non-modified biochar (i.e., pristine biochar) was produced from municipal sludge by pyrolysis at 600°C and no further treatment.

Modified biochars produced from municipal sludge were:

(1) $FeCl_3$-modified biochar using solution containing 1.4 M $FeCl_3$,

(2) $ZnCl_2$-modified biochar using solution containing 2 M $ZnCl_2$,

(3) KOH-modified biochar using solution containing 2 M KOH, and

(4) $FeCl_3$/$ZnCl_2$-modified biochar using solution containing 2 M $ZnCl_2$ and 1.4 M $FeCl_3$.

Modified biochars were produced by mixing 2 g of dried municipal sludge and 40 mL of respective modification solution at 400 rpm for 24 h, followed by drying at 105°C for 24 h to ensure that all water has evaporated. Pyrolysis of the dried mixture was done at 600°C. After cooling down, it was removed from the muffle furnace and 20 mL 1 M HCl was added to the biochar and allowed to soak for 2 h. Once the soaking was complete, the contents were transferred to the vacuum filtration system and washed using deionized water until the pH of the filtrate was between 6 and 8. Then, the washed modified biochar was dried in the oven at 105°C for 24 h. After the $FeCl_3$-modified biochar was fully dried, it was crushed using an agate mortar and pestle (Fisherbrand™, Fisher Scientific, USA) and stored in air-tight glass vials.

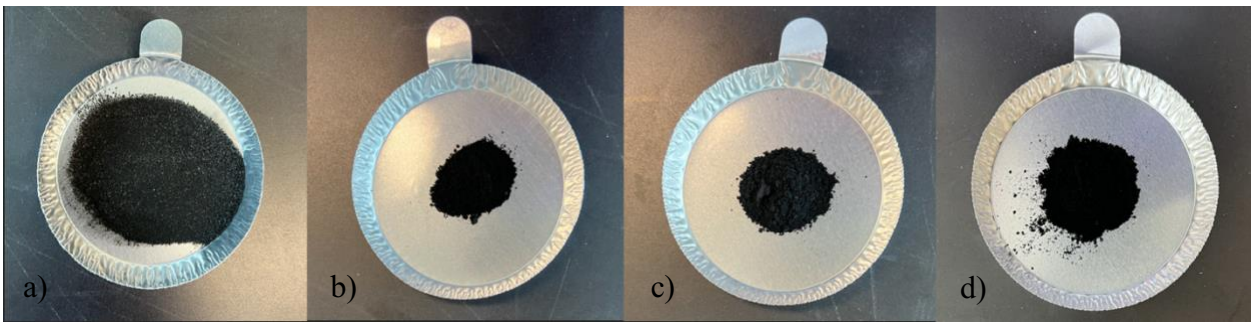

Figure 3.2: Engineered sludge biochar from municipal waste. a) Non-modified biochar, b) $FeCl_3$-modified biochar, c) KOH-modified biochar, and d) $FeCl_3$/$ZnCl_2$-modified biochar.

3.3. Characterization of Sludge and Biochars

3.3.1. Surface Area and Porous Properties

The surface area and porous properties of the biochar were determined using a surface area analyzer (Autosorb iQ, Quantachrome, USA). The material biochar was outgassed before N_2 adsorption at 120°C for 4 h. The surface area and porous properties were calculated using the Brunauer-Emmett-Teller (BET) method.

3.3.2. Point of Zero Charge

The method for pH_{pzc} was previously described in detail by Nguyen et al. (2022) and Jang et al. (2018). Briefly, the pH of 0.01 M NaCl solution was adjusted using 0.1 M HCl or 0.1 M NaOH according to the pH range of 2 – 10. Once the pH ($pH_{initial}$) was adjusted, 5 mg of biochar were added to falcon tubes containing of 25 mL of 0.01 M NaCl with adjusted pH. The tube was filled with N_2 gas to minimize the CO_2 effect in the head space of bottle. The falcon tubes were sealed and placed on a platform shaker, providing continuous agitation at 150 rpm for 48 h. After 48 h, the equilibrium pH (pH_{final}) will be recorded. For each container, ΔpH was calculated using Eq. 3.1. ΔpH vs. pH_{inital} was plotted and the pH_{pzc} was indicated by the pH at ΔpH = 0.

$$\Delta pH = pH_{initial} - pH_{final} \qquad \text{Eq. 3.1}$$

3.3.3. Surface Functional Groups

Fourier transform infrared (FTIR) spectroscopy (Nicolet™ iS50 FT-IR Spectrometer, Thermo Scientific, USA) analysis was performed to assess the materials between 400 and 4000 cm^{-1} at 4 cm^{-1} resolution.

3.3.4. Crystallographic Structures

Phase identification of the crystal structure properties was determined using X-ray diffractometer (XRD Ultima IV, Rigaku, Japan) using a scanning rate of 2° min^{-1} between 5 and 90° 2θ angles and a cobalt tube at 38 kV and 38 mA.

3.3.5. Elemental Distribution

The chemical state and binding energies of the sludge, and pre and post adsorption biochars were studied using an x-ray photoelectron spectroscopy equipped with monochromatic Al Kα source (hν = 1486.6 eV) at a power of 210 W (XPS Kratos AXIS Ultra, Shimadzu, USA).

3.3.6. Thermostability and Proximate Analysis

The thermostability of the biochar was determined by heating the biochar to 900°C from room temperature using a heating rate of 20°C min^{-1} with N_2 as purge gas using a thermogravimetric analyzer (Discovery TGA, TA Instruments, USA) equipped with platinum pan. The moisture, volatile matter, ash, and fixed carbon content by weight loss was also determined based on the method presented by Crombie et al. (2013).

3.3.7. Ultimate Analysis

The elemental composition in terms of carbon (C), nitrogen (N), hydrogen (H), and sulphur (S) concentrations was determined using an elemental analyzer (2400 Series II CHNOS analyzer, PerkinElmer, USA). The elemental oxygen content was estimated by difference (100 – C(%) – H(%) – N(%) – S(%) – Ash(%)) on a dry-mass basis.

3.3.8. Scanning Electron Microscopy (SEM)

The surface morphology of the sludge-produced biochars will be analyzed using a scanning electron microscopy (SEM) (EVO M10, Zeiss, Germany) at 15.0 kV. A magnification of range from 250 x to 10.0 Kx was used.

3.4. Preparation and Characterization of PFAS Spiked Pre-UV Secondary Effluent

All experiments were done using pre-UV secondary effluent as the media. The pre-UV secondary effluent alone or spiked with either PFOS, PFOA or PFBS obtained pre and post experiment were characterized based on chemical oxygen demand (COD), total organic carbon (TOC), phosphorus (PO_4), nitrite (NO_2), and sulfate (SO_4) concentrations. The COD was obtained using a Hach Company (Germany) TNT 822 COD kit with a testing range between 20 – 1500 mg L^{-1}. The TOC was determined using TOC analyzer (TOC-L series, Shimadzu) with a potassium hydrogen phthalate (99%) standard of 50 ppm. Hach Company testing kits TNT 844, TNT 839, and TNT 865 were used to determine the phosphorus (PO_4), nitrite (NO_2), and sulfate (SO_4) concentrations, respectively.

The PFOS and the PFOA concentrations were determined using ultra-performance liquid chromatography-quadrupole time of flight mass spectrometry UPLC-QTOF-MS (Xevo G2-S, Waters). Fitted with a perfluorinated compound (PFC)-free kit, containing a PFC isolator column the UPCL system isolated the background contaminants from the analytes in the sample. The isolator column was inserted between mixer of the binary solvent manager (BSM) and the injector of the sample manager, in the flow path. The electrospray ionization (ESI) source was operated in negative ion mode. The compounds were monitored at 498.93 m/z (PFOS) and 413.92 m/z (PFOA). The chromatographic separations were performed using an ACQUITY UPLC® BEH C18 column (1.7 µm, 2.1 × 50 mm, Waters, USA) with mobile phases of 0.1% formic acid in water (A), and 0.1% formic acid in acetonitrile (B). The elution gradient was 0-0.5 min, 5% B; 0.5-3 min, increased from 5% to 95% B; then returned to the initial condition 95% B at 3.1 min and held for 1 min to equilibrate the column with a flow rate of 0.4 mL/min. The injection volume was 2

µL, and the column temperature was maintained at 40 ˚C. The PFOS and PFOA data was determined using MassLynx (Waters, USA) and was processed using TargetLynx (Waters, USA).

3.5. Adsorption Experiments Using Biochar for PFAS Removal

3.5.1. Instrumentation

An APX-200 analytical balance (Denver Instruments, USA) was used to measure the mass of the biochars. Erlenmeyer flasks containing biochar and spiked pre-UV secondary effluent solution were placed in a platform shaker (New Brunswick™ Innova® 2100 platform shaker, Eppendorf Inc., USA) at an agitation speed of 200 rpm and 20°C. After the appropriate contact time, samples were filtered using a syringe filter PES 0.22 µm and stored in 50 mL falcon tubes. PES filters were used to ensure that the remaining PFOS/PFOA is not removed from the samples before analysis (Chandramouli et al., 2014; Winchell et al., 2021). Samples were stored at 4°C until analysis. Prior to analysis, a 2 mL sample was added to a polypropylene plastic vial. The concentration of the model compound was then determined with a time-of-flight mass spectrometer (UPLC-QTOF-MS, Xevo G2S, Waters, USA).

3.5.2. Effect of Biochar Type

The different biochar types studied include non-modified sludge biochar, $FeCl_3$-modified sludge biochar, $ZnCl_2$-modified sludge biochar, KOH-modified sludge biochar, and $FeCl_3$/$ZnCl_2$-modified sludge biochar. Adsorption experiments were performed to compare the effect of different biochars on the removal of PFAS spiked pre-UV secondary effluent over a 24-hour contact time at pH 6.5. All experiments were completed in duplicate. Batch adsorption testing was performed for each model compound (PFOS or PFOA). Into an Erlenmeyer flask, 30 mL of a 25

mg L^{-1} PFAS solution was added, along with a biochar concentration of 1 g L^{-1} and covered. Each of these flasks was placed in the platform and shaken at 200 rpm for 24 hrs. Blank samples (i.e., biochar added to non-spiked pre-UV secondary effluent) underwent the same adsorption process to determine if any biochar leaching occurred. After the 24-hour contact period, the contents of the flasks were filtered and stored to be analyzed by the UPLC-QTOFMS (Xevo G2S). The concentration of PFAS (25 mg L^{-1}) and adsorbent doses (1 g L^{-1}) were determined based on the literature as summarized in Tables 2.3 to 2.5.

3.5.3. Effect of Adsorbent Dosage Experiments

The effect of the adsorbent dosage was studied by varying the amount of biochar added to a specific volume of PFAS compound for a contact time of 24 h at the effluent pH 6.5. The adsorbent dosages evaluated were 0.01, 0.05, 0.1, 0.5, and 1.0 g L^{-1} for PFOS and 0.25, 0.5, 0.75, 1.0, and 1.25 g L^{-1} for PFOA. All experiments were completed in duplicate. In each experiment, 30 mL of 25 mg L^{-1} PFAS spiked pre-UV secondary effluent was added to an Erlenmeyer flask with a varying $FeCl_2$-modified biochar dose and covered. Then, the optimal dosage was determined for further experiments.

3.5.4. Kinetic Experiments

The adsorption kinetics were determined using different contact times from 15 min to 24 h. Every contact time required a single batch experiment. A 30 mL sample of 25 mg L^{-1} PFAS spiked pre-UV secondary effluent was added to Erlenmeyer flasks containing $FeCl_3$-modified biochar at a concentration determined to be the best adsorbent dosage. The start time and biochar

mass were recorded. Experiments were completed in duplicate. Based on the kinetic experiments, the adsorption equilibrium was determined.

3.5.5. Isotherm Experiments

A specific dosage of modified biochar at decreasing intervals from the determined best adsorbent dosage were added to Erlenmeyer flasks with 30 mL of 25 mg L^{-1} PFAS spiked pre-UV secondary effluent. The flasks were covered and placed into a platform shaker for the contact time determined to be the equilibrium time. Experiments were completed in duplicate.

3.5.6. Desorption Experiments

Desorption experiments were conducted to determine if the PFAS compounds leach from the biochar after adsorption. First, adsorption experiments were performed using 25 mg L^{-1} PFAS spiked pre-UV secondary effluent. Calculated amounts of PFAS spiked pre-UV secondary effluent and biochar (based on the best adsorbent dosage) were added to a 500 mL Erlenmeyer flask and covered. The flasks were placed into a platform shaker at 200 rpm for the determined equilibrium time. The supernatant was separated from the adsorbent using vacuum filtration, the biochar was collected on the glass microfilter membrane. The post-adsorption biochar was then oven-dried at 50°C until completely dry.

Desorption of PFAS compounds from modified biochar was evaluated at 24 h and 7 days of contact times using oven-dried post-adsorption modified biochar at the same concentrations applied in the adsorption experiments (kinetic experiments). The post-adsorption biochar was added to a flask with 30 mL of non-spiked pre-UV secondary effluent and shaken for 24 hr and 7-

day contact time. Every contact time required a single batch experiment. Experiments were performed in duplicate.

3.5.7. Regeneration Experiments

Thermal regeneration uses a stream of nitrogen gas and high temperatures to aid in the release of the volatile organic fluorine from the biochar saturated with PFOS and PFOA. Post-adsorption biochar was collected by first performing adsorption experiments at equilibrium conditions with fresh $FeCl_3$-modified biochar. After adsorption, the post-adsorption biochar was separated from the solution using vacuum filtration. The post-adsorption biochar was collected on the glass microfilter membrane. Then, the post-adsorption biochar was regenerated through pyrolysis at 600°C (same pyrolysis conditions presented in section 3.2: using the muffle furnace in 99% pure N_2 at 2 L min^{-1} environment at a heating rate of 10°C min^{-1} and residence time at 600°C of 2 h). After regeneration, the regenerated biochar was applied in adsorption experiments at equilibrium time using PFAS spiked pre-UV secondary effluent at biochar dosage defined as the optimal adsorbent dosage. Experiments were performed in duplicate. After contact time, the contents of the flasks were filtered using a glass membrane and vacuum filtration system, the biochar was collected. A total of five regeneration cycles were completed for PFOS and PFOA compounds.

4. Results and Discussion

4.1. Characterization of Biochar

4.1.1. Surface Area and Porous Properties

The surface area and porous properties of non-modified biochar and $FeCl_3$-modified biochar are described in Table 4.1. The surface area of the non-modified biochar was determined to be 7.87 m^2 g^{-1} using a surface area analyzer and the BET method. The surface area of $FeCl_3$-modified biochar is 32 times greater than non-modified biochar at 246.97 m^2 g^{-1}. This supports the higher adsorption rate of $FeCl_3$-modified biochar compared to non-modified biochar as well. Increasing the surface area increases the number of available adsorbent sites for the PFOS and PFOA to attach. There is an increase in pore volume from non-modified biochar, 0.04 m^3 g^{-1}, to $FeCl_3$-modified biochar, 0.26 m^3 g^{-1} as well. Again, this increases the adsorption capacity and in turn the removal of PFOS and PFOA from the pre-UV secondary effluent. As depicted by the surface area and porous properties, the $FeCl_3$-modified biochar is a mesoporous material.

Table 4.1: Surface area and porous properties

	Sludge	Non-modified biochar	$FeCl_3$-modified biochar
Total Surface Area (m^2/g)	1.44	7.87	246.97
Micropore Surface Area (m^2/g)	0.00	0.00	53.10
Mesopore Surface Area (m^2/g)	1.44	7.87	193.87
Total Pore Volume (cm^3/g)	0.02	0.04	0.26
Micropore Pore Volume (cm^3/g)	0.00	0.00	0.03
Mesopore Pore Volume (cm^3/g)	0.02	0.04	0.23

4.1.2. Point of Zero Charge

The point of zero charge was determined based on the method described by Nguyen et al. (2022) and Jang et al. (2018). The pH_{pzc} of non-modified biochar was determined (Eq. 3.1) to be 8 which is significantly higher than $FeCl_3$-modified biochar with a pH_{pzc} of 3 (Figure 4.1). At a pH equivalent to the pH_{pzc} electrostatic interaction should be involved in the adsorption process, however, electrostatic repulsion may occur at a pH greater than the defined pH_{pzc} (Chen et al., 2017; Guo et al., 2017). Based on this it is assumed that $FeCl_3$-modified biochar is able to perform regardless of neutral pH allowing it to be a feasible PFAS adsorption solution for municipal wastewater as treatment plants must maintain a pH between the range of 6.5 – 8.5.

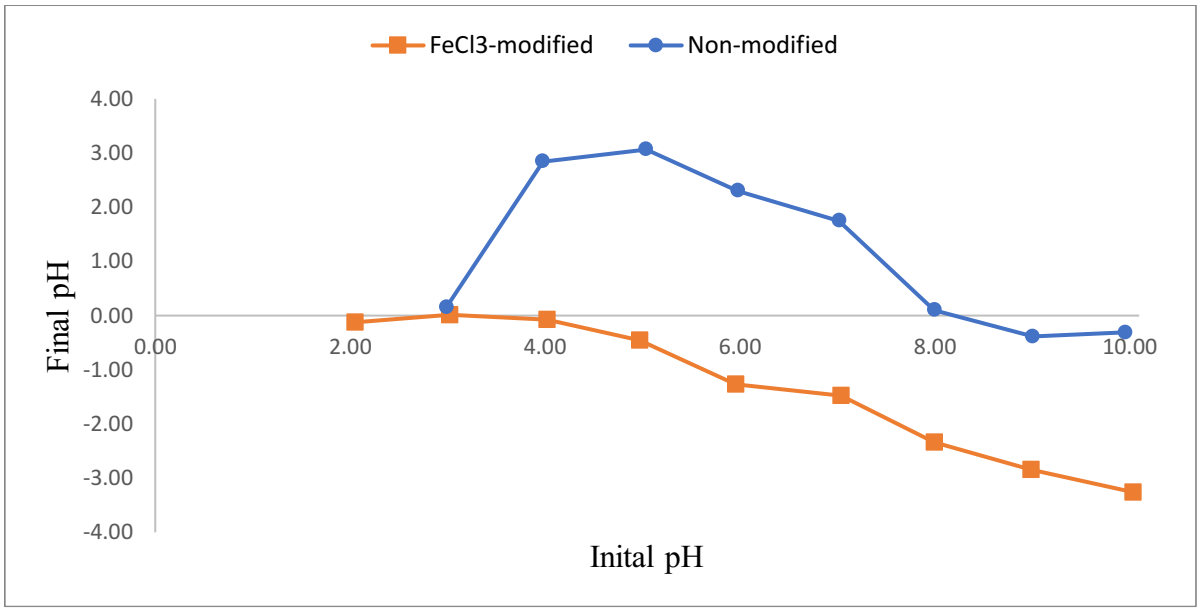

Figure 4.1: Point of zero charge for non-modified biochar and $FeCl_3$-modified biochar.

4.1.3. Scanning Electron Microscopy (SEM)

Based on SEM images for biochar produced using municipal sludge as a feedstock has the potential for greater adsorption when compared to other pyrolyzed biomass feedstocks such as rice husk (Deng et al., 2013). This is due to increased roughness correlating to high surface area and

exposed functional groups (Chia et al., 2012; Song et al., 2021). The roughness of the material surface studied shows $FeCl_3$-modified biochar to be the roughest and municipal sludge to smoothest. This is confirmed by the surface area and porous properties as $FeCl_3$-modified biochar has a surface area 32 greater than non-modified biochar increasing its adsorption capacity. The XRD and SEM results show that the production of $FeCl_3$-modified biochar by the method presented in this work was successful. The production of $FeCl_3$-modified biochar is further supported by the presence of Fe2p displayed in the XPS survey scan.

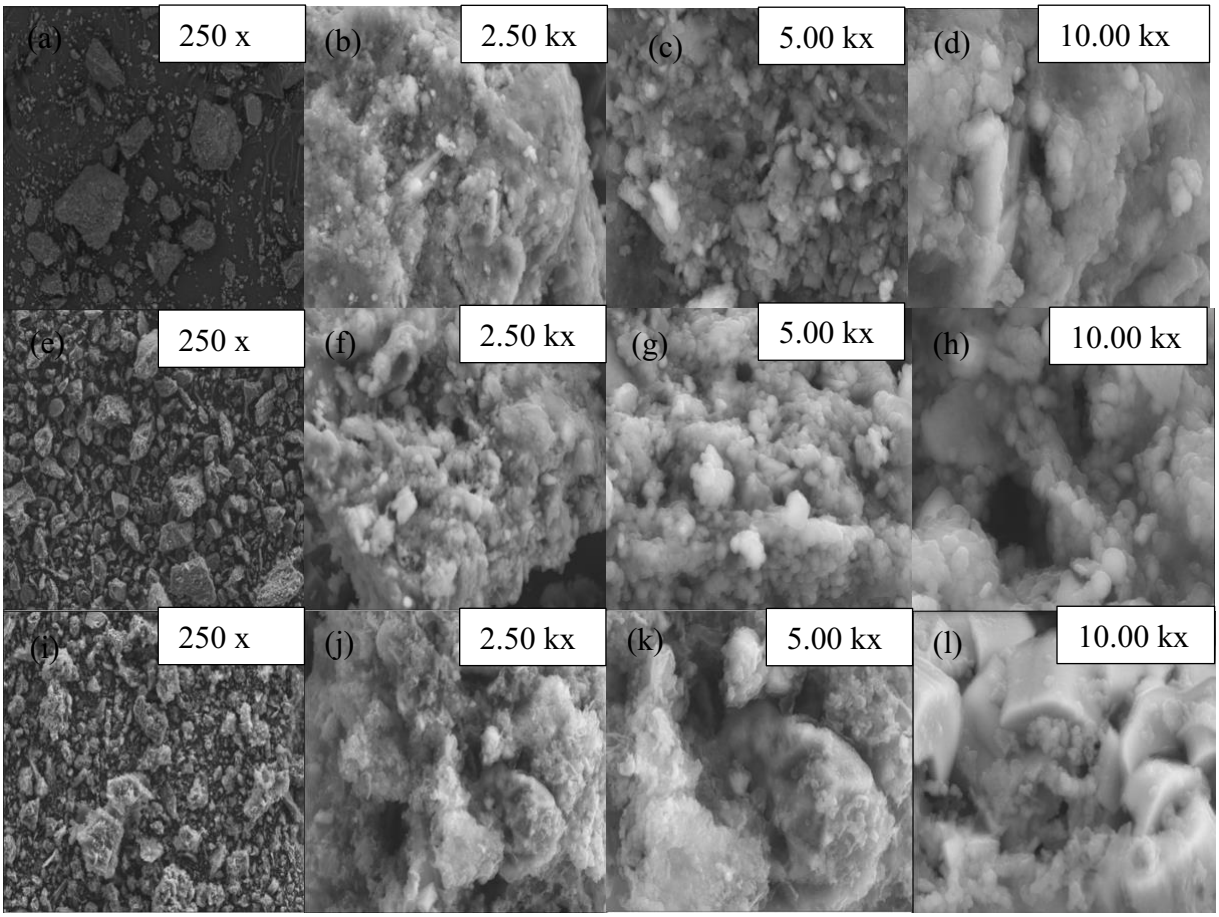

Figure 4.2: SEM images of sludge at (a) 250 x, (b) 2.50 kx, (c) 5.00 kx, and (d) 10.00 kx, non-modified biochar at (e) 250 x, (f) 2.50 kx, (g) 5.00 kx, and (h) 10.00 kx, and $FeCl_3$-modified biochar at (i) 250 x, (j) 2.50kx, (k) 5.00 kx, and (l) 10.00 kx.

4.1.4. Surface Functional Group

The FTIR spectra of the municipal sludge, non-modified biochar, and $FeCl_3$-modified biochar are presented in Figure 4.3. The FTIR spectra has the potential to distinguish subtle differences between biochar samples that would not be observed visually (Chia et al., 2012). FTIR spectra shows the changes of functional groups on the surface of the material when pyrolyzed from sludge into biochar. Dried sludge was analyzed, displaying band lengths of 3405 cm^{-1} (-OH stretching vibrations of hydrogen-bonded hydroxyl groups), 2925 cm^{-1} (asymmetric aliphatic C-H stretching vibrations), 1656 cm^{-1} and 1552 cm^{-1} (aromatic C=C stretching vibrations and C=O stretching vibrations), 1454 cm^{-1} (- COH bending vibration), and 1060 cm^{-1} (carbohydrate C-O stretching vibrations). The peak observed at 3405 cm^{-1} indicates the presence of phenol and alcohol and the peak at 2925 cm^{-1} indicates the presence of alkane groups (Ghodke et al., 2021). The board peak at 1060 cm^{-1} indicates the presence of polysaccharides. Wavelengths below 800 cm^{-1} such as 531 cm^{-1} and 465 cm^{-1} indicate aromatic C-H bending vibrations (CH deformation) (Chia et al., 2012; Liu et al., 2015; Nzediegwu et al., 2021). The FTIR spectra determined for municipal sludge is similarly described in a study of sewage sludge conducted by Ghodke et al. in 2021.

There is a notable increase in baseline adsorption from sludge to the pyrolyzed engineered biochar (non-modified and $FeCl_3$-modified) this could be to carbonization (Liu et al., 2015). The ignition temperatures used in the production of non-modified biochar resulted in two peaks disappearing from 3400-1600 cm^{-1}. The FTIR spectra for non-modified biochar show bands at 1590 cm^{-1} (C=O stretching vibrations), 1013 cm^{-1} (C-O stretching vibrations), 776 cm^{-1}, 693 cm^{-1}, 440 cm^{-1}, and 421 cm^{-1} (C-H bending vibration/ CH deformation). Based on Figure 4.3 it can be observed that the intensity of the peak decreased with the addition of high temperatures for the

band range of 1600-800 cm^{-1}, suggesting ignition loss of -OH and aliphatic C-H content and decrease of C=O and C-O content at 600 °C. A reduction in carbon, hydrogen, and oxygen is seen in the ultimate analysis as well.

The FTIR spectra for $FeCl_3$-modified biochar displays aromatic C-H stretching at 3066 cm^{-1}, expressing the presence of lignin residue as a result of pyrolysis. Wavelengths at 2124 cm^{-1} (C=O stretching vibrations), 1564 cm^{-1} (C=O stretching vibrations), 1062 cm^{-1} (C-O stretching vibrations), 796 cm^{-1}, 778 cm^{-1}, 694 cm^{-1}, 449 cm^{-1} (C-H bending vibrations/ CH deformation). The bands at 3066 cm^{-1} and 2124 cm^{-1} show very low intensity whereas the intensity increases below 800 cm^{-1}. The increase in C-H bending vibrations intensity indicates the formation of a functional group being formed at high temperatures (Yuan et al., 2011).

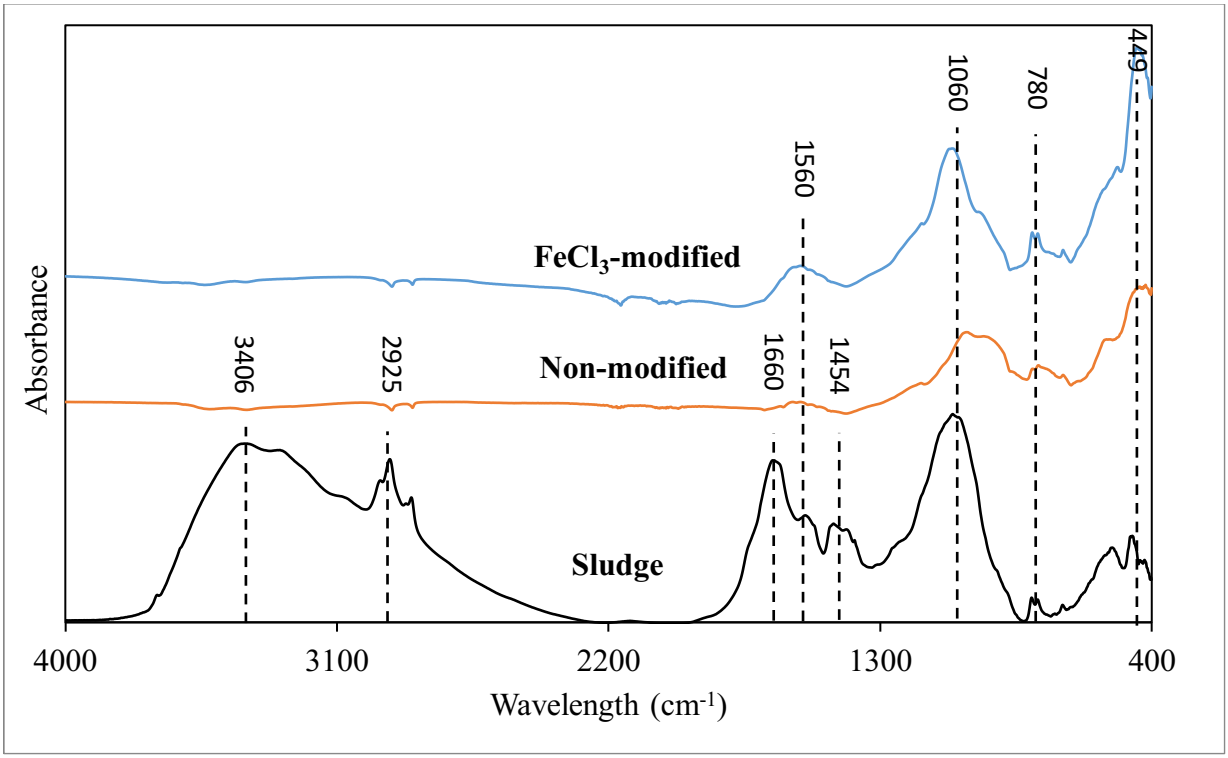

Figure 4.3: FTIR peaks of municipal sludge, non-modified biochar, and $FeCl_3$-modified biochar.

4.1.5. Crystallographic Structures

XRD analysis is used to identify the phases associated with the crystallinity of the sludge, non-modified biochar, and $FeCl_3$-modified biochar. The XRD patterns represented in Figure 4.4 range between $2\theta = 25° - 85°$. The dried sludge displayed a broad diffraction peak at approximately $2\theta = 32$, similar to non-modified biochar. After the pyrolysis process, muscovite microcrystals appeared in the XRD pattern and an increase in quartz microcrystals is observed in the non-modified biochar. As described by Song et al. (2021) the presence of muscovite microcrystals and increase in peak intensity show that biochar was formed during the pyrolysis process.

$FeCl_3$-modified biochar displays broad diffraction peaks at $2\theta = 32$, $2\theta = 38$, and $2\theta = 42$ and smaller broad peaks at $2\theta = 25$, $2\theta = 48$, $2\theta = 58$, and $2\theta = 64$. After the $FeCl_3$-modified biochar pyrolysis synthesis process, graphite C is no longer shown, however, Fe_2O_3 hematite and quartz crystals are seen in larger quantities. The emergence of Fe_2O_3 hematite in the XRD pattern further demonstrates the presence of additional functional groups in the biochar as the FTIR spectra indicated. The increase in peak intensity further indicates the interaction between the 1.4 M $FeCl_3$ solution and municipal sludge biochar and the successful production of $FeCl_3$-modified biochar (Álvarez et al., 2020; Song et al., 2021).

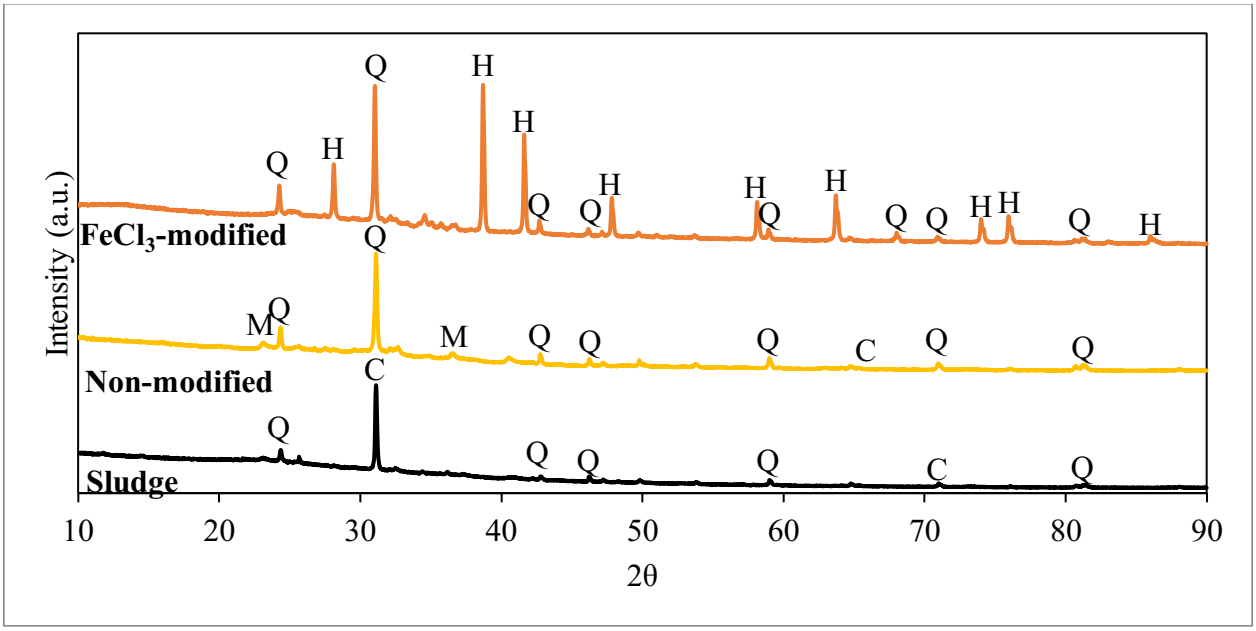

Figure 4.4: XRD diffractograms of municipal sludge, non-modified biochar, and $FeCl_3$-modified biochar. Where C is graphite C, Q is quartz, M is muscovite, and H is Fe_2O_3 hematite.

4.1.6. Elemental distribution

Using XPS survey spectra (Figure 4.5) of municipal sludge, non-modified biochar, and $FeCl_3$-modified biochar the physical or chemical adsorption can be determined. C1s, N1s, and O1s peaks are observed along with Si2s. Fe2p and Cl1s peaks are found in $FeCl_3$-modified biochar. The deconvolution peaks for the main components (C and O) were also identified.

The deconvolution peaks of carbon and oxygen were evaluated to better describe the adsorbent and adsorption mechanisms. The main elements in AC and modified AC are C 1s (280 eV) and O 1s (533 eV) (Alonso-de-Linaje et al., 2021, The international XPS database, 2022).

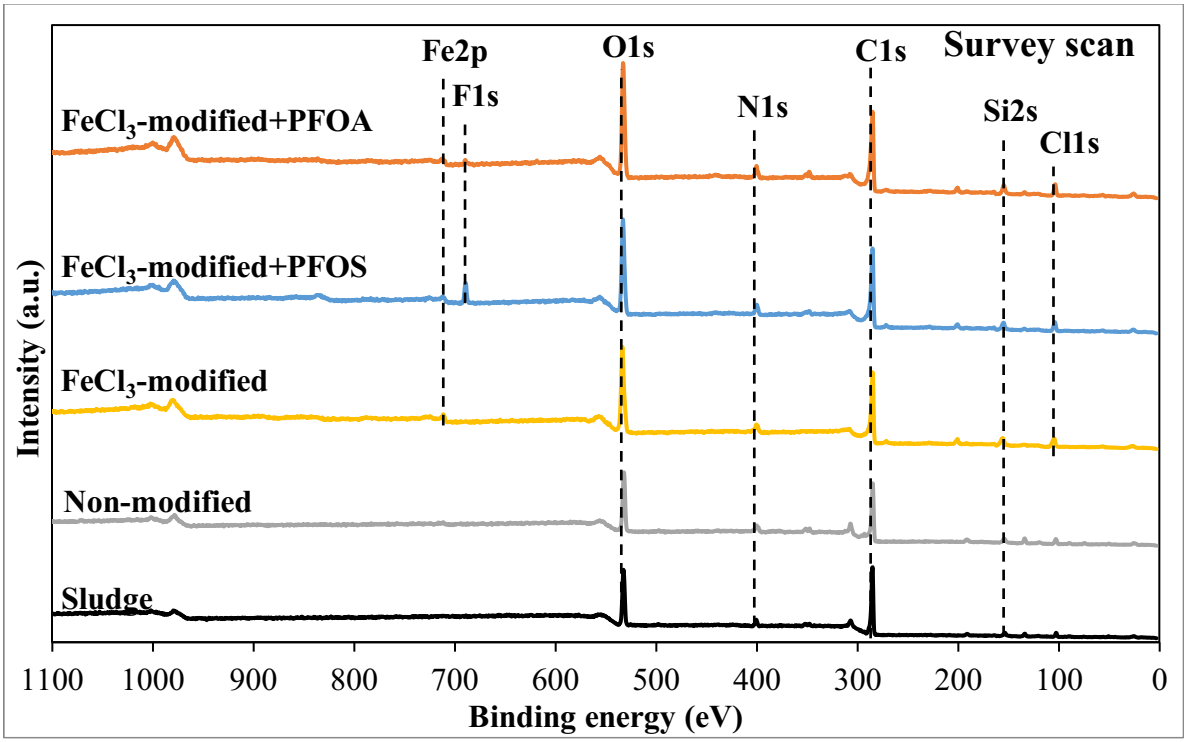

Figure 4.5: XPS analysis of municipal sludge, non-modified biochar, $FeCl_3$-modified biochar pre and post PFOS and PFOA adsorption

There are four deconvolution peaks of carbon (Figure 4. 6) for municipal sludge and three deconvolution peaks of carbon for non-modified biochar and $FeCl_3$-modified biochar. The binding energy of C1s is detected at 284.5 eV with a chemical state C=C and a concentration of 58.2%. The second carbon peak for municipal sludge has a binding energy of 288.03, 286.04, and 285.05, indicating C-F (7.2%), C-O (20.02%), and C=O (14.58%). The deconvolution peaks of non-modified biochar and $FeCl_3$-modified biochar have a chemical state of C=C, C-F, and C=O (Deng et al., 2012; Song et al, 2022). These peaks indicate the presence of carboxylate groups (Zhi & Liu, 2016; Song et al, 2021). The surface C=C content increases to 68. 79% when municipal sludge is pyrolyzed to produce non-modified biochar but is reduced to 55.4% during the production of $FeCl_3$-modified biochar. The C=O ratio increased from 14.58% (sludge) to 34.82% ($FeCl_3$-modified biochar), indicating that oxygen containing functional groups may be detrimental to

biochar adsorption. Supporting the increased removal rate for $FeCl_3$-modified biochar compared to non-modified biochar (28.06%) as its O/C ratio is higher. Adsorption onto oxygen containing functional groups may be achieved through hydrogen bonding and hydrophobic interaction (Inyang and Dickenson, 2015; Song et al., 2022). Hydrogen bonding and hydrophobic interaction are both types of physical adsorption.

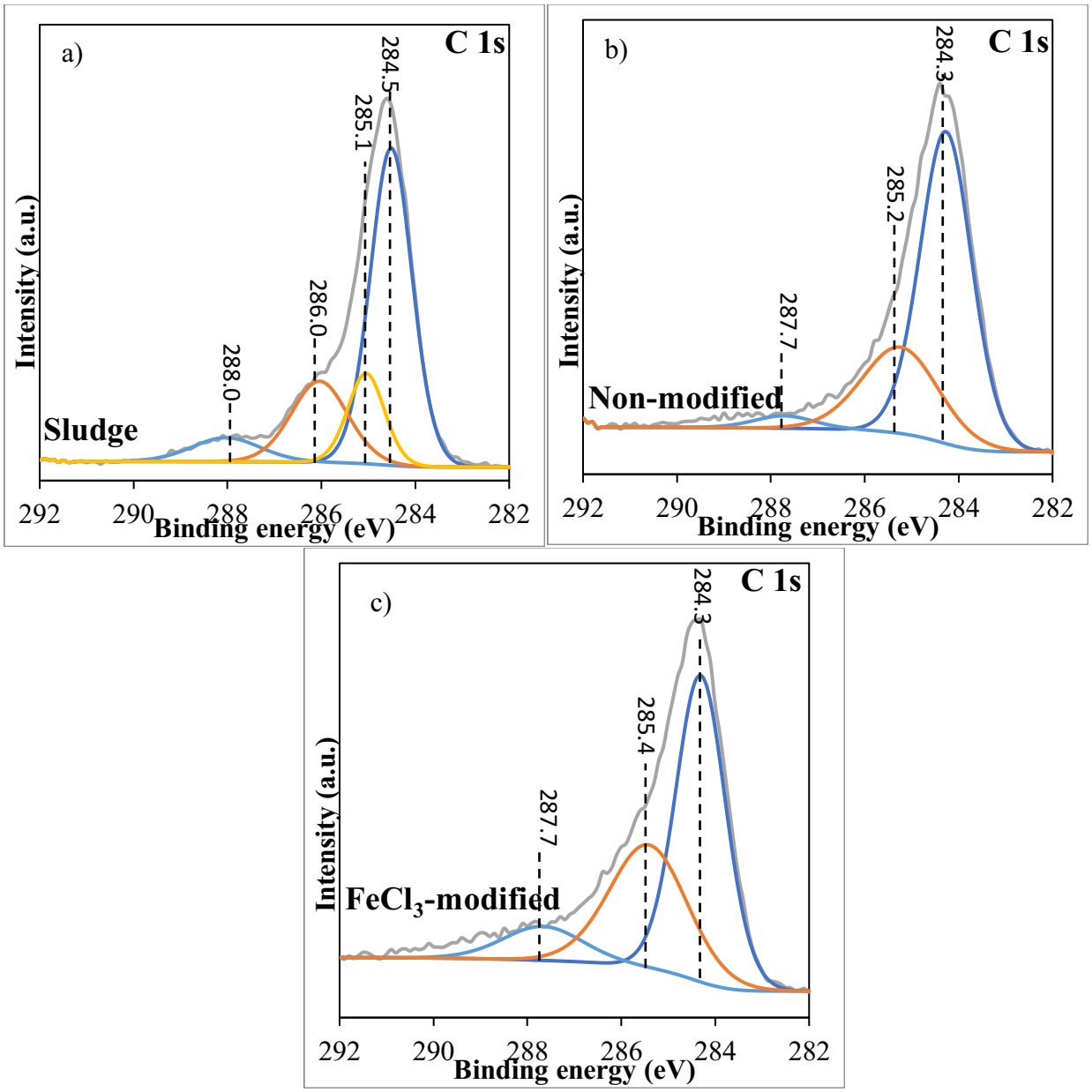

Figure 4.6: XPS analysis deconvolution peaks of carbon for a) municipal sludge, b) non-modified biochar c) $FeCl_3$-modified biochar pre adsorption.

The deconvolution peaks of oxygen are displayed in Figure 4.7. There are two deconvolution peaks of oxygen for municipal sludge and non-modified biochar and three deconvolution peaks of oxygen for $FeCl_3$-modified biochar. The deconvolution peaks of oxygen for municipal sludge, non-modified biochar, and, $FeCl_3$-modified biochar can be attributed to C=O (approximately 530.8 eV) and O-H (approximately 532.0 eV) (Wang et al., 2016; Song et al., 2021; The international XPS database, 2022; Wang et al., 2022). The peak area of O-H decreases from 94.7% (sludge) to 89.9% (non-modified biochar) and 74.73% ($FeCl_3$-modified biochar). The XPS area ratio for C=O increases with temperature increase with the highest area ratio appearing for $FeCl_3$-modified biochar, showing an increase in carbon, this is in agreement with the ultimate analysis.

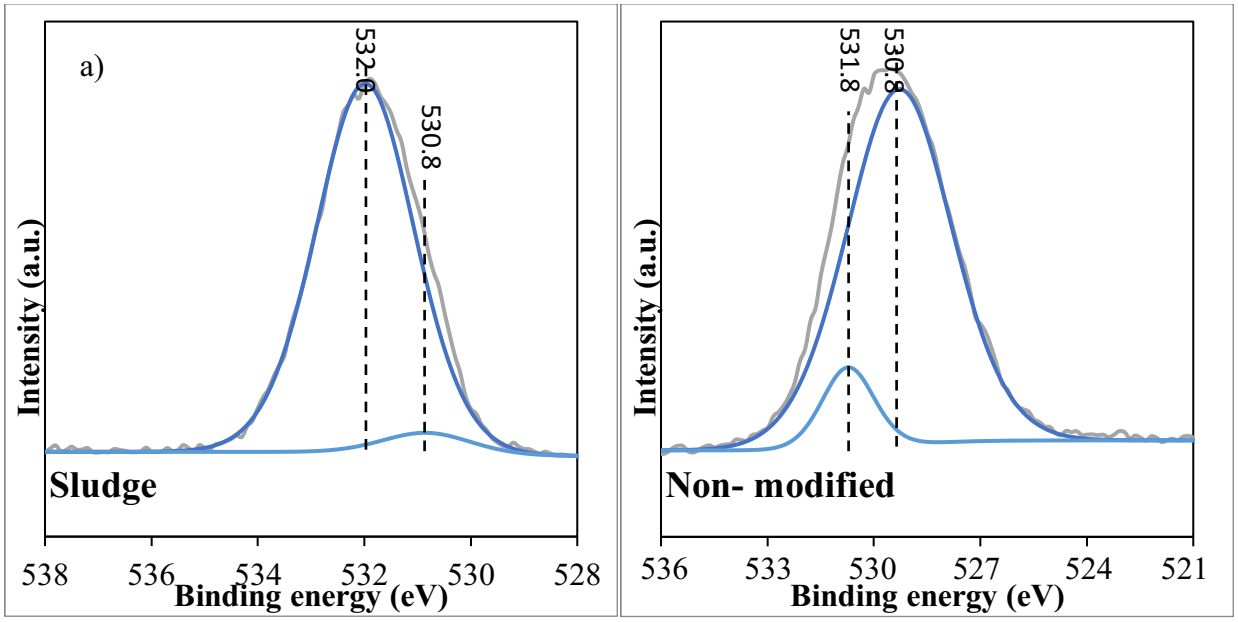

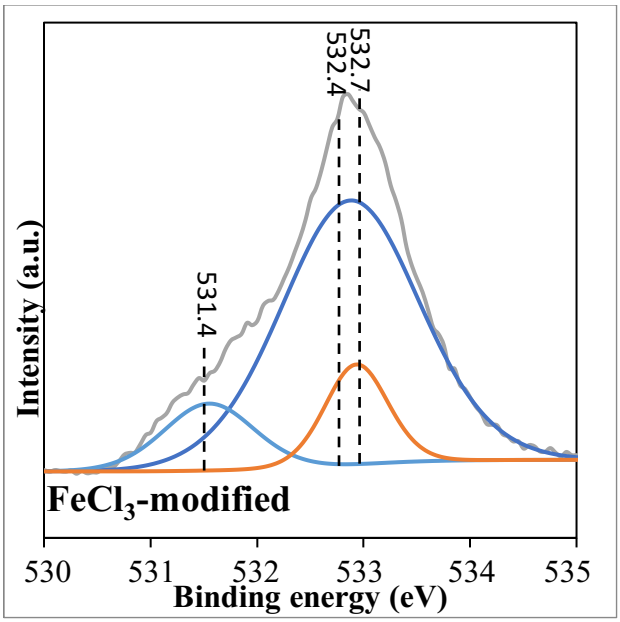

Figure 4.7: XPS analysis deconvolution peaks of oxygen for a) municipal sludge, b) non-modified biochar c) $FeCl_3$-modified biochar pre adsorption.

Table 4.2: Deconvolution peaks of Carbon

	$FeCl_3$-modified biochar			$FeCl_3$-modified biochar + PFOS			$FeCl_3$-modified biochar + PFOA		
	Deconvolution peaks of C								
	C1s 1	C1s 2	C1s 3	C1s 1	C1s 2	C1s 3	C1s 1	C1s 2	C1s 3
Position (eV)	281.51	284.87	282.62	281.58	284.52	282.76	281.61	284.65	283
Real (eV)	284.31	287.67	285.42	284.34	287.32	285.56	284.41	287.45	285.8
Conc. (%)	55.35	9.83	34.82	49.44	19.87	30.69	53.75	20.91	25.35

Table 4.3: Deconvolution Peaks of Oxygen

$FeCl_3$-modified biochar	$FeCl_3$-modified biochar + PFOS	$FeCl_3$-modified biochar + PFOA
Deconvolution peaks of O		

	O1s 1	O1s 2	O1s 3	O1s 1	O1s 2	O1s 3	O1s 1	O1s 2	O1s 3
Position (eV)	530.24	527.59	530.36	528.23	529.8	530.53	529.5	527.61	529.92
Real (eV)	533.04	530.39	533.16	531.03	532.6	533.33	532.3	530.41	532.72
Conc. (%)	74.73	12.37	12.9	25.78	49.92	24.3	80.86	7.04	12.1

4.1.7. Thermostability and ultimate analysis

The TGA study determined mass loss using a thermogravimetric analyzer. Using a 10°C min^{-1} heating rate, a 10 mg sample was combusted from 25 to 900 °C. The mass loss is shown in Figure 4.8. Based on this the thermostability, moisture content, and ash content of the sludge, non-modified biochar, and $FeCl_3$-modified biochar were analyzed (Table 4.5). As the temperature increased volatile matter and other combustible content burn off. This is described at the burnout temperature where the curve starts to plateau (Nzediegwu et al., 2021; Elanchezhiyan et al., 2021). Typically, there are four different regions of the TGA/DTG curve, region one shows the mass loss associated with moisture loss. Region two describes the degradation of carbohydrates, region three shows the degradation of aromatic compounds and region four depicts the decomposition of inorganic content and thermally stable compounds (Hernandez-Mena et al., 2014; Fan et al., 2018).

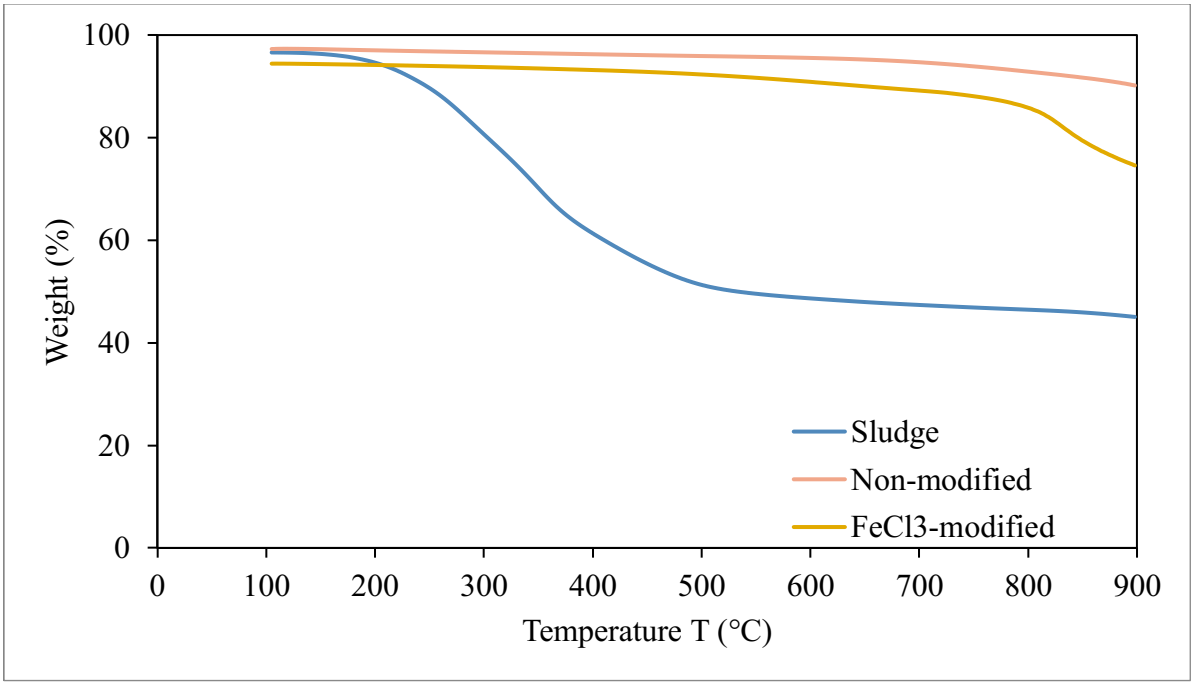

Figure 4.8: Thermogravimetric analysis of municipal sludge, non-modified biochar, and $FeCl_3$-modified biochar.

The TGA analysis of municipal sludge is typical for sewage sludge (Shahbeing & Nosrati, 2020; Ghodke et al., 2021). The TGA curve (Figure 4.9) displays that at 560 °C the thermal decomposition is almost complete and considered approximately stable as the mass loss after this point is 4.4%. The mass loss at temperatures greater than 560 °C indicates the degradation of large complex molecules of aromatic compounds such as proteins (Nzediegwu et al., 2021; Ghodke et al., 2021). The TGA curve shows mass loss starting at 200 °C (3.4% mass loss) and continuing to 560 °C (50.5% mass loss). The mass loss observed up until 200 °C is mainly related to moisture loss. The mass loss occurring from 200 – 560 °C can be attributed to the thermal degradation of carbohydrates such as saccharides. The drop in the DTG curve from 150 to 500 °C is also attributed to the thermal degradation of carbohydrates (Hernandez-Mena et al., 2014; Fan et al., 2018;

Nzediegwu et al., 2021). Based on this the pyrolysis zone for sludge was in the temperature range of 200 – 560 °C.

The TGA results for non-modified biochar show that the thermal decompaction occurs at much high temperatures (600 °C) compared to municipal sludge (200 °C). This suggests that non-modified biochar is more thermally stable, and less combustible material is present. Based on the TGA curve a mass loss of 4.5% is observed at 600 °C and a total mass loss of 9.8% at 900 °C. At 600 °C inorganic content and thermally stable components begin to degrade as shown in the TGA. The DTG plot indicates that at 150 °C to 560 °C carbohydrates begin to thermally degrade and at 600 °C – 780 °C aromatic compounds (proteins) are decomposed. Inorganic content and thermally stable compounds begin to degrade at 800 °C to 900 °C (Fan et al., 2018; Shahbeing & Nosrati, 2020).

$FeCl_3$-modified biochar has a higher moisture content resulting in more mass loss (2.7%) at ignition temperatures of 105 °C. Similar, to non-modified biochar, $FeCl_3$-modified biochar is more thermally stable, indicating that inorganic content and thermally stable components begin to degrade at 800 °C. The DTG curve for $FeCl_3$-modified biochar shows that in temperature region 720 °C – 760 °C aromatic compound is degraded and at 800 °C – 900 °C inorganic content and thermally stable components decomposed.

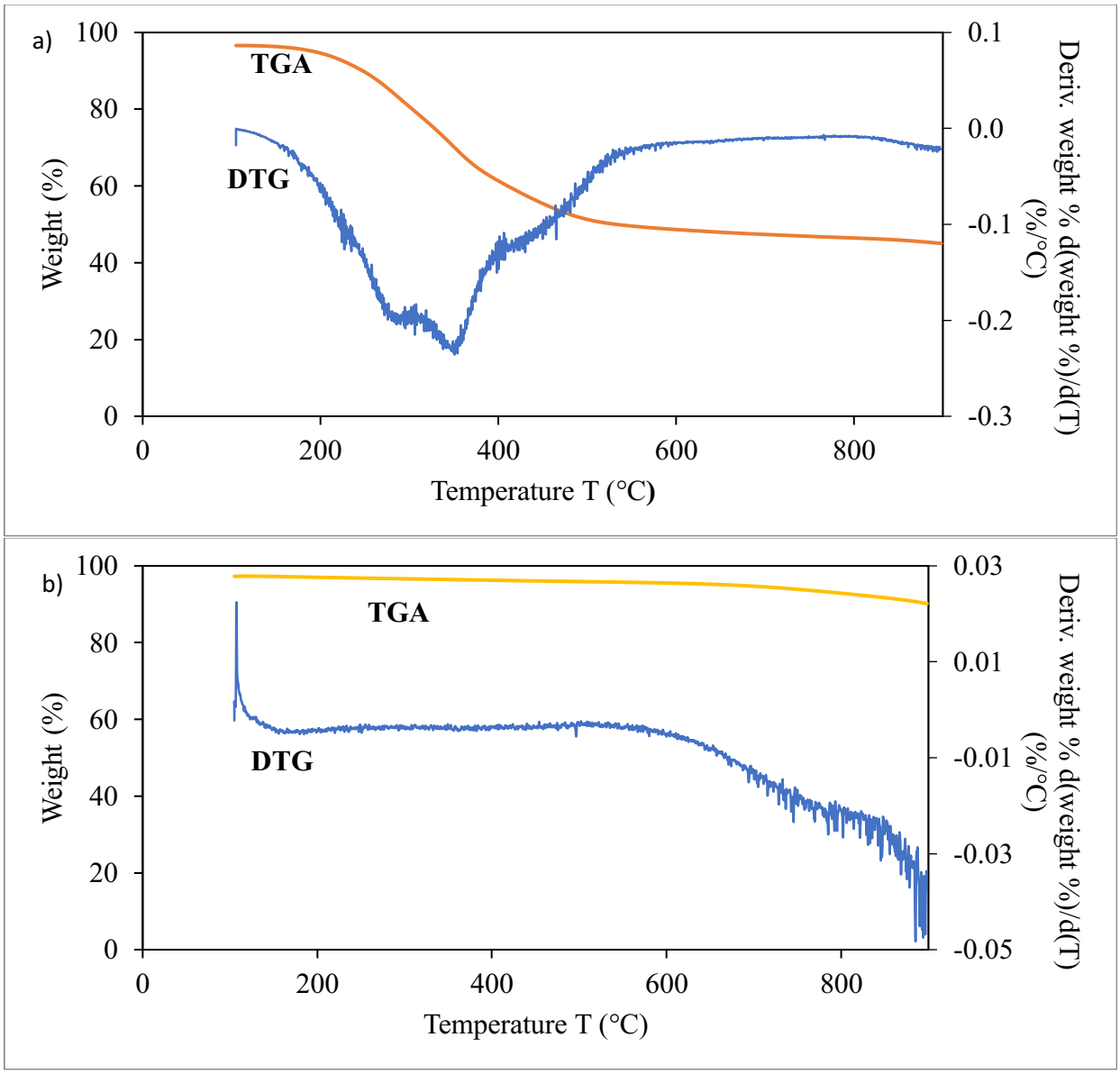
a)
TGA
DTG
Weight (%)
Deriv. weight % d(weight %)/d(T) (%/°C)
Temperature T (°C)
b)
TGA
DTG
Weight (%)
Deriv. weight % d(weight %)/d(T) (%/°C)
Temperature T (°C)

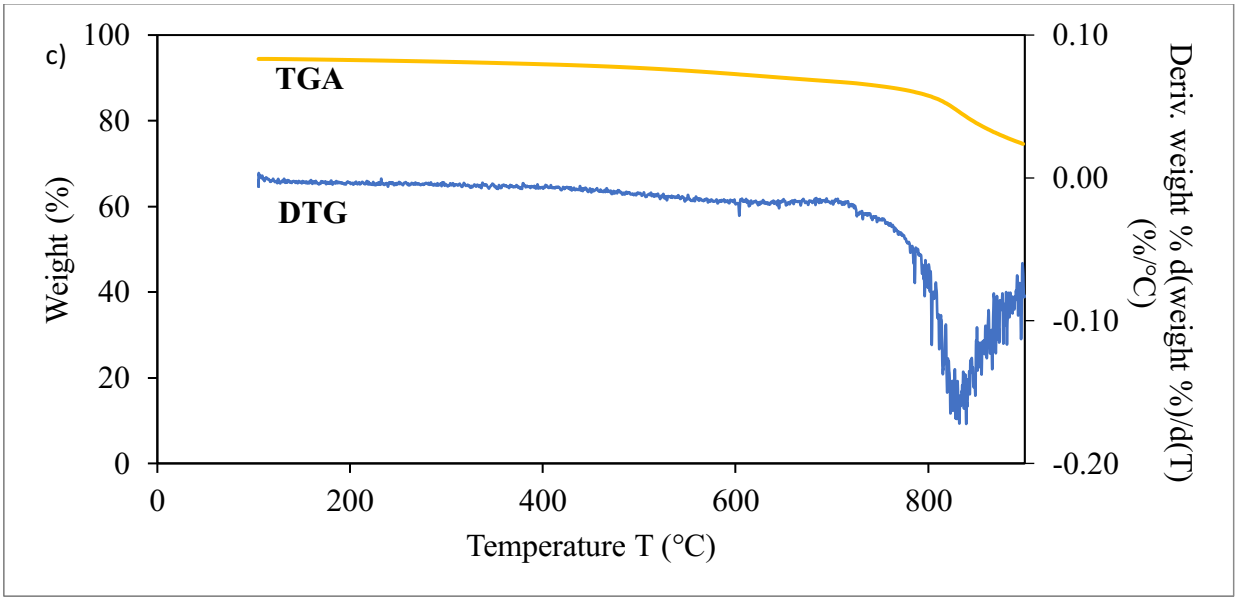

Figure 4.9: TGA and DTG characterization of (a) municipal sludge, (b) non-modified biochar, and (c) FeCl3-modified biochar.

The TGA analysis affirms the release of volatile matter in the form is pyrolysis gas as the maximum mass loss of non-modified biochar and $FeCl_3$-modified biochar is 35.1% and 49.2% compared to municipal sludge (64.4%) at 900 °C. The moisture content was determined as mass loss occurring at temperatures lower than 105 °C. As shown in Figure 4.9 the moisture content of $FeCl_3$-modified biochar was higher than in sludge and non-modified biochar. This could be attributed to $FeCl_3$-modified biochar having a higher surface area and pore volume allowing increased adsorption of water (Álvarez et al., 2020). The results showed that the volatile matter from municipal sludge was reduced from 53.3% to 10.6% (non-modified biochar) and 25.3% ($FeCl_3$-modified biochar) while the fixed carbon was increased from 7.7% to 21.8% (non-modified biochar) and 12.5% ($FeCl_3$-modified biochar) after production using pyrolysis. These results indicate that effective carbonization occurred. The ash content of non-modified biochar and $FeCl_3$-modified biochar was observed to increase to 64.89% and 50.77% from 35.63% in sludge. Karaca et al. (2018) and Deng et al (2013) reported similar TGA and ultimate analysis values for municipal

sludge. The ultimate analysis of sludge, non-modified biochar, and $FeCl_3$-modified biochar is shown in Table 4.5. Typically, with the addition of heat the O concentration decreases due to devolatilization (Nzedieqwu et al., 2021). Consequently, when the O content decreases the C, H, and N concentrations are decreased. The addition of Fe maintains the O content at 15.34% compared to non-modified biochar at 2.47%. The concentration of C decreased for sludge-based biochar as the high ash content impedes C recovery (Álvarez et al., 2020; Nzedieqwu et al., 2021). The total carbon has been found to be higher in biochar containing Fe (Álvarez et al., 2020). This concurs with the finding of this study as $FeCl_3$-modified biochar has a C content of 29.28%, whereas non-modified biochar is 27.8%. The pyrolysis of sludge to produce non-modified biochar and $FeCl_3$-modified biochar increased carbonization, reducing the H/C, O/C, and (N+O)/C values. However, $FeCl_3$-modified biochar has higher H/C, O/C, and (N+O)/C ratios than non-modified biochar increasing aromatically, stability, and oxygen containing functional groups. The O/C ratio decreases with increasing temperatures the adsorption mechanism shifts from ion exchange mechanism to physical adsorption (Uttran et al., 2018). A decreasing H/C value with increasing temperature indicates the formation of more stable and aromatic rings (Shakya et al., 2022).

Table 4.4: Thermogravimetric analysis and ultimate analysis of sludge, non-modified biochar, and $FeCl_3$-modified biochar.

Characteristics		Sludge	Non-modified biochar	$FeCl_3$-modified Biochar
TGA Analysis (%)	Moisture	3.4	2.7	5.6
	Volatile matter	53.3	10.6	24.0
	Ash	35.63	64.89	50.77
	Fixed C	7.7	21.8	12.5
Ultimate Analysis (%)	Carbon	32.91	27.80	29.28
	Hydrogen	4.87	0.97	1.6
	Nitrogen	5.29	3.87	3.01
	Oxygen	20.69	2.47	15.34

Sulfur	0.61	0.00	0.00
H/C	1.78	0.42	0.66
O/C	0.47	0.07	0.39
(N+O)/C	0.61	0.19	0.48

4.2. Effect of Different Biochar Types

Different biochar types were evaluated to determine which would be the most effective in removing PFOS, PFOA, and PFB compounds from pre-UV secondary effluent. Five different types of biochar were used: non-modified biochar, $FeCl_3$-modified biochar, $ZnCl_2$-modified biochar, KOH-modified biochar, and $FeCl_3$/$ZnCl_2$-modified biochar. A biochar dosage of 1.0 g L^{-1} was used to evaluate each biochar type. The results of the effect of biochar type on the adsorption of PFOS and PFOA compounds are shown in Figure 4.10. Using a biochar dose of 1.0 g L^{-1}, no removal of PFB was seen with any of the different types of engineered biochar. Based on previous research by Zhoa et al. (2016), it is observed that short-chain PFAS are less likely to be adsorbed than long-chain PFAS. This is possibly due to the favorable partitioning of short-chain PFAS into the aqueous phase whereas long-chain PFAS show favorable partitioning to the solid phase. Long-chain PFAS being more hydrophobic compared to short-chain PFAS could also play a role as hydrophobicity interaction is a potential adsorption mechanism (Yadav et al., 2022; Lenka et al., 2021). $ZnCl_2$-modified biochar was determined to be an ineffective adsorbent for PFAS as no removal occurred using a 1.0 g L^{-1} dosage and a contact time of 24 hours at a pH of 6.5.

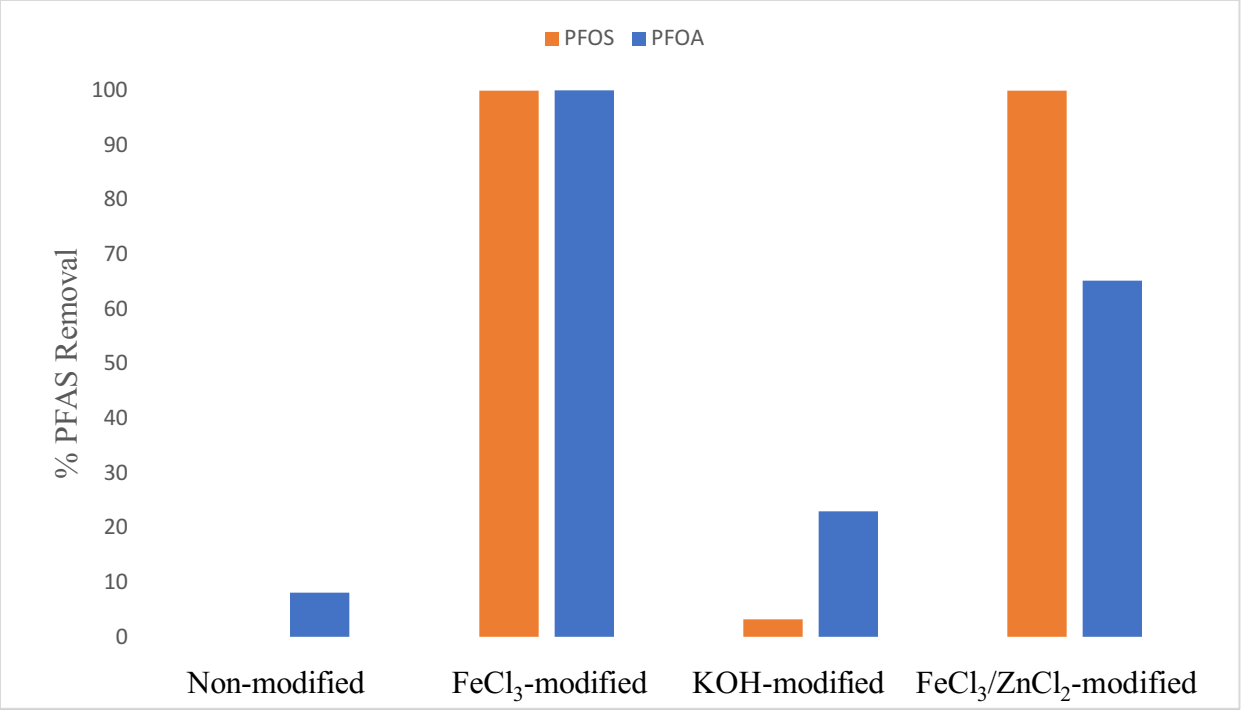

Figure 4.10: Effect of biochar type for PFOS, and PFOA. Adsorption conditions: initial PFAS spiked pre-UV secondary effluent concentration: 25 mg L^{-1} (pH 6.5); contact time: 24 h; agitation speed: 200 rpm; adsorbent concentration: 1.0 g L^{-1}

The non-modified biochar showed no removal of PFOS and 8.11% removal of PFOA. KOH-modified biochar removed 3.23% of PFOS and 22.94% of PFOA. The highest PFOS and PFOA removal was observed using $FeCl_3$-modified biochar and $FeCl_3/ZnCl_2$-modified biochar. The former removed 99.98% and 100% of PFOS and PFOA, respectively, while the latter removed 100% and 65.16% of PFOS and PFOA, respectively. $FeCl_3$-modified biochar was the biochar selected for further adsorption experiments (kinetic, isotherm, desorption, and regeneration experiments) based on the great removal of both PFOS and PFOA observed, while also requiring less chemical to produce the biochar.

4.3. Effect of Adsorbent Dosage Experiments

The first step in assessing the biochar as an adsorbent is to determine the effect of the adsorbent dosage. Biochar dosages between 0.05 to 1.25 g L^{-1} were evaluated and the results of the effect of adsorbent dosage on the adsorption of PFOS and PFOA compounds are shown in Figure. 4.11.

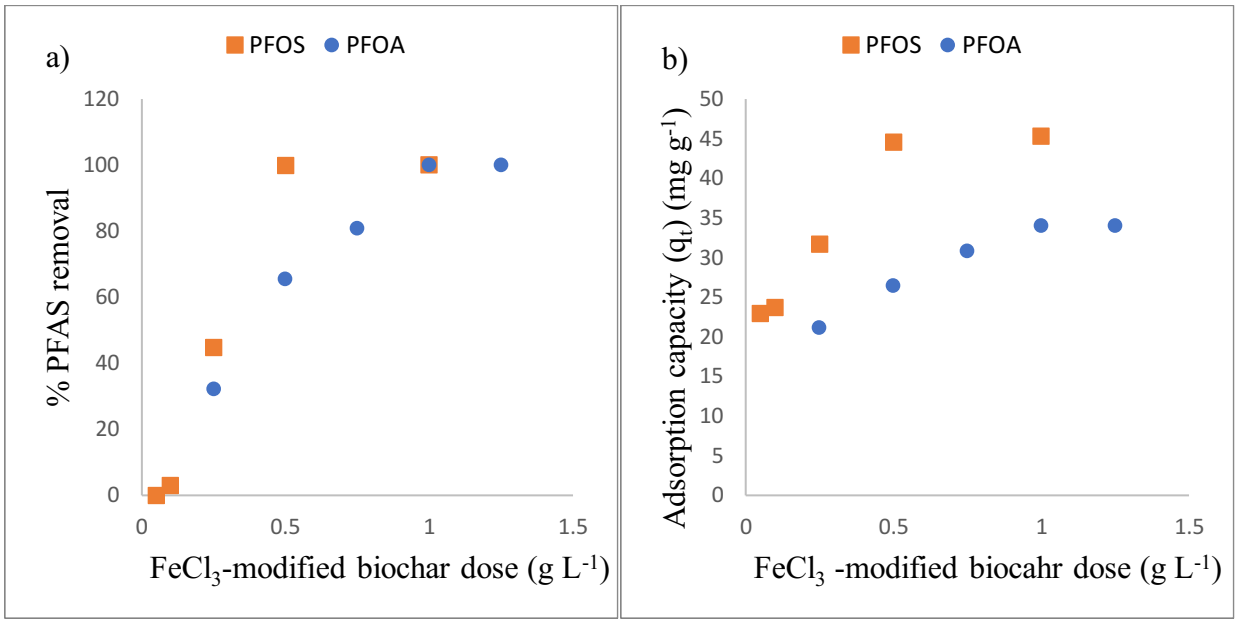

Figure 4.11: Effect of adsorbent dosage for $FeCl_3$-modified biochar on adsorption of PFOS and PFOA in terms of (a) percentage of removal and (b) adsorption capacity. Adsorption conditions: initial PFAS spiked pre-UV secondary effluent concentration: 25 mg L^{-1} (pH 6.5); contact time: 24 h; agitation speed: 200 rpm.

Using the lowest $FeCl_3$-modified biochar dosage of 0.05 g L^{-1}, no removal of PFOS was observed. The amount of PFAS adsorbed increased as the adsorbent dosage increased, determining the optimal absorbent dose for PFOS to be 0.5 g L^{-1} with a removal percent of 99.89%. The removal of PFOS tends to be relatively stable once the dosage of 0.5 g L^{-1} or higher is used. $FeCl_3$-modified biochar dosages were also studied for PFOA removal, using dosages of 0.25, 0.5, 0.75, 1.0, and 1.25 g L^{-1}. A $FeCl_3$-modified biochar dose of 0.75 g L^{-1} is determined to be optimal with

PFOA removal of 80.71%. Similar concentrations were used in a study conducted by Ochoa-Herrera and Sierra-Alvarez (2008) using GAC as the adsorbent.

Studies of the adsorption of PFOS and PFOA compounds in distilled water also applied a similar range of adsorbent dosages. For example, distilled water containing GAC was used at a range of 0.1 – 1.0 g L^{-1} in the adsorption of PFOS. The PFOS concentration was also similar using 15 – 300 mg L^{-1}. Although, the contact time for these experiments was extended to 48 h (Ochoa-Herrera and Sierra-Alvarez, 2008; Chen et al., 2011; Gagliano et al., 2021).

Based on the preliminary adsorption dosage data, the optimal dosage of $FeCl_3$-modified biochar dosage was 0.5 g L^{-1} and 0.75 g L^{-1} for PFOS and PFOA adsorption, respectively. These optimal dosages were applied in the following adsorption experiments (kinetics, isotherm, desorption, and regeneration experiments). In addition to PFOS having a higher molecular weight and lower water solubility (0.55 mg L^{-1}) than PFOA (3.3 g L^{-1}), the presence of the hydrophobic sulfonic acid group typically results in stronger adsorption affinity (lnyang & Dickenson, 2017). So, a lower adsorbent dosage is needed to reach optimal removal of PFOS compared to PFOA. The hydrophobic surface of $FeCl_3$-modified biochar and its favorable exposed functional groups also play a part in the increased adsorption at moderately low dosages.

4.4. Kinetics Study

The study of kinetics adsorption determines how fast the adsorbate attaches to the adsorbent surface. Understanding the adsorption kinetic provided insight into how full-scale operations should be designed with optimum operating conditions (Song et al., 2020; Benally et al., 2019). The kinetic experiments were performed from 5 min to 24 h. As shown in Figure 4.12 PFOS and

PFOA are rapidly removed by the $FeCl_3$-modified biochar during the initial stages. PFOS and PFOA removal begins to plateau around 4 hours and 6 hours.

It was observed that after 5 minutes 18.48% of PFOS were removed. The removal jumped to 30.19% after 15 minutes and 61.32% after 30 minutes. At a contact time of 1 hour, the adsorption rate slowed down removing 81.73% before reaching equilibrium at 4 hours (98.33%). $FeCl_3$-modified biochar adsorbed 42.54% of PFOA after 5 minutes and continued to jump at 15 minutes (54.16%) and 30 minutes (62.5%) before the adsorption rate slowed down and equilibrium was reached at 6 hours (80.71%). Based on Figure 4.12 (b) the adsorption equilibrium for PFOS and PFOA is determined to be 4 hrs and 6 hours, respectively, as the adsorption capacity does not fluctuate significantly. The q_e value for PFOS (36.71 mg/g) is slightly higher than for PFOA (28.34 mg/g), which could be a result of the more hydrophobic properties of PFOS and their tendency for the formation of the hemi-micelle and micelle in internal pores (Guo et al., 2017).

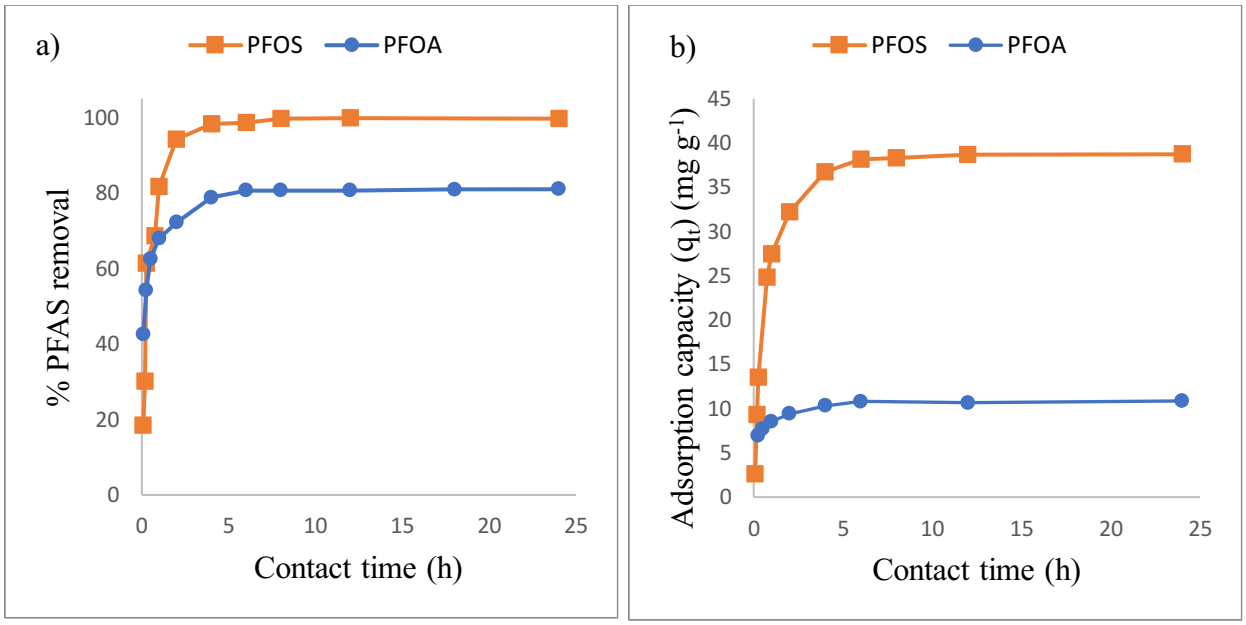

Figure 4.12: (a) The removal of PFOS and PFOA using $FeCl_3$-modified biochar and (b) the adsorption capacity of $FeCl_3$-modified biochar for PFOS and PFOA adsorption over time.

Adsorption conditions: initial PFAS spiked pre-UV secondary effluent concentration: 25 mg L^{-1} (pH 6.5); agitation speed: 200 rpm; adsorbent concentration: 0.5 g L^{-1} (PFOS), 0.75 g L^{-1} (PFOA).

The kinetics models PFO (Eq. 2.3), PSO (Eq. 2.4), Elovich (Eq. 2.5), and IPD (Eq. 2.6) kinetic models were applied to the experimental kinetic data to evaluate the adsorption of PFOS and PFOA onto $FeCl_3$-modified biochar (Figure 4.13). The fitted kinetic parameters are presented in Table 4.6.

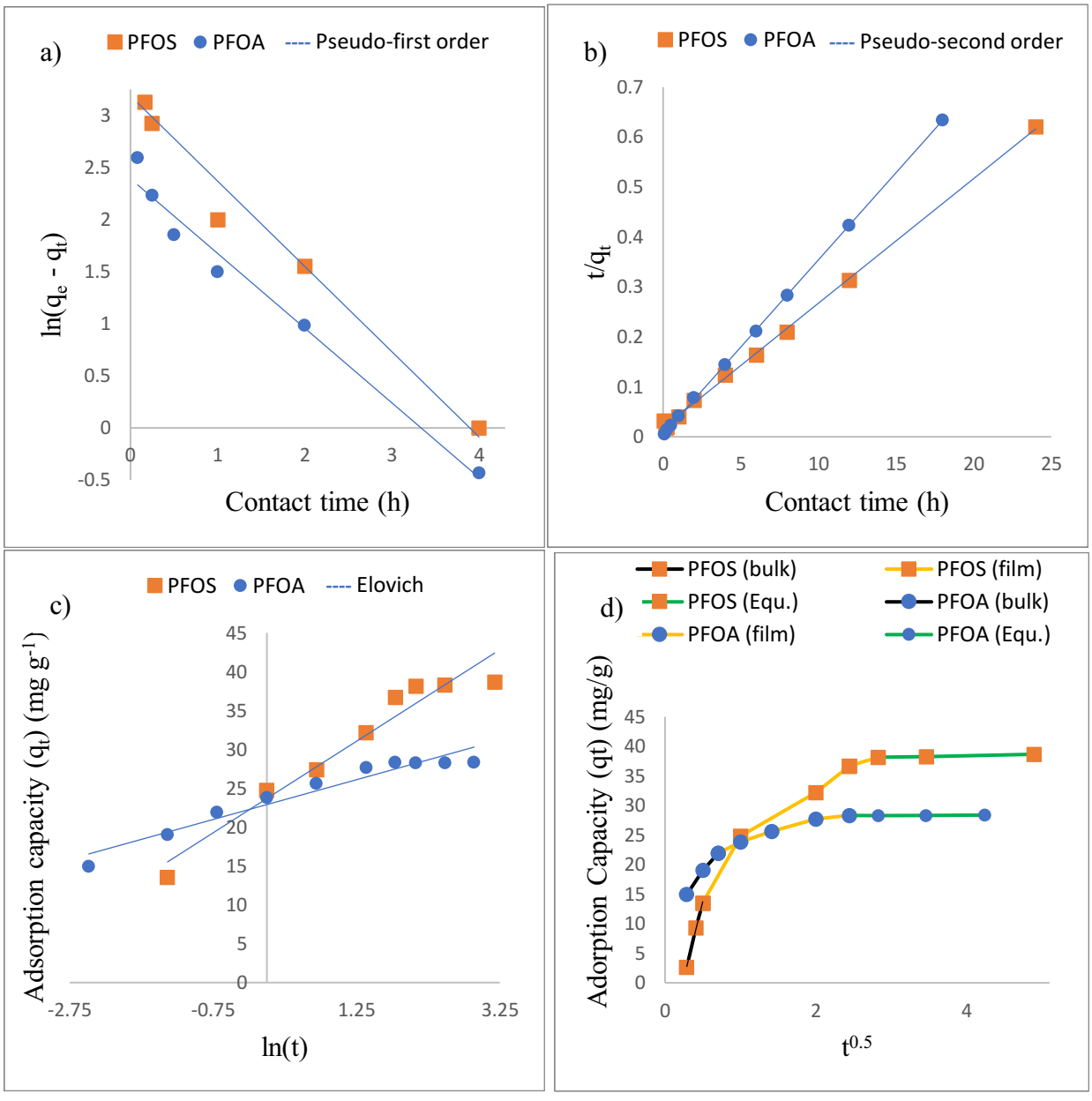

Figure 4.13: (a) Pseudo-first order, (b) pseudo-second order, (c) Elovich, and (d) intraparticle diffusion kinetic models for the adsorption of PFOS and PFOA on $FeCl_3$-modified biochar using 0.5 g L^{-1} and 0.75 g L^{-1}, respectively.

As seen from the kinetics parameters presented in Table 4.6, the correlation coefficient (R^2) values for the PSO model were 1.0 and 1.0 for PFOS and PFOA adsorption and were higher than those obtained for the PFO model. Therefore, the adsorption process of PFOS and PFOA on $FeCl_3$-modified biochar is best described by the PSO kinetic model. The experimental q_e value for removal of PFOS and PFOA was determined to be 36.71 mg g^{-1} and 28.34 mg g^{-1} where the calculated q_e are 40.16 mg g^{-1} and 28.65 mg g^{-1}, respectively. The $q_{e.exp}$ and $q_{e.cal}$ are similar further indicating the good fitting of the PSO model to the adsorption data. The rate constants, K_{pso} for PFOS and PFOA are 0.04 g mg^{-1} h^{-1} and 0.25 g mg^{-1} h^{-1}. As the PSO rate constant decreases the adsorption capacity (q_e) increases.

The Elovich kinetic model assumes that the surface of the adsorbent is energetically heterogeneous. The Elovich model R^2 value for PFOS was 0.95 and for PFOA was 0.94. The Elovich parameters indicate important interactions between the PFOS/PFOA and the adsorbent. The initial adsorption rate (α) (mg g^{-1} h^{-1}) expresses the affinity between PFOS/PFOA and adsorbent, and β is the desorption constant (Guo et al., 2017; Fagbayigbo et al., 2022). $FeCl_3$-modified biochar has an initial adsorption rate of 64.4 (mg g^{-1} h^{-1}) and 62.27 (mg g^{-1} h^{-1}) for PFOS and PFOA, respectively indicating PFOS is adsorbed more quickly than PFOA.

The IPD model was used to evaluate the diffusion mechanism during the adsorption process. The IPD models for PFOS and PFOA are shown in Figure 4.13 with the kinetics parameter displayed in Table 4.6. Since the plot does not pass through the origin, intraparticle diffusion is not the rate-limiting step and film diffusion must be taken into consideration (Islam et al., 2018).

The IPD plot is multilinear two linear regions before equilibrium is reached. There are three possible regions of diffusion that occur in the adsorption process, bulk, film, and pore (Ofomaja, 2010; Benally et al., 2019; Song et al., 2021). The first stage of the IPD model occurred rapidly and could be interpreted as bulk diffusion (boundary layer diffusion). The next subsequent stage occurred more slowly describing the mass transfer through the film layer surrounding the adsorbent. The last region of the IPD model for PFOS shows the equilibrium stage which was reached after 4 hours and 6 hours. The bulk intraparticle diffusion rate constant, $K_{i,bulk}$ for PFOS and PFOA adsorption are 51.72 mg g^{-1} $min^{-0.5}$ and 16.76 mg g^{-1} $min^{-0.5}$. Intraparticle diffusion rate constants, $K_{i,film}$ were determined to be 10.98 mg g^{-1} $min^{-0.5}$ and 3.64 mg g^{-1} $min^{-0.5}$ for PFOS and PFOA, respectively. The PFOS rate constant is significantly higher than PFOA in both bulk and film stages.

The intercept, c_i is an indicator of the effect the boundary layer plays. The larger the c_i value the more significant of a role that phase plays in the determination of the rate-limiting step (Ofomaja, 2010; Benally et al., 2019). The IPD c_i for PFOS removal is negative in the bulk phase indicating that adsorption occurs quickly, which agrees with the rate constant. The larger c_i of the film phase indicates that it plays a more dominate in limiting the speed of adsorption. The c_i for the film stage is also larger than the bulk stage for PFOA adsorption. The c_i for PFOA adsorption during both the bulk and film stages are higher than PFOS, indicating that the PFOA adsorption process takes longer. This is reflected by the equilibrium time for each compound. Based on the intraparticle diffusion rate constant (K_i) and intercept (c_i) for bulk and film diffusion, film diffusion is rate limiting for the adsorption of both PFOS and PFOA compounds.

The additional sulfonic functional group along with the lower water solubility allows PFOS to be adsorbed onto $FeCl_3$-modified biochar more rapidly, reducing the adsorption equilibrium time

compared to PFOA. $FeCl_3$-modified biochar performs well when compared to other literature where adsorption equilibriums range from 24 hours to days, showing similar removal of PFOS and PFOA. The PSO rate constant and adsorption capacity for the removal of PFOS and PFOA was higher compared to HWC and PWC (Inyang & Dickenson, 2017) and GAC (Yu et al., 2009, Senevirathna et al., 2010). $FeCl_3$-modified biochar performed similarly to PAC for the adsorption of PFOS (Son et al., 2020). The improved $FeCl_3$-modified biochar adsorption of PFOS and PFOA due to the increased surface area, pore volume, hydrophobicity, and decrease in H/C and O/C ratios associated with the modification of Fe to municipal sludge produced biochar.

Table 4.5: Summary of modeling kinetic parameters obtained for adsorption of PFOS and PFOA compound on FeCl3-modified biochar.

Kinetic models and parameters		PFOS	PFOA
$q_{eq.exp}$[c]		36.71 mg g^{-1}	28.34 mg g^{-1}
Pseudo-first order	$q_{eq.PFO}$ (mg g^{-1})	24.27	10.95
	K_{PFO} (h^{-1})	0.82	0.72
	R^2	0.97	0.98
Pseudo-second order	$q_{eq.PSO}$ (mg g^{-1})	40.16	28.65
	K_{PSO} (h^{-1})	0.04	0.25
	R^2	1.0	1.0
Elovich	α (mg g^{-1} min^{-1})	64.40	62.27
	B (mg g^{-1})	0.17	0.39
	R^2	0.95	0.94
Intraparticle diffusion	$K_{i,bulk}$ (mg g^{-1} $min^{-0.5}$)	51.72	16.76

	$c_{i,\ bulk}$	-12.14	10.28
	R^2	1.0	1.0
	$K_{i,\ film}$ (mg g^{-1} $min^{-0.5}$)	10.98	3.64
	$c_{i,\ film}$	10.47	19.98
	R^2	0.94	0.96

4.5. Equilibrium Study

Based on the kinetic data, it was determined that the equilibrium time for PFOS and PFOA is 4 h and 6 h (Figure 4.13), respectively. Then the equilibrium study was performed using a concentration of PFOS/PFOA of 25 mg L^{-1} with a $FeCl_3$-modified biochar dosage range of 0.05 g L^{-1} – 1.0 g L^{-1} (PFOS) and 0.25 g L^{-1} – 1.25 g L^{-1} (PFOA).

Langmuir (Eq. 2.7) and Freundlich (Eq. 2.8) isotherm models were applied to experimental $FeCl_3$-modified biochar adsorption data for the removal of PFOS and PFOA (Figure. 4.14). The isotherm parameters for each model are shown in Table 4.7.

As seen in Figure 4.14, the Langmuir isotherm has a higher R^2 value for PFOS and PFOA compared to the Freundlich model. The R^2 when fitted to the Langmuir model were 1.0 for PFOS and 0.95 for PFOA. The R^2 value of the Freundlich model were 0.97 for PFOS and 0.92 for PFOA. The Freundlich isotherm model is commonly used in heterogeneous surface adsorbents. The Langmuir equation assumes that there is no interaction between the adsorbate molecules and that the adsorption is localized in a monolayer (Ochoa-Herrera & Sierra-Alvarez, 2008; Deng et al., 2013, Guo et al, 2017). It also assumes that once the adsorbate occupies a site, no further adsorption can take place at that site. So, the well-fitting Langmuir model to the experimental data indicated that monolayer adsorption occurred for PFOS/PFOA. The maximum adsorption capacity, q_{max} for the removal of PFOS and PFOA were 54.95 mg g^{-1} and 12.53 mg g^{-1}. The q_{max} value for $FeCl_3$-

modified biochar removal of PFOS and PFOA may be associated with their hydrophobic C-F chain. This is consistent with their logK_{ow} values and again indicates adsorption may occur through hydrophobic interaction (Deng et al., 2013). The Langmuir affinity constant, b_L values of PFOA were higher than PFOS.

Adsorption isotherms reported in the literature differ between Langmuir or Freundlich as the best fit for the removal of PFOS and PFOA based on different variations of initial concentrations and adsorbent properties. Ochoa-Herrera and Sierra-Alvarez (2008), Inyang and Dickenson (2017), Yu et al. (2009), and Deng et al. (2013) all reported that the Langmuir isotherm provided the best fit for experimental adsorption of PFOS and PFOA. $FeCl_3$-modified biochar had a higher maximum adsorption capacity than GAC, AC, HWC, and PWC (Yu et al., 2009; Inyang and Dickenson, 2017) but Ochoa- Herrera and Sierra-Alvarez (2008) reported a higher q_{max} for PAC.

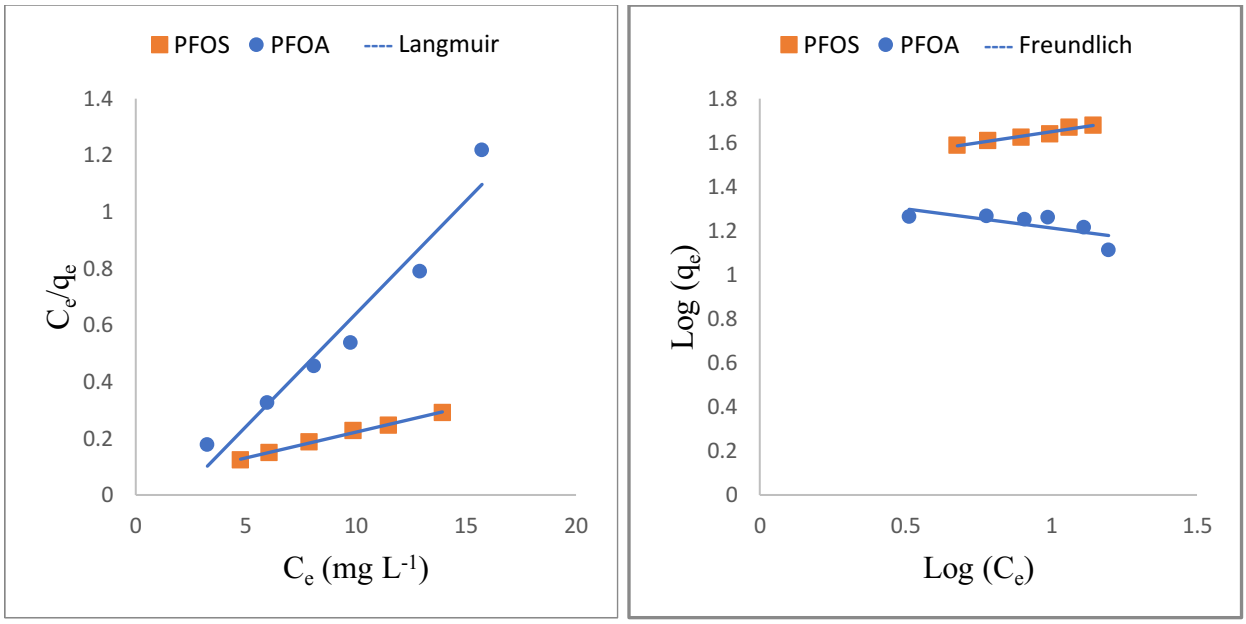

Figure 4.14: Langmuir and Freundlich isotherms applied to the adsorption of PFOS and PFOA compounds using $FeCl_3$-modified biochar. Adsorption conditions: initial PFAS compound concentration: 25 mg L^{-1} (pH 6.5); contact time: 4 hours (PFOS), and 6 hours (PFOA),

respectively; agitation speed: 200 rpm; adsorbent concentration: 0.1 g L^{-1} to 0.5 g L^{-1} for PFOS, and 0.25 g L^{-1} to 1.25 g L^{-1} for PFOA, respectively.

Table 4.6: Summary of modeling isotherm parameters obtained for adsorption of PFOS and PFOA compound on $FeCl_3$-modified biochar.

Isotherm	Parameters	PFOS	PFOA
Langmuir	q_{max} (mg g^{-1})	54.95	12.53
	b (L mg^{-1})	0.46	0.51
	R^2	1.0	0.95
Freundlich	K_f	28.25	24.34
	n_f	5.04	5.76
	R^2	0.97	0.52

4.6. Desorption Study

The desorption of PFOS and PFOA from $FeCl_3$-modified biochar was determined at contact times of 24 hours and 7 days. As shown in Table 4.8, no desorption was seen at a contact time of 24 h for either PFOS or PFOA. Once the $FeCl_3$-modified biochar reaches adsorption equilibrium no PFOS or PFOA is leaching even after 24 hours. At a contact time of 7 days, no desorption was observed of PFOS and desorption of the PFOA was 5.3%. The desorption of PFOA from $FeCl_3$-modified biochar although small shows the stronger attraction of PFOS. This could be due to the weak adsorption affinity of PFOA as they contain a carboxyl group instead of a sulfonic group. Askeland et al (2020) also reported higher desorption of PFOA than PFOS in biochar. However, they reported a higher concentration of desorption than seen with $FeCl_3$-modified biochar. The very weak desorption further indicates that $FeCl_3$-modified biochar is a suitable option for the removal of PFOS and PFOA in water/wastewater treatment.

Table 4.7: Desorption values for PFOS and PFOA

	Desorption Percent	
Contact time	PFOS	PFOA
24 hours	0	0
7 days	0	5.3

4.7. Regeneration Study

The regeneration of spent biochar was studied over five cycles using thermal regeneration and the results were summarized in Table 4.9. As shown in Figure 4.15 removal of PFOS was reduced to 84.68% after the first regeneration cycle of spent $FeCl_3$-modified biochar. After five cycles, only 33% PFOS removal was obtained. After each $FeCl_3$-modified biochar regeneration cycle for PFOS adsorption a 15-20% reduction in biochar mass was observed. Whereas, a 10-15% reduction in biochar mass was noted after each $FeCl_3$-modified biochar regeneration cycle for PFOS adsorption. The removal of PFOA after the first cycle of regeneration increased slightly to 100%, over the next three regeneration cycles this removal was maintained. After the fifth regeneration cycle, the removal of PFOA using $FeCl_3$-modified biochar decreased to 99.08% removal still showing promising removal after regeneration. The increase in removal with the first four regeneration cycles may be due to the addition of heat (600 °C, over two hours) burning off the previous PFOA adsorbed while increasing the surface area and porous volume of the material. The lower regeneration of PFOS-saturated $FeCl_3$-modified biochar may be due to the sulfonic group's stronger attachment compared to the PFOA carboxyl group. This is not seen in the regeneration of $FeCl_3$-modified biochar for the removal of PFOS as the sulfonic functional group makes it more thermally stable and thermal regeneration at 600 °C less efficient. There is very little documentation in the literature on the thermal regeneration of adsorbent for the removal of PFOS

and PFOA. Gagliano et al. (2021) achieved GAC regeneration of 90% using microwave regeneration at 700 °C after the first cycle. The regeneration was reduced to 65% after the fifth cycle.

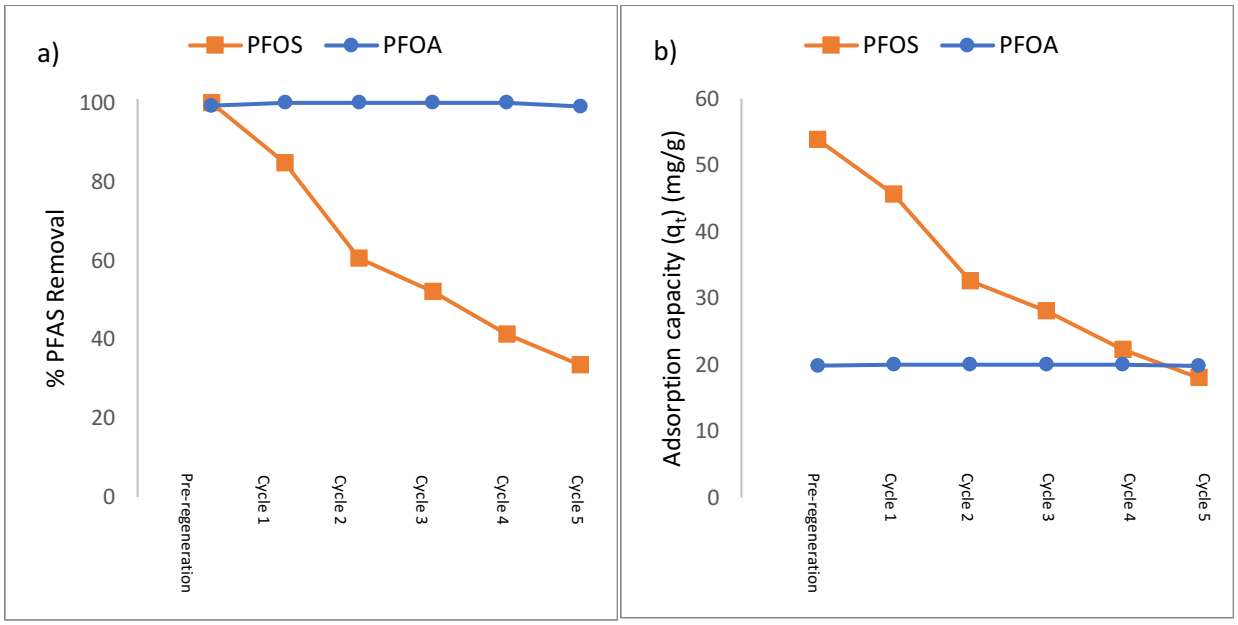

Figure 4.15: a) The removal of PFOS and PFOA over five regeneration cycles and b) the adsorption capacity of PFOS and PFOA over five regeneration cycles Adsorption conditions: initial PFAS compound concentration: 25 mg L^{-1} (pH 6.5); contact time: 4 hours (PFOS), and 6 hours (PFOA); agitation speed: 200 rpm; adsorbent concentration: 0.5 g L^{-1} for PFOS, and 0.75 g L^{-1} for PFOA; regeneration temperature: 600 °C.

Table 4.8: Removal and adsorption capacity after each regeneration cycle

	PFOS		PFOA	
	Removal (%)	qt (mg g^{-1})	Removal (%)	qt (mg g^{-1})
Pre-regeneration	99.89	53.87	80.71	19.85

Cycle 1	84.68	45.61	100	20.00
Cycle 2	60.59	32.64	100	20.00
Cycle 3	52.11	28.07	100	20.00
Cycle 4	41.36	22.28	100	20.00
Cycle 5	33.47	18.03	99.08	19.82

4.8. Characterization of Pre-UV Secondary Effluent

The pre-UV secondary effluent (SE) was characterized at three different stages: (1) pre-UV SE alone, (2) PFAS-spiked pre-UV SE before adsorption, and (3) PFAS-spiked pre-UV SE after adsorption. The wastewater was characterized for PFOS and PFOA as shown in Table 4.10.

Table 4.9: Pre-UV secondary effluent characteristics

	COD (mg L^{-1})	TOC (mg L^{-1})	Phosphorus (mg L^{-1})	Nitrite (mg L^{-1})	Sulfate (mg L^{-1})
Pre-UV SE	33.1	8.035	0.554	0.008	167.0
PFOS Pre-UV SE (pre)	32.1	9.479	0.624	0.00	180.0
PFOS Pre-UV SE (post)	23.3	5.521	0.654	0.011	167.5
PFOA Pre-UV SE (pre)	36.5	14.32	0.609	0.046	167.5
PFOA Pre-UV SE (post)	13.7	6.745	0.751	0.024	172.5

As demonstrated through this characterization, treatment using $FeCl_3$-modified biochar as an adsorbent reduced the overall COD and TOC of the wastewater. Where a COD reduction of 27.30% and 62.41% in PFOS and PFOA spiked pre-UV SE and a TOC reduction of 41.76% and 52.90%, respectively. The higher removal of COD and TOC in the PFOA spiked wastewater could be due to the longer equilibrium time associated. Furthermore, it could help explain the lower PFOA removal compared to PFOS as more active sites are occupied by organic molecules.

4.9. Adsorption Mechanisms

4.9.1. Surface Functional Groups

The FTIR peaks for $FeCl_3$-modified biochar before adsorption and after PFOS and PFOA adsorption are shown in Figure 4.16. The three major bands centered around 449, 1062, and 1564 are attributed to C-H bending vibration, C–F stretching vibrations, and C=O vibrations (Wu, 2007, Nzedieqwu et al., 2021).

At wavelengths below 800 cm^{-1} the aromatic C-H bending vibration can be observed. This is evident in $FeCl_3$-modified biochar pre and post PFOS and PFOA adsorption as the biochar was pyrolyzed at high temperatures (600 °C). Given the hydrophobic properties of the C–F chain in PFAS, hydrophobic interactions should be responsible for the adsorption capacities as CF_2 and CF_3 are generally adsorbed by hydrophobic interaction. The C-F band ranges from 1000-1400 cm^{-1} generally when hydrophobic properties are responsible for adsorption (Hassan et al., 2020; Lin-Vien et al., 1991). The C-F band for $FeCl_3$-modified biochar post PFOS and PFOA adsorption are 1056 cm^{-1} and 1057 cm^{-1} indicating that hydrophobic interaction is prominent. The third peak observed occurred at 1563 cm^{-1} and 1562 cm^{-1} indicating C=O stretching vibrations. C=O stretching vibrations often occur at a wavelength ranging from 1500-1700 cm^{-1} (Hassan et al., 2020; Lv et al., 2020). Dominant hydrophobic interaction indicates that physical adsorption occurred between the adsorbent and the adsorbate.

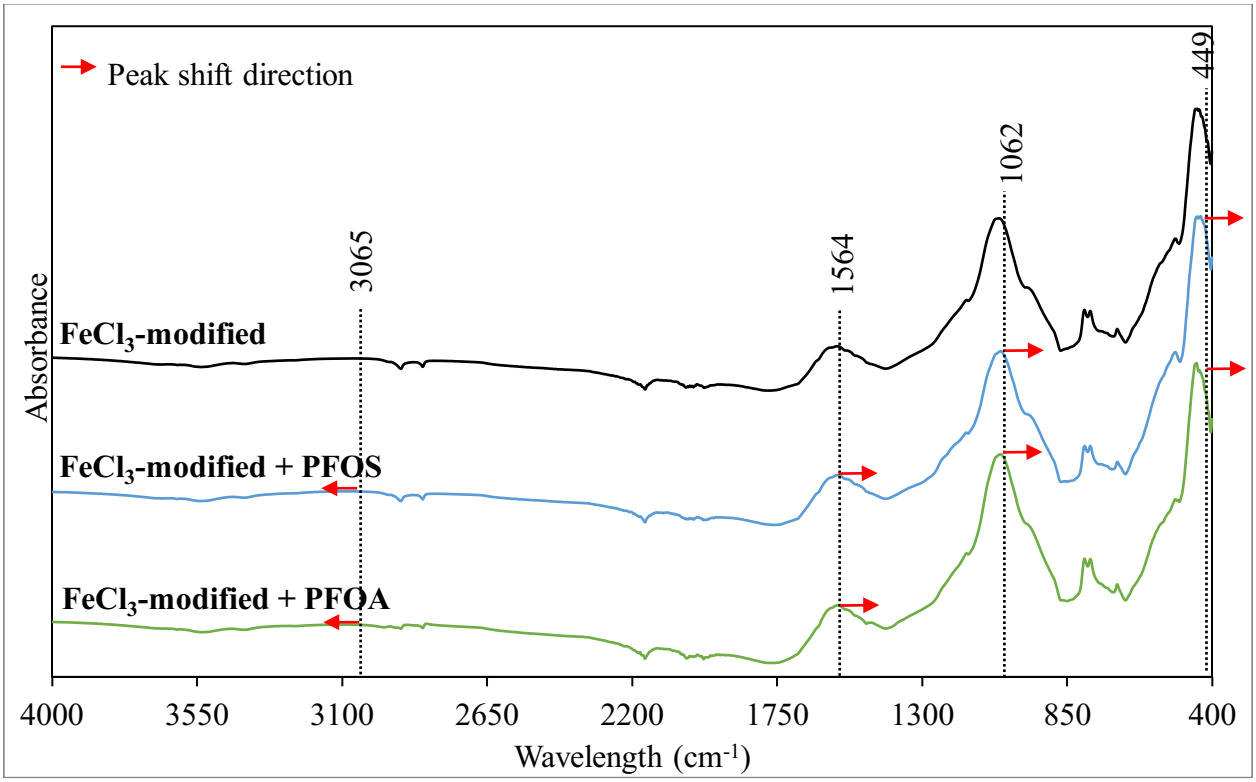

Figure 4.16: FTIR spectra of $FeCl_3$-modified biochar and FeCl3-modified biochar post PFOS and PFOA adsorption.

4.9.2. Elemental Distribution

Using XPS analysis (Figure 4.17) of $FeCl_3$-modified biochar post PFOS and PFOA can help determind differences in adsorption. The XPS survey scan depicts the presence of Fe and Cl in pre and post adsorption $FeCl_3$-modified biochar. C1s, N1s, and O1s peaks are seen in the $FeCl_3$-modified biochar before adsorption, and they are present after adsorption as well with the addition of F1s peak. The F1s peak indicates that PFOS and PFOA compounds are being adsorbed. The deconvolution peaks of carbon and oxygen were evaluated to better describe the adsorbent and adsorption mechanisms.

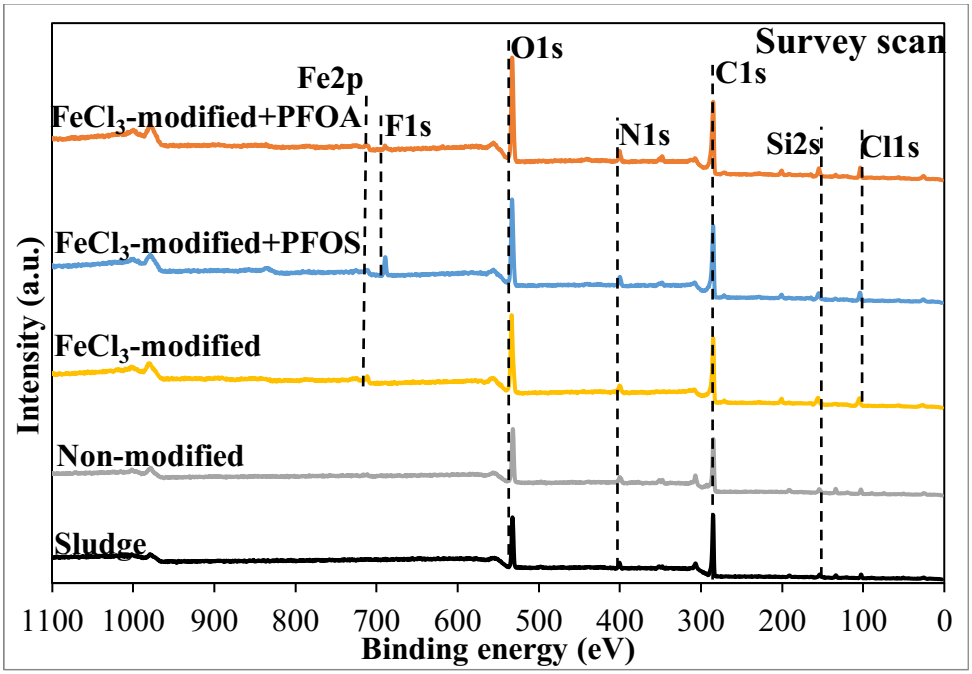

Figure 4.17: XPS analysis of municipal sludge, non-modified biochar, $FeCl_3$-modified biochar pre and post PFOS and PFOA adsorption

There are three deconvolution peaks of carbon for non-modified biochar, $FeCl_3$-modified biochar pre and post PFOS and PFOA adsorption (Figure 4.18). The peaks occur at approximal binding energies 284 eV (C=C), 285 eV (ketonic C=O), and 288 eV (C-F). After adsorption, a decrease in C=C and C=O area ratios is seen while C-F increased. Indicating the adsorption of PFOS and PFOA onto the $FeCl_3$-modified biochar surface. The C=C concentration for $FeCl_3$-modified biochar post adsorption indicates an increasing concentration of PFOS and PFOA. The lower concentration of C=C for the adsorption of PFOS indicates a stronger adsorption affinity than PFOA (Alonso-de-Linaje et al., 2021).

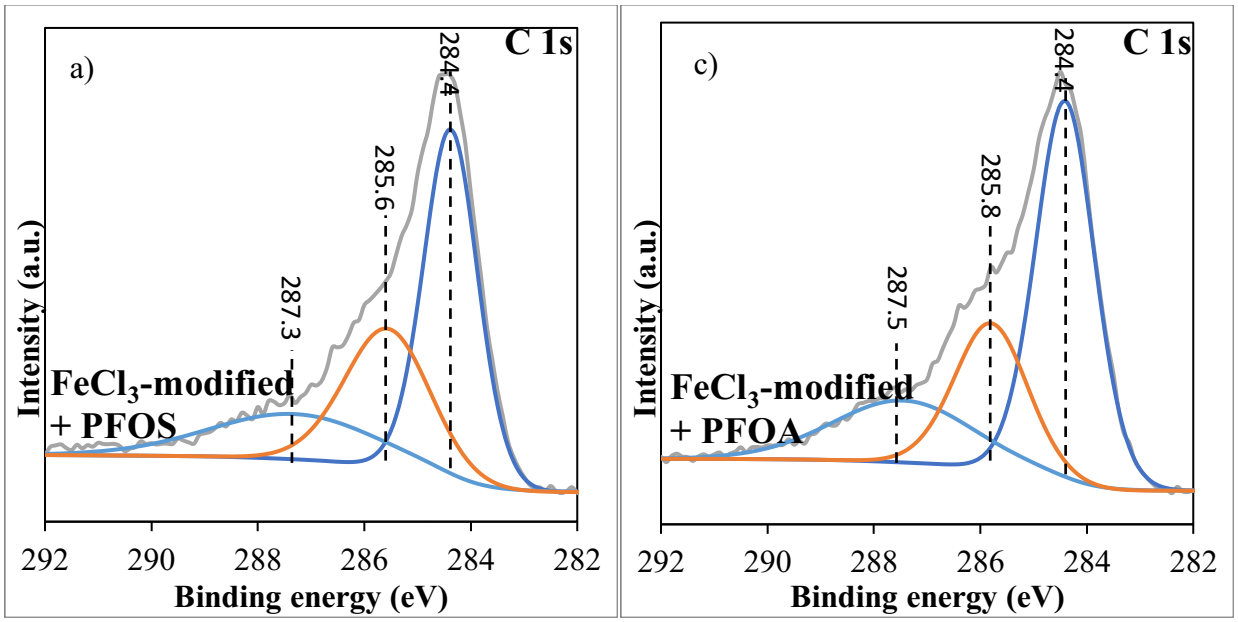

Figure 4.18: XPS analysis deconvolution peaks of carbon for a) municipal sludge, b) non-modified biochar c) $FeCl_3$-modified biochar pre adsorption d) $FeCl_3$-modified biochar post PFOS adsorption, and e) $FeCl_3$-modified biochar post PFOA adsorption.

There are three deconvolution peaks of oxygen for $FeCl_3$-modified biochar pre and post PFOS and PFOA adsorption (Figure 4.18). The deconvolution peaks of oxygen for $FeCl_3$-modified biochar pre and post adsorption have binding energies of 530.4 (C=O), 531.0 (C=O), 532.0 (-OH), and 533.0 (- OH), (Wang et al., 2016; Song et al., 2020; Elanchezhiyan et al., 2021). There is a significant decrease in the area ratio of -OH from PFOS adsorption to PFOA adsorption (37.8%). The presence of hydroxyl groups helps to facilitate adsorption, therefore increasing PFOS adsorption (Zhi & Liu, 2016).

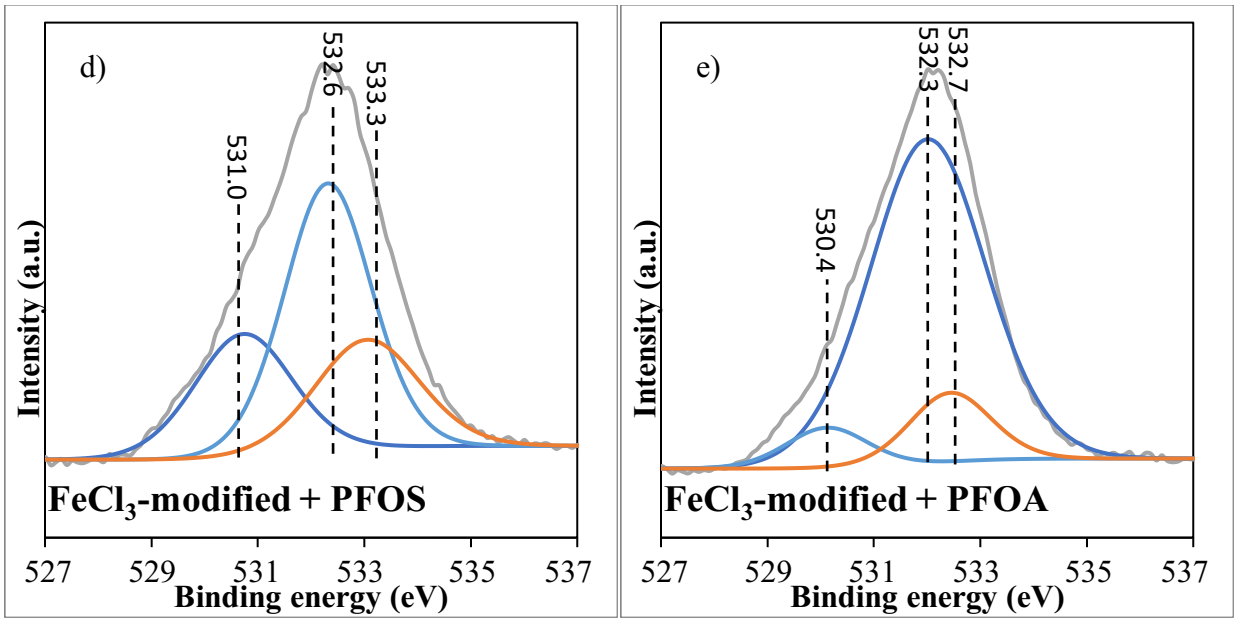

Figure 4.19: XPS analysis deconvolution peaks of oxygen for a) municipal sludge, b) non-modified biochar c) $FeCl_3$-modified biochar pre adsorption d) $FeCl_3$-modified biochar post PFOS adsorption, and e) $FeCl_3$-modified biochar post PFOA adsorption.

5. Conclusion

In summary, the information presented in this thesis focuses on the adsorption of PFOS and PFOA compounds from spiked pre-UV secondary effluent using municipal sludge-produced $FeCl_3$-modified biochar. The literature review portrays the gaps in current knowledge related to the study of PFPS and PFOA from real wastewater and outlines the current technologies being researched. The emphasis of this study was to gain a better understanding of the adsorption processes through underlying characterization and adsorption mechanisms using a real wastewater medium.

The results of this study demonstrated that mesoporous $FeCl_3$-modified biochar can successfully be synthesized and used to adsorb persistent and toxic organic contaminants such as PFOS and PFOA from pre-UV secondary effluent. Sludge, non-modified biochar, and the $FeCl_3$-

modified biochar were characterized using BET, FTIR, SEM, XRD, XPS, TGA, and Ultimate analysis. FTIR, SEM, XRD, and XPS confirm the carbonization and presence of Fe in the $FeCl_3$-modified biochar. BET, TGA, and the ultimate analysis highlight the increased surface area, pore volume, thermal stability, H/C ratio, and O/C ratio giving $FeCl_3$-modified biochar a better adsorption capacity. Resulting in higher removal efficiency for PFOS (99.89%) and PFOA (80.71%) compared to other engineered biochar. The pseudo-second order kinetic model and Langmuir isotherm model best fit the experimental PFOS and PFOA adsorption data. Providing insight into the adsorption equilibrium and adsorption capacity indicating that adsorption occurs in monolayer.

The enhanced removal efficiency of $FeCl_3$-modified biochar is attributed to the increase in surface area, pore volume, and lower O/C ratio compared to non-modified biochar. PFOS has a favorable exposed functional group providing a stronger adsorption affinity compared to the PFOA. Based on the IDP model the rate-limiting step of the adsorption process was determined to be film diffusion.

Over the duration of 7 days no desorption of PFOS was noted and very little (5.3%) was observed for PFOA. Thermal regeneration is also a potential option for $FeCl_3$-modified biochar as the removal rate remained acceptable (84.68%, 60.58%, 52.11%, 41.36%) for PFOS, diminishing to 33.47% after five cycles. Where, thermal regeneration increased the removal rate for the removal of PFOA, maintaining a removal of 100% over four cycles, then reducing to 99.08% after the fifth cycle. Based on the FTIR characterization of $FeCl_3$-modified biochar, hydrogen bonding and hydrophobic interaction are considered the dominant mechanisms that govern $FeCl_3$-modified biochar of PFOS and PFOA adsorption indicating that physical adsorption is occurring. This is further supported by the XPS data analysis using deconvolution peaks of carbon and oxygen.

Overall, $FeCl_3$-modified biochar derived from municipal waste makes the treatment process economically competitive with other currently available PFAS treatment technologies while promoting a circular economy. Additionally, the beneficial reuse of municipal waste (sludge) for addressing persistent emerging contaminants provides a sustainable approach to non-hazardous waste management.

6. Recommendations

This research lays the groundwork for further study around PFOS and PFOA adsorption using engineered sludge-based biochar in wastewater. Additional experimentation using lower concentrations of PFOS and PFOA could be performed to confirm the adsorption performance of $FeCl_3$-modified. It would be beneficial to further evaluate the removal rate and adsorption capacities of $FeCl_3$-modified biochar at different preparation temperatures. As the adsorption capacity is largely impacted by feedstock type and operation condition during synthesis. Further study into the upper end of the acceptable wastewater pH range (8.2-8.5) would increase the scope of feasibility for large-scale implementation, as this study only assesses PFOS and PFOA removal using engineered biochar with a pH of 6.5. The adsorption kinetics of $FeCl_3$-modified biochar could be further evaluated using different temperatures providing further understanding of the adsorption mechanisms (physical/chemical adsorption). Using solid phase extraction or a triple quad mass spectrometer could aid in the analysis and detection of PFOS and PFOA.

References

Alonso-de-Linaje, V., Mangayayam, M. C., Tobler, D. J., Rives, V., Espinosa, R., & Dalby, K. N. (2021). Enhanced sorption of perfluorooctane sulfonate and perfluorooctanoate by hydrotalcites. *Environmental Technology & Innovation*, *21*, 101231. https://doi.org/10.1016/j.eti.2020.101231

Álvarez, M. L., Gascó, G., Palacios, T., Paz-Ferreiro, J., & Méndez, A. (2020). Fe oxides-biochar composites produced by hydrothermal carbonization and pyrolysis of biomass waste. *Journal of Analytical and Applied Pyrolysis*, *151*, 104893. https://doi.org/10.1016/j.jaap.2020.104893

Arrieta-Cortes, R., Farias, P., Hoyo-Vadillo, C., & Kleiche-Dray, M. (2017). Carcinogenic risk of emerging persistent organic pollutant perfluorooctane sulfonate (PFOS): A proposal of Classification. *Regulatory Toxicology and Pharmacology*, *83*, 66–80. https://doi.org/10.1016/j.yrtph.2016.11.021

Askeland, M., Clarke, B. O., Cheema, S. A., Mendez, A., Gasco, G., & Paz-Ferreiro, J. (2020). Biochar sorption of PFOS, PFOA, pfhxs and pfhxa in two soils with contrasting texture. *Chemosphere*, *249*, 126072. https://doi.org/10.1016/j.chemosphere.2020.126072

Banks, D., Jun, B.-M., Heo, J., Her, N., Park, C. M., & Yoon, Y. (2020). Selected advanced water treatment technologies for perfluoroalkyl and Polyfluoroalkyl Substances: A Review. *Separation and Purification Technology*, *231*, 115929. https://doi.org/10.1016/j.seppur.2019.115929

Benally, C., Messele, S. A., & Gamal El-Din, M. (2019). Adsorption of organic matter in oil sands process water (OSPW) by carbon xerogel. *Water Research*, *154*, 402–411. https://doi.org/10.1016/j.watres.2019.01.053

Chandramouli, B., Benskin, J. P., Hamilton, M. C., & Cosgrove, J. R. (2014). Sorption of per- and polyfluoroalkyl substances (pfass) on Filter Media: Implications for Phase Partitioning Studies. *Environmental Toxicology and Chemistry*, *34*(1), 30–36. https://doi.org/10.1002/etc.2751

Chen, W., Zhang, X., Mamadiev, M., & Wang, Z. (2017). Sorption of perfluorooctane sulfonate and perfluorooctanoate on polyacrylonitrile fiber-derived activated carbon fibers: In comparison with activated carbon. *RSC Advances*, *7*(2), 927–938. https://doi.org/10.1039/c6ra25230c

Chen, X., Xia, X., Wang, X., Qiao, J., & Chen, H. (2011). A comparative study on sorption of perfluorooctane sulfonate (PFOS) by chars, ash and carbon nanotubes. *Chemosphere*, *83*(10), 1313–1319. https://doi.org/10.1016/j.chemosphere.2011.04.018

Chia, C. H., Gong, B., Joseph, S. D., Marjo, C. E., Munroe, P., & Rich, A. M. (2012). Imaging of mineral-enriched biochar by FTIR, Raman and Sem–EDX. *Vibrational Spectroscopy*, *62*, 248–257. https://doi.org/10.1016/j.vibspec.2012.06.006

Chou, W.-C., & Lin, Z. (2020). Probabilistic human health risk assessment of perfluorooctane sulfonate (PFOS) by integrating in vitro, in vivo toxicity, and human epidemiological studies using a Bayesian-based dose-response assessment coupled with physiologically based pharmacokinetic (PBPK) modeling approach. *Environment International*, *137*, 105581. https://doi.org/10.1016/j.envint.2020.105581

Crombie, K., Mašek, O., Sohi, S. P., Brownsort, P., & Cross, A. (2012). The effect of pyrolysis conditions on biochar stability as determined by three methods. *GCB Bioenergy*, *5*(2), 122–131. https://doi.org/10.1111/gcbb.12030

Dai, X., Xie, Z., Dorian, B., Gray, S., & Zhang, J. (2019). Comparative study of pfas treatment by UV, UV/ozone, and fractionations with air and ozonated air. *Environmental Science: Water Research & Technology*, *5*(11), 1897–1907. https://doi.org/10.1039/c9ew00701f

Dalahmeh, S. S., Alziq, N., & Ahrens, L. (2019). Potential of biochar filters for onsite wastewater treatment: Effects of active and inactive biofilms on adsorption of per- and polyfluoroalkyl substances in laboratory column experiments. *Environmental Pollution*, *247*, 155–164. https://doi.org/10.1016/j.envpol.2019.01.032

Deng, S., Niu, L., Bei, Y., Wang, B., Huang, J., & Yu, G. (2013). Adsorption of perfluorinated compounds on aminated rice husk prepared by atom transfer radical polymerization. *Chemosphere*, *91*(2), 124–130. https://doi.org/10.1016/j.chemosphere.2012.11.015

Deng, S., Zheng, Y. Q., Xu, F. J., Wang, B., Huang, J., & Yu, G. (2012). Highly efficient sorption of perfluorooctane sulfonate and perfluorooctanoate on a quaternized cotton prepared by atom transfer radical polymerization. *Chemical Engineering Journal*, *193-194*, 154–160. https://doi.org/10.1016/j.cej.2012.04.005

Elanchezhiyan, S. S. D., Preethi, J., Rathinam, K., Njaramba, L. K., & Park, C. M. (2021). Synthesis of magnetic chitosan biopolymeric spheres and their adsorption performances for PFOA and PFOS from aqueous environment. *Carbohydrate Polymers*, *267*, 118165. https://doi.org/10.1016/j.carbpol.2021.118165

Environmental Protection Agency. (n.d.). *Health effects support document for perfluorooctane sulfonate (PFOS)*. EPA. Retrieved August 11, 2022, from https://www.epa.gov/sites/default/files/2016-05/documents/pfos_hesd_final_508.pdf

Environmental Protection Agency. (n.d.). *Health effects support document for perfluorooctanoic acid (PFOA) - US EPA*. EPA. Retrieved August 11, 2022, from https://www.epa.gov/sites/default/files/2016-05/documents/pfoa_hesd_final-plain.pdf

Environmental Protection Agency. (n.d.). *Our Current Understanding of the Human Health and Environmental Risks of PFAS*. EPA. Retrieved August 11, 2022, from https://www.epa.gov/pfas/our-current-understanding-human-health-and-environmental-risks-pfas

Environmental Protection Agency. (n.d.). *Perfluorooctane Sulfonate*. EPA. Retrieved August 11, 2022, from https://tdb.epa.gov/tdb/contaminant?id=10940

Environmental Protection Agency. (n.d.). *Perfluorooctanoic Acid*. EPA. Retrieved August 11, 2022, from https://tdb.epa.gov/tdb/contaminant?id=10520

Fagbayigbo, B. O., Opeolu, B. O., Fatoki, O. S., Olatunji, O. S., Akharame, M. O., & Human, I. S. (2022). Sorption and partitioning of perfluorooctanoic acid (PFOA) and perfluorooctane sulfonate (PFOS) onto sediments of Diep and Plankenburg River Systems Western Cape, South Africa. *Environmental Technology & Innovation*, *25*, 102110. https://doi.org/10.1016/j.eti.2021.102110

Fan, Q., Sun, J., Chu, L., Cui, L., Quan, G., Yan, J., Hussain, Q., & Iqbal, M. (2018). Effects of chemical oxidation on surface oxygen-containing functional groups and adsorption behavior of biochar. *Chemosphere*, *207*, 33–40. https://doi.org/10.1016/j.chemosphere.2018.05.044

Gagliano, E., Falciglia, P. P., Zaker, Y., Karanfil, T., & Roccaro, P. (2021). Microwave regeneration of granular activated carbon saturated with pfas. *Water Research*, *198*, 117121. https://doi.org/10.1016/j.watres.2021.117121

Gagliano, E., Sgroi, M., Falciglia, P. P., Vagliasindi, F. G. A., & Roccaro, P. (2020). Removal of poly- and perfluoroalkyl substances (PFAS) from water by adsorption: Role of pfas chain length, effect of organic matter and challenges in adsorbent regeneration. *Water Research*, *171*, 115381. https://doi.org/10.1016/j.watres.2019.115381

Ghodke, P. K., Sharma, A. K., Pandey, J. K., Chen, W.-H., Patel, A., & Ashokkumar, V. (2021). Pyrolysis of sewage sludge for sustainable biofuels and value-added biochar production. *Journal of Environmental Management*, *298*, 113450. https://doi.org/10.1016/j.jenvman.2021.113450

Government of Canada. (2021, July 29). *Per- and polyfluoroalkyl substances (PFAS)*. Canada.ca. Retrieved August 11, 2022, from https://www.canada.ca/en/health-canada/services/chemical-substances/other-chemical-substances-interest/per-polyfluoroalkyl-substances.html

Guo, H., Liu, Y., Ma, W., Yan, L., Li, K., & Lin, S. (2018). Surface molecular imprinting on carbon microspheres for fast and selective adsorption of perfluorooctane sulfonate. *Journal of Hazardous Materials*, *348*, 29–38. https://doi.org/10.1016/j.jhazmat.2018.01.018

Guo, W., Huo, S., Feng, J., & Lu, X. (2017). Adsorption of perfluorooctane sulfonate (PFOS) on corn straw-derived biochar prepared at different pyrolytic temperatures. *Journal of the Taiwan Institute of Chemical Engineers*, *78*, 265–271. https://doi.org/10.1016/j.jtice.2017.06.013

Hamid, H., & Li, L. (2016). Role of wastewater treatment plant (WWTP) in environmental cycling of poly- and perfluoroalkyl (PFAS) compounds. *Ecocycles*, *2*(2), 43–53. https://doi.org/10.19040/ecocycles.v2i2.62

Hang, X., Chen, X., Luo, J., Cao, W., & Wan, Y. (2015). Removal and recovery of perfluorooctanoate from wastewater by nanofiltration. *Separation and Purification Technology*, *145*, 120–129. https://doi.org/10.1016/j.seppur.2015.03.013

Hassan, M., Liu, Y., Naidu, R., Du, J., & Qi, F. (2020). Adsorption of perfluorooctane sulfonate (PFOS) onto metal oxides modified biochar. *Environmental Technology & Innovation*, *19*, 100816. https://doi.org/10.1016/j.eti.2020.100816

Hernandez-Mena*, L. E., Pécora, A. A. B., & Beraldo, A. L. (2014). Slow Pyrolysis of Bamboo Biomass: Analysis of Biochar Properties. *Italian Association of Chemical Engineering*, *37*. https://doi.org/10.3303/CET1437020

Higgins, C. P., & Luthy, R. G. (2006). Sorption of perfluorinated surfactants on sediments. *Environmental Science & Technology*, *40*(23), 7251–7256. https://doi.org/10.1021/es061000n

Ho, S.-H., Chen, Y.-di, Yang, Z.-kai, Nagarajan, D., Chang, J.-S., & Ren, N.-qi. (2017). High-efficiency removal of lead from wastewater by biochar derived from anaerobic digestion sludge. *Bioresource Technology*, *246*, 142–149. https://doi.org/10.1016/j.biortech.2017.08.025

Inyang, M., & Dickenson, E. R. V. (2017). The use of carbon adsorbents for the removal of perfluoroalkyl acids from potable reuse systems. *Chemosphere*, *184*, 168–175. https://doi.org/10.1016/j.chemosphere.2017.05.161

Jang, H. M., Yoo, S., Choi, Y.-K., Park, S., & Kan, E. (2018). Adsorption isotherm, kinetic modeling and mechanism of tetracycline on pinus taeda-derived activated biochar. *Bioresource Technology*, *259*, 24–31. https://doi.org/10.1016/j.biortech.2018.03.013

Karaca, C., Sözen, S., Orhon, D., & Okutan, H. (2018). High temperature pyrolysis of sewage sludge as a sustainable process for energy recovery. *Waste Management*, *78*, 217–226. https://doi.org/10.1016/j.wasman.2018.05.034

Kothawala, D. N., Köhler, S. J., Östlund, A., Wiberg, K., & Ahrens, L. (2017). Influence of dissolved organic matter concentration and composition on the removal efficiency of perfluoroalkyl substances (pfass) during drinking water treatment. *Water Research*, *121*, 320–328. https://doi.org/10.1016/j.watres.2017.05.047

Kucharzyk, K. H., Darlington, R., Benotti, M., Deeb, R., & Hawley, E. (2017). Novel treatment technologies for pfas compounds: A critical review. *Journal of Environmental Management*, *204*, 757–764. https://doi.org/10.1016/j.jenvman.2017.08.016

Lenka, S. P., Kah, M., & Padhye, L. P. (2021). A review of the occurrence, transformation, and removal of poly- and perfluoroalkyl substances (PFAS) in wastewater treatment plants. *Water Research*, *199*, 117187. https://doi.org/10.1016/j.watres.2021.117187

Lin-Vien, D., Colthup, N. B., Fateley, W. G., & Grasselli, J. G. (1991). *The Handbook of Infrared and Raman characteristic frequencies of organic molecules*. Academic Press.

Liu, Y., He, Z., & Uchimiya, M. (2015). Comparison of biochar formation from various agricultural by-products using FTIR spectroscopy. *Modern Applied Science*, *9*(4). https://doi.org/10.5539/mas.v9n4p246

Liu, Z., Bentel, M. J., Yu, Y., Ren, C., Gao, J., Pulikkal, V. F., Sun, M., Men, Y., & Liu, J. (2021). Near-quantitative defluorination of perfluorinated and fluorotelomer carboxylates and sulfonates with integrated oxidation and reduction. *Environmental Science & Technology*, *55*(10), 7052–7062. https://doi.org/10.1021/acs.est.1c00353

Lv, S., Li, C., Mi, J., & Meng, H. (2020). A functional activated carbon for efficient adsorption of phenol derived from pyrolysis of rice husk, Koh-activation and EDTA-4NA-modification. *Applied Surface Science*, *510*, 145425. https://doi.org/10.1016/j.apsusc.2020.145425

Militao, I. M., Roddick, F. A., Bergamasco, R., & Fan, L. (2021). Removing pfas from aquatic systems using natural and renewable material-based adsorbents: A Review. *Journal of Environmental Chemical Engineering*, *9*(4), 105271. https://doi.org/10.1016/j.jece.2021.105271

Momina, M., Shahadat, M., & Isamil, S. (2018). Regeneration performance of clay-based adsorbents for the removal of industrial dyes: A Review. *RSC Advances*, *8*(43), 24571–24587. https://doi.org/10.1039/c8ra04290j

Murray, C. C., Marshall, R. E., Liu, C. J., Vatankhah, H., & Bellona, C. L. (2021). Pfas treatment with granular activated carbon and ion exchange resin: Comparing chain length, empty bed contact time, and cost. *Journal of Water Process Engineering*, *44*, 102342. https://doi.org/10.1016/j.jwpe.2021.102342

Nguyen, V.-T., Vo, T.-D.-H., Nguyen, T.-B., Dat, N. D., Huu, B. T., Nguyen, X.-C., Tran, T., Le, T.-N.-C., Duong, T.-G.-H., Bui, M.-H., Dong, C.-D., & Bui, X.-T. (2022). Adsorption of norfloxacin from aqueous solution on biochar derived from spent coffee ground: Master variables and response surface method optimized adsorption process. *Chemosphere*, *288*, 132577. https://doi.org/10.1016/j.chemosphere.2021.132577

Nzediegwu, C., Naeth, M. A., & Chang, S. X. (2021). Carbonization temperature and feedstock type interactively affect chemical, fuel, and surface properties of hydrochars. *Bioresource Technology*, *330*, 124976. https://doi.org/10.1016/j.biortech.2021.124976

Ofomaja, A. E. (2010). Intraparticle diffusion process for lead(ii) biosorption onto Mansonia Wood Sawdust. *Bioresource Technology*, *101*(15), 5868–5876. https://doi.org/10.1016/j.biortech.2010.03.033

Ochoa-Herrera, V., & Sierra-Alvarez, R. (2008). Removal of perfluorinated surfactants by sorption onto granular activated carbon, zeolite and sludge. *Chemosphere*, *72*(10), 1588–1593. https://doi.org/10.1016/j.chemosphere.2008.04.029

Pachkowski, B., Post, G. B., & Stern, A. H. (2019). The derivation of a reference dose (RFD) for Perfluorooctane Sulfonate (PFOS) based on immune suppression. *Environmental Research*, *171*, 452–469. https://doi.org/10.1016/j.envres.2018.08.004

Panieri, E., Baralic, K., Djukic-Cosic, D., Buha Djordjevic, A., & Saso, L. (2022). Pfas molecules: A major concern for the human health and the environment. *Toxics*, *10*(2), 44. https://doi.org/10.3390/toxics10020044

Schröder, H. F., & Meesters, R. J. W. (2005). Stability of fluorinated surfactants in advanced oxidation processes—a follow up of degradation products using flow injection–mass spectrometry, liquid chromatography–mass spectrometry and liquid chromatography–multiple stage mass spectrometry. *Journal of Chromatography A*, *1082*(1), 110–119. https://doi.org/10.1016/j.chroma.2005.02.070

Senevirathna, S. T. M. L. D., Tanaka, S., Fujii, S., Kunacheva, C., Harada, H., Shivakoti, B. R., & Okamoto, R. (2010). A comparative study of adsorption of perfluorooctane sulfonate (PFOS) onto granular activated carbon, ion-exchange polymers and non-ion-exchange polymers. *Chemosphere*, *80*(6), 647–651. https://doi.org/10.1016/j.chemosphere.2010.04.053

Simonin, J.-P. (2016). On the comparison of pseudo-first order and pseudo-second order rate laws in the modeling of adsorption kinetics. *Chemical Engineering Journal*, *300*, 254–263. https://doi.org/10.1016/j.cej.2016.04.079

Shakya, A., Vithanage, M., & Agarwal, T. (2022). Influence of pyrolysis temperature on biochar properties and cr(vi) adsorption from water with groundnut shell biochars: Mechanistic approach. *Environmental Research*, *215*, 114243. https://doi.org/10.1016/j.envres.2022.114243

Son, H., Kim, T., Yoom, H.-S., Zhao, D., & An, B. (2020). The adsorption selectivity of short and long per- and polyfluoroalkyl substances (pfass) from surface water using powder-activated carbon. *Water*, *12*(11), 3287. https://doi.org/10.3390/w12113287

Song, J., Messele, S. A., Meng, L., Huang, Z., & Gamal El-Din, M. (2021). Adsorption of metals from oil sands process water (OSPW) under natural ph by sludge-based biochar/Chitosan composite. *Water Research*, *194*, 116930. https://doi.org/10.1016/j.watres.2021.116930

Song, J., How, Z. T., Huang, Z., & Gamal El-Din, M. (2022). Biochar/iron oxide composite as an efficient peroxymonosulfate catalyst for the degradation of model naphthenic acids compounds. *Chemical Engineering Journal*, *429*, 132220. https://doi.org/10.1016/j.cej.2021.132220

Sörengård, M., Lindh, A.-S., & Ahrens, L. (2020). Thermal desorption as a high removal remediation technique for soils contaminated with per- and polyfluoroalkyl substances (pfass). *PLOS ONE*, *15*(6). https://doi.org/10.1371/journal.pone.0234476

Tchobanoglous, G., Burton, F. L., & Stensel, H. D. (2014). *Wastewater Engineering. treatment and Reuse*. McGraw-Hill.

The international XPS database. The International XPS Database 1. (2022, July 5). Retrieved November 7, 2022, from https://xpsdatabase.com/

Trojanowicz, M., Bojanowska-Czajka, A., Bartosiewicz, I., & Kulisa, K. (2018). Advanced oxidation/reduction processes treatment for aqueous perfluorooctanoate (PFOA) and perfluorooctanesulfonate (PFOS) – a review of recent advances. *Chemical Engineering Journal*, *336*, 170–199. https://doi.org/10.1016/j.cej.2017.10.153

Umpleby, R. J., Baxter, S. C., Bode, M., Berch, J. K., Shah, R. N., & Shimizu, K. D. (2001). Application of the freundlich adsorption isotherm in the characterization of molecularly imprinted polymers. *Analytica Chimica Acta*, *435*(1), 35–42. https://doi.org/10.1016/s0003-2670(00)01211-3

U.S. National Library of Medicine. (n.d.). *Perfluorobutanesulfonic acid*. National Center for Biotechnology Information. PubChem Compound Database. Retrieved September 11, 2022, from https://pubchem.ncbi.nlm.nih.gov/compound/67815

U.S. National Library of Medicine. (n.d.). *Perfluorooctanesulfonic acid*. National Center for Biotechnology Information. PubChem Compound Database. Retrieved September 11, 2022, from https://pubchem.ncbi.nlm.nih.gov/compound/74483

U.S. National Library of Medicine. (n.d.). *Perfluorooctanoic acid*. National Center for Biotechnology Information. PubChem Compound Database. Retrieved September 11, 2022, from https://pubchem.ncbi.nlm.nih.gov/compound/Perfluorooctanoic-acid

Uttran, A., Loh, S. K., Kong, S.-H., & Bachmann, R. T. (2018). Adsorption of NPK fertiliser and humic acid on palm kernel shell biochar. *Journal of Oil Palm Research*, *30*, 472–483. https://doi.org/10.21894/jopr.2018.0029

Vo, H. N., Nguyen, T. M., Ngo, H. H., Guo, W., & Shukla, P. (2022). Biochar sorption of perfluoroalkyl substances (pfass) in aqueous film-forming foams-impacted groundwater: Effects of PFASS properties and groundwater chemistry. *Chemosphere*, *286*, 131622. https://doi.org/10.1016/j.chemosphere.2021.131622

Wang, B., Lee, L. S., Wei, C., Fu, H., Zheng, S., Xu, Z., & Zhu, D. (2022). Covalent triazine-based framework: A promising adsorbent for removal of perfluoroalkyl acids from aqueous solution. *Environmental Pollution*, *216*, 884–892. https://doi.org/10.1016/j.envpol.2016.06.062

Wang, Y., Zhang, H., Zhu, Y., Dai, Z., Bao, H., Wei, Y., & Cai, W. (2016). Au-NP-decorated crystalline feocl nanosheet: Facile synthesis by laser ablation in liquid and its exclusive gas sensing response to hcl at room temperature. *Advanced Materials Interfaces*, *3*(9), 1500801. https://doi.org/10.1002/admi.201500801

Winchell, L. J., Wells, M. J. M., Ross, J. J., Fonoll, X., Norton, J. W., Kuplicki, S., Khan, M., & Bell, K. Y. (2021). Analyses of per- and polyfluoroalkyl substances (PFAS) through the urban water cycle: Toward achieving an integrated analytical workflow across aqueous, solid, and gaseous matrices in water and wastewater treatment. *Science of The Total Environment*, *774*, 145257. https://doi.org/10.1016/j.scitotenv.2021.145257

Worch, E. (2012). *Adsorption technology in water treatment*. De Gruyter.

Xiang, W., Zhang, X., Chen, J., Zou, W., He, F., Hu, X., Tsang, D. C. W., Ok, Y. S., & Gao, B. (2020). Biochar technology in wastewater treatment: A critical review. *Chemosphere*, *252*, 126539. https://doi.org/10.1016/j.chemosphere.2020.126539

Xu, B., Ahmed, M. B., Zhou, J. L., Altaee, A., Wu, M., & Xu, G. (2017). Photocatalytic removal of perfluoroalkyl substances from water and wastewater: Mechanism, kinetics and controlling factors. *Chemosphere*, *189*, 717–729. https://doi.org/10.1016/j.chemosphere.2017.09.110

Yadav, S., Ibrar, I., Al-Juboori, R. A., Singh, L., Ganbat, N., Kazwini, T., Karbassiyazdi, E., Samal, A. K., Subbiah, S., & Altaee, A. (2022). Updated review on Emerging Technologies for pfas contaminated water treatment. *Chemical Engineering Research and Design*, *182*, 667–700. https://doi.org/10.1016/j.cherd.2022.04.009

Yang, L., He, L., Xue, J., Ma, Y., Xie, Z., Wu, L., Huang, M., & Zhang, Z. (2020). Persulfate-based degradation of perfluorooctanoic acid (PFOA) and perfluorooctane sulfonate (PFOS) in aqueous solution: Review on influences, mechanisms and prospective. *Journal of Hazardous Materials*, *393*, 122405. https://doi.org/10.1016/j.jhazmat.2020.122405

Yu, Q., Zhang, R., Deng, S., Huang, J., & Yu, G. (2009). Sorption of perfluorooctane sulfonate and perfluorooctanoate on activated carbons and resin: Kinetic and isotherm study. *Water Research*, *43*(4), 1150–1158. https://doi.org/10.1016/j.watres.2008.12.001

Yuan, J.-H., Xu, R.-K., & Zhang, H. (2011). The forms of alkalis in the biochar produced from crop residues at different temperatures. *Bioresource Technology*, *102*(3), 3488–3497. https://doi.org/10.1016/j.biortech.2010.11.018

Yuan, Y., Feng, L., He, X., Liu, X., Xie, N., Ai, Z., Zhang, L., & Gong, J. (2022). Efficient removal of PFOA with an IN2O3/persulfate system under solar light via the combined process of surface radicals and photogenerated holes. *Journal of Hazardous Materials*, *423*, 127176. https://doi.org/10.1016/j.jhazmat.2021.127176

Zeng, Z., Song, B., Xiao, R., Zeng, G., Gong, J., Chen, M., Xu, P., Zhang, P., Shen, M., & Yi, H. (2019). Assessing the human health risks of perfluorooctane sulfonate by in vivo and in vitro studies. *Environment International*, *126*, 598–610. https://doi.org/10.1016/j.envint.2019.03.002

Zhi, Y., & Liu, J. (2016). Surface modification of activated carbon for enhanced adsorption of perfluoroalkyl acids from aqueous solutions. *Chemosphere*, *144*, 1224–1232. https://doi.org/10.1016/j.chemosphere.2015.09.097

Zdravkov, B., Čermák, J., Šefara, M., & Janků, J. (2007). Pore classification in the characterization of porous materials: A perspective. *Open Chemistry*, *5*(4), 1158. https://doi.org/10.2478/s11532-007-0039-3

Zhao, P., Xia, X., Dong, J., Xia, N., Jiang, X., Li, Y., & Zhu, Y. (2016). Short- and long-chain Perfluoroalkyl substances in the water, suspended particulate matter, and surface sediment of a turbid river. *Science of The Total Environment*, *568*, 57–65. https://doi.org/10.1016/j.scitotenv.2016.05.221

Appendices

Calibration Curve

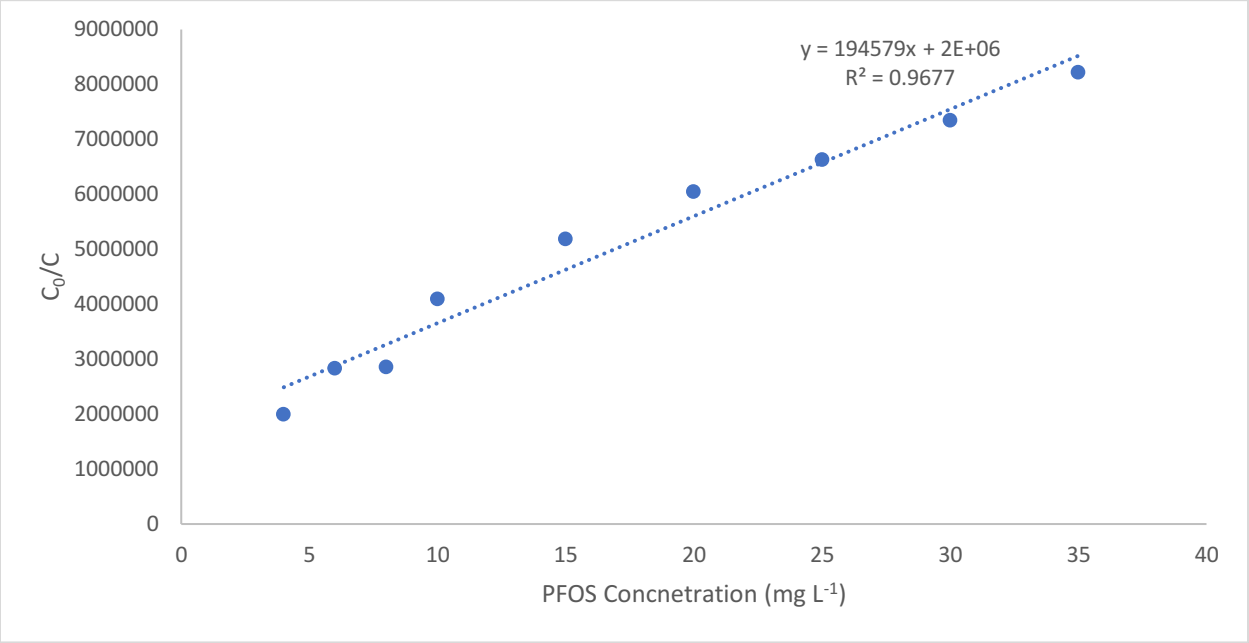

Figure 7.1: Calibration curve for PFOS from concentrations 4 mg L-1 to 35 mg L-1.

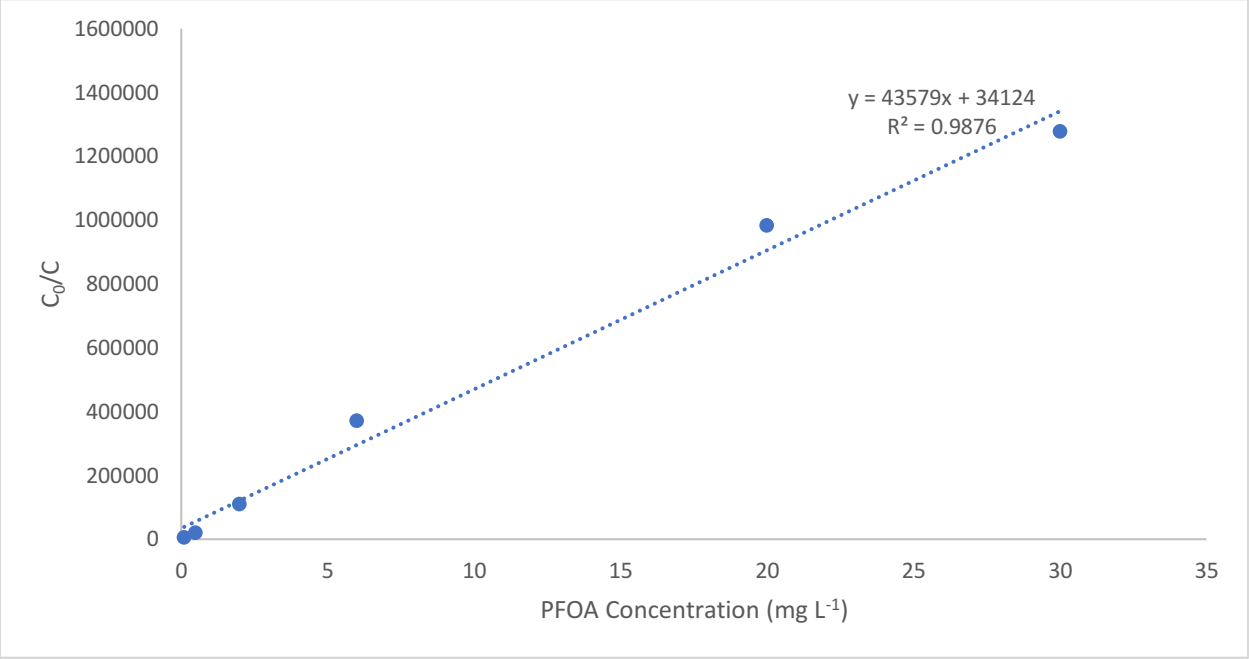

Figure 7.2: Calibration curve for PFOA from concentrations 0.1 mg L^{-1} to 30 mg L^{-1}.

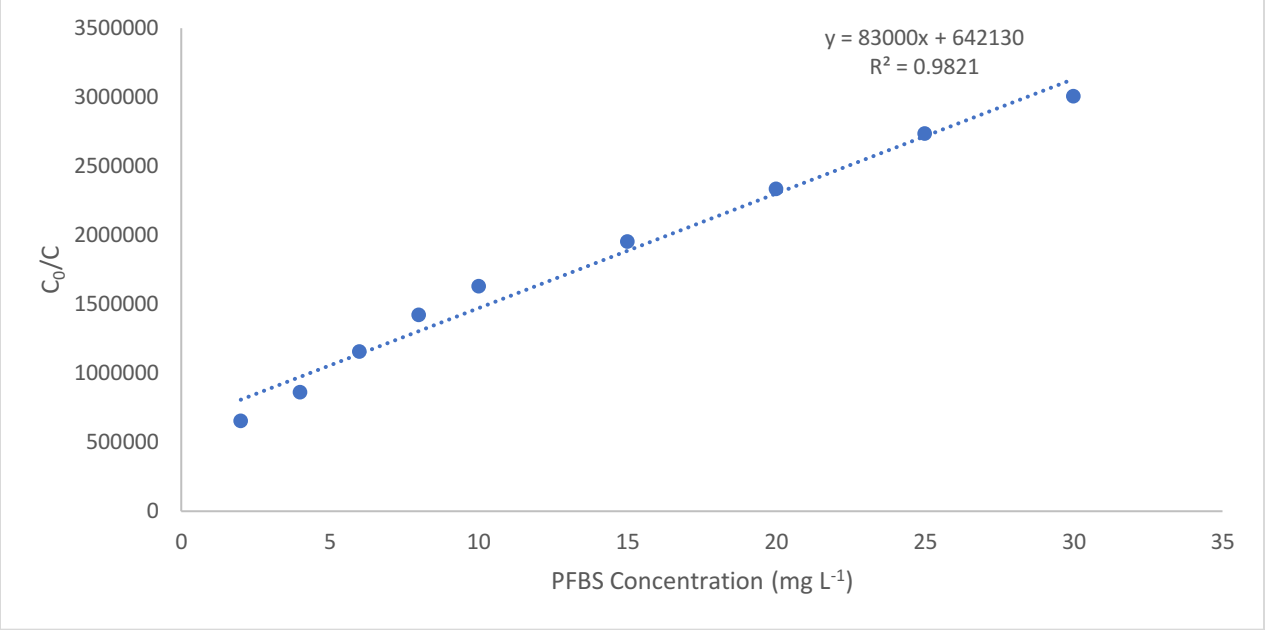

Figure 7.3: Calibration curve for PFOS from concentrations 2 mg L^{-1} to 30 mg L^{-1}.

AOP Data

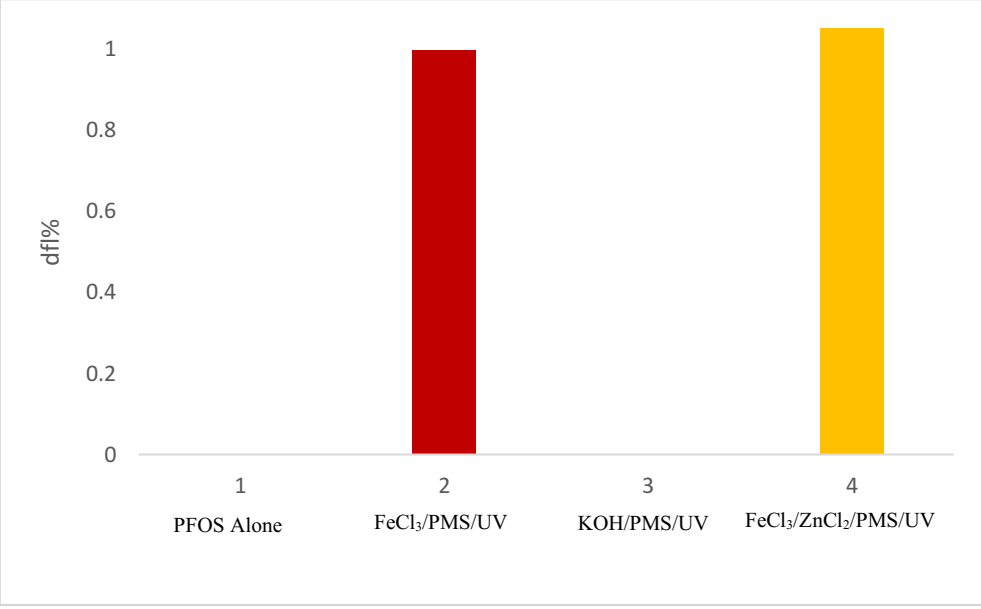

Figure 7.4: Defluorination percent of PFOS using various adsorbents, UV irradiation, and PMS as a catalyst. Adsorption conditions: initial PFOS spiked pre-UV secondary effluent concentration: 10 mg L^{-1} (pH 4.5); contact time: 4 h; adsorbent concentration: 0.05 g L^{-1}; PMS concentration: 0.5 g L^{-1}.

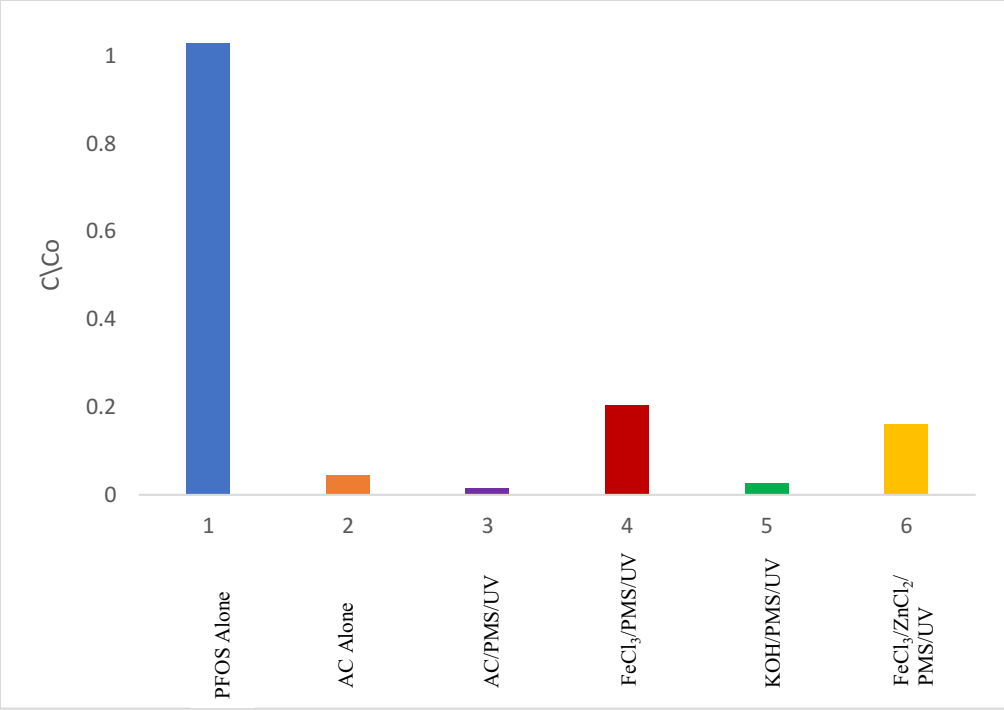

Figure 7.5: Removal of PFOS using various adsorbents and PMS as a catalyst. Adsorption conditions: initial PFOS spiked pre-UV secondary effluent concentration: 10 mg L^{-1} (pH 4.5); contact time: 4 h; adsorbent concentration: 0.05 g L^{-1}; PMS concentration: 0.5 g L^{-1}.

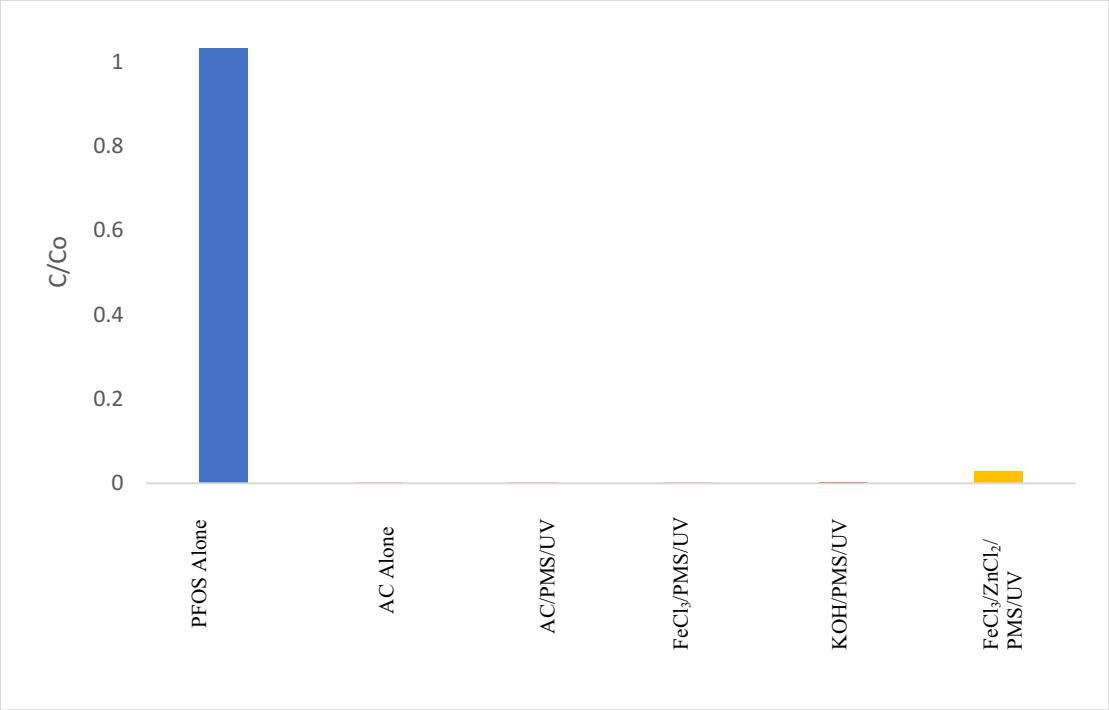

Figure 7.6: Removal of PFOS using various adsorbents, UV irradiation, and PMS as a catalyst. Adsorption conditions: initial PFOS spiked pre-UV secondary effluent concentration: 10 mg L^{-1} (pH 4.5); contact time: 4 h; adsorbent concentration: 0.05 g L^{-1}; PMS concentration: 0.5 g L^{-1}.

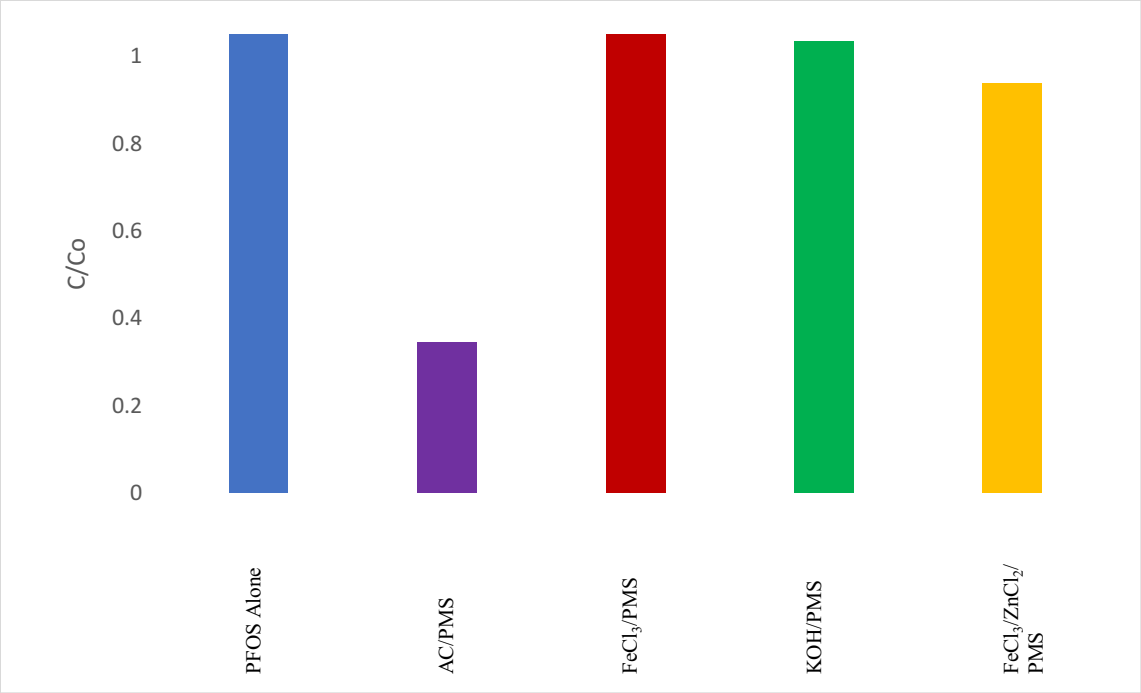

Figure 7.7: Removal of PFOS using various adsorbents (AC, $FeCl_3$-modified biochar, KOH-modified biochar, and $FeCl_3/ZnCl_2$-modified biochar) and PMS as a catalyst. Adsorption conditions: initial PFOS spiked pre-UV secondary effluent concentration: 10 mg L^{-1} (pH 8.5); contact time: 4 h; adsorbent concentration: 0.05 g L^{-1}; PMS concentration: 0.5 g L^{-1}.

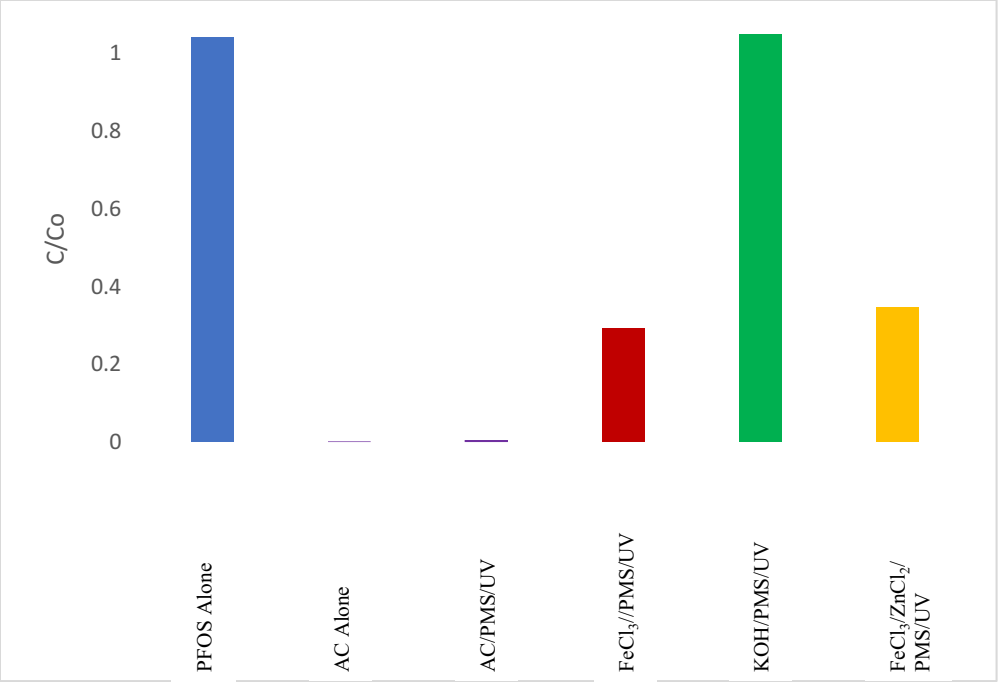

Figure 7.8: Removal of PFOS using various adsorbents (AC, $FeCl_3$-modified biochar, KOH-modified biochar, and $FeCl_3/ZnCl_2$-modified biochar), UV irradiation, and PMS as a catalyst. Adsorption conditions: initial PFOS spiked pre-UV secondary effluent concentration: 10 mg L^{-1} (pH 8.5); contact time: 4 h; adsorbent concentration: 0.05 g L^{-1}; PMS concentration: 0.5 g L^{-1}